Behavioural pharmacology predicts disrupted signalling pathways and candidate therapeutics from zebrafish mutants of Alzheimer's disease risk genes

François Kroll[1,2], Joshua Donnelly[1], Güliz Gürel Özcan[1], Eirinn Mackay[1], Jason Rihel[1*]

[1]Department of Cell and Developmental Biology, University College London, London, United Kingdom

[2]Institut de la Vision, Sorbonne Université, Paris, France

* Corresponding author: j.rihel@ucl.ac.uk

By exposing genes associated with disease, genomic studies provide hundreds of starting points that should lead to druggable processes. However, our ability to systematically translate these genomic findings into biological pathways remains limited. Here, we combine rapid loss-of-function mutagenesis of Alzheimer's risk genes and behavioural pharmacology in zebrafish to predict disrupted processes and candidate therapeutics. FramebyFrame, our expanded package for the analysis of larval behaviours, revealed that decreased night-time sleep was common to F0 knockouts of all four late-onset Alzheimer's risk genes tested. We developed an online tool, ZOLTAR, which compares any behavioural fingerprint to a library of fingerprints from larvae treated with 3,674 compounds. ZOLTAR successfully predicted that *sorl1* mutants have disrupted serotonin signalling and identified betamethasone as a drug which normalises the excessive day-time sleep of *presenilin-2* knockout larvae with minimal side effects. Predictive behavioural pharmacology offers a general framework to rapidly link disease-associated genes to druggable pathways.

Introduction

To prevent or slow down disease, therapies must target the biological processes that cause the disease. Genomic approaches like family studies or genome-wide association studies (GWASs) can help in this quest for causal processes by exposing genes that are mutated before disease onset. For finding causal processes, studying the genome, rather than the transcriptome or epigenome, is advantageous because the chronology from genomic variant to disease is unambiguous, providing a strong argument for causality. In theory, all we need to do after a genomic study is follow the thread from each gene to the biological process in which it is involved. We know from the genomic study that this process increased or reduced risk when it was altered by mutations in the gene, so modulating more forcefully the process with a drug may unlock a larger therapeutic benefit. In practice, the path from genomic variant to druggable process is far from straightforward.

Research on Alzheimer's disease (AD) exemplifies well both the benefit and challenge of translating genomic studies into druggable biological processes. Family studies of early-onset AD in the 1990's[1] identified causal mutations in amyloid precursor protein (*APP*)[2,3], presenilin 1 (*PSEN1*)[4], and presenilin 2 (*PSEN2*)[5]. Subsequent work demonstrated that amyloid beta (Aβ), a small peptide which forms aggregates in AD patients' brains[6], was generated by cleavage of APP by γ-secretase[7,8], of which the catalytic subunit is PSEN1 or PSEN2[9,10]. Consequently, the field naturally converged on the amyloid hypothesis of AD, which posits that the disease is caused by toxic aggregates of Aβ[11]. Today, antibodies against Aβ such as lecanemab show promise in slowing down disease progression[12]. This story shows that, although a great challenge, genomic studies (family studies of early-onset AD) can be successfully translated into a causal process (Aβ aggregation) that is now targeted by disease-modifying drugs (lecanemab).

However, the beneficial effects from targeting Aβ aggregation currently remain modest despite substantial reductions in brain amyloid burden[12]. To completely stop disease progression, anti-amyloid therapy will likely need to be combined with drugs modulating other processes that contribute to the disease[13]. GWASs have identified tens of genomic loci where sequence variation is associated with late-onset AD, offering an opportunity to discover new causal processes of AD that potentially go beyond the amyloid hypothesis. For example, analysis of cell types enriched for open chromatin at AD-associated loci pointed to a possible critical role of monocytes, macrophages, and microglia in AD progression[14,15]. Although GWASs are designed to generate new hypotheses, AD-associated loci have rarely been exploited to find new causal processes in an unbiased, systematic manner. Given the challenges inherent to linking genomic variants to causal biological events, new genomic associations are often first more narrowly interpreted in the context of the amyloid

hypothesis. While this interpretation may be correct, it tends to create a self-fulfilling prophecy which leaves little room for the discovery of new causal processes[16,17].

As AD is primarily a disease of the old age, research often focuses on patients or animal models after disease onset. However, this approach also hinders the discovery of new *causal* processes from genomic studies because it largely annuls the advantage of unambiguous chronology—since genomic variants were unambiguously present before disease onset, they must have modulated a process which contributed causally to disease initiation. In patients or animals after disease onset, many biological processes are disrupted, but only a small proportion may be genuinely causal for disease progression and therefore make suitable targets for disease-modifying therapies. For example, one may find that dopamine is lacking in the basal ganglia of patients and animal models of Parkinson's disease. Treatment with levodopa, a dopamine precursor, temporarily relieves motor symptoms, but does not slow down disease progression, so dopamine deficiency was not in fact a causal process[18]. Therefore, perhaps counterintuitively, studying the consequences of AD-associated mutations *early* in life seems more likely to identify processes that are genuinely causal to disease, as any disrupted process that is identified is less likely to be a secondary disease consequence.

In practice, how can we quickly follow the thread from a disease-associated gene to a (druggable) biological process in which it is involved? In this work, we describe a behavioural pharmacology approach to link genes associated with a disease to likely causal biological processes using zebrafish larvae. Our strategy predicts from the behavioural profile of knockout zebrafish the likely causal processes and potential compounds that rescue the phenotype. In previous work[19], we introduced the use of zebrafish F0 knockouts to study complex traits such as behaviour. In this study, we demonstrate how the F0 knockout method renders this behavioural pharmacology approach fast and scalable to the parallel study of tens of disease-associated genes, rather than one at a time[20,21]. As genomic studies of AD can likely be further exploited to find causal processes, we used Alzheimer's risk genes as a case study for our strategy. The strategy is not specific to any one disease or set of genes. In theory, any measurable change in behaviour could be used to predict the underlying causal pathways and small molecules that normalise this change.

Results

Most Alzheimer's risk genes are present in zebrafish and expressed early in development

GWASs point to small portions of the genome where variation in sequence is associated with variation in disease risk, but do not readily specify the genes whose altered function are responsible for this association. Therefore, as a starting point, we used a meta-analysis of GWASs on AD that found 37 significant loci and annotated each with the most likely causal gene using mainly statistical colocalisation[22,23]. To add confidence to these calls, we cross-referenced these causal gene predictions with a transcription-wide association study and risk gene pre-mRNAs that undergo differential splicing in AD brains[24]. Finally, we added to our list the three genes which can cause early-onset AD when mutated: *PSEN1*[4], *PSEN2*[5], and *APP*[2,3], yielding a list of 40 genes associated with AD risk (Supplementary file 1).

Of these 40 Alzheimer's risk genes, 30 (75%) had at least one annotated orthologue in the zebrafish genome (source: Ensembl). Of those, 17 had one orthologue (e.g. the only zebrafish orthologue of human *SORL1* was *sorl1*); 11 had two orthologues (e.g. the zebrafish orthologues of human *APP* were *appa* and *appb*); and 2 had more than two orthologues (e.g. the zebrafish orthologues of human *MS4A6E* included *ms4a17a*, *ms4a17c.2*, *tmem176l*, and more) (Fig. 1a). A human gene often has two or more zebrafish orthologues because of a teleost-specific whole-genome duplication event around 340 million years ago[25]. There were no annotated orthologues for 10 Alzheimer's risk genes, including *TREM2*.

Next, we used a published single-cell RNA sequencing (scRNA-seq) dataset of the developing zebrafish brain[26] to ask whether the orthologues of the Alzheimer's risk genes were expressed in zebrafish embryos and larvae. Most of the genes (33/42) were detectable as early as 12 hours post-fertilisation (hpf) and remained expressed throughout development (Fig. 1b). At 5 days post-fertilisation (dpf), 38 of the 42 orthologues (90%) were expressed.

From these observations, we selected seven high-confidence Alzheimer's risk genes for further study in zebrafish; the orthologues of the three early-onset Alzheimer's genes: *psen1*, *psen2*, *appa*/*appb*; and four genes associated with late-onset AD: *apoea*/*apoeb*, *cd2ap*, *clu*, *sorl1*. We chose *APOE* as it is the most well-known genetic risk factor for late-onset AD[27]. *CD2AP*, *CLU*, and *SORL1* were chosen because non-coding variants within or near those genes are repeatedly found by GWASs[28,29]. At the *CD2AP* locus, *CD2AP* was highly likely to be the causal gene by colocalisation[22]. At the *CLU* locus, both *PTK2B* and *CLU* were likely causal[22], but differential splicing of *CLU* correlated with risk of AD[24]. The top variant at the *SORL1* locus was within an intron of *SORL1*[22], but rare protein-coding variants in

SORL1 were likely causal for some early-onset AD patients through haploinsufficiency or deleterious effects on protein function[30–32].

For these selected Alzheimer's risk genes, we more carefully examined their expression patterns in larval zebrafish. From the scRNA-seq dataset[26], most of these genes were broadly expressed in the 5-dpf larva in different neuronal populations and other cell types (Fig. 1–supplement 1 and 2). *apoeb* was highly expressed specifically in epidermis progenitors, Müller glia in the retina, and microglia (Fig. 1c), as observed previously[33–36]. Across clusters, the highest expression of *clu* was in radial glia (Fig. 1–supplement 2c, cluster 30). To confirm and extend these observations, we used in situ hybridization chain reaction (HCR) to label mRNA in 6-dpf larvae. As we observed in the scRNA-seq data, most genes tested (*appa*, *appb*, *psen1*, *psen2*, *apoea*, *cd2ap*, *sorl1*) were broadly expressed throughout the 6-dpf brain (Fig. 1d and Fig. 1–supplement 3 and 4). *apoeb* expression was restricted to cells in the forebrain and optic tectum (Fig. 1d and Fig. 1–supplement 4b). Based on the scRNA-seq dataset (Fig. 1c) and literature[33,37], these cells are likely *ccl34b.1*$^{+}$ amoeboid microglia derived from primitive myeloid precursors from the rostral blood island. Additionally, *apoeb* was detected in cells bordering the hindbrain ventricle, which are likely radial glia/astrocytes[38,39]. Contrary to the widespread expression found in the scRNA-seq dataset, *clu* expression was largely restricted to the diencephalic and myelencephalic choroid plexuses (Fig. 1d and Fig. 1–supplement 4d), confirming a previous report[40].

In summary, around 75% of Alzheimer's risk genes had at least one clear orthologue in zebrafish and most of these were expressed in the brain of 5–6-dpf zebrafish larvae, suggesting they play a role in early brain development or function.

Fig. 1: Most Alzheimer's risk genes are found in zebrafish and expressed early in development.

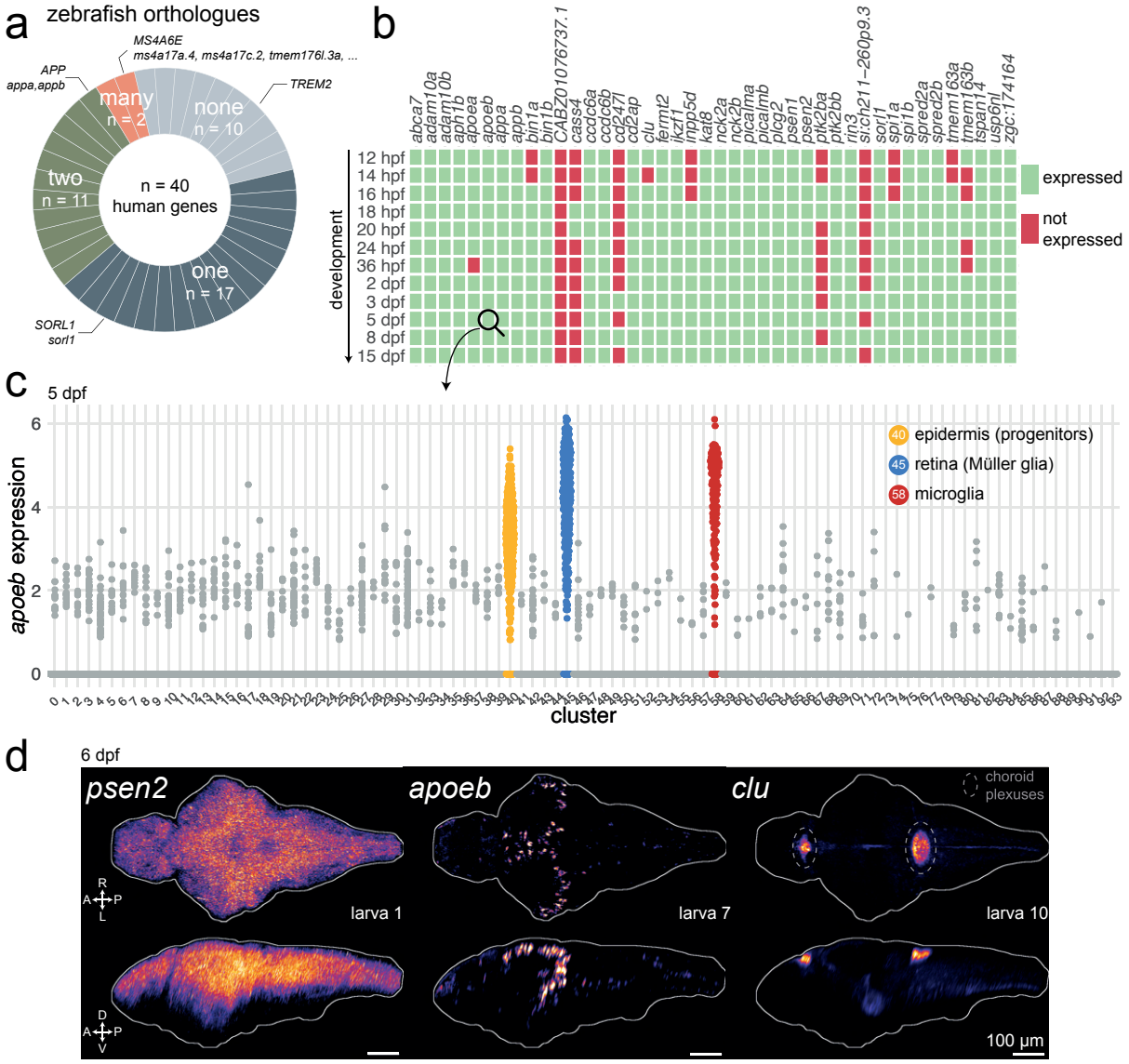

a, Of 40 Alzheimer's risk genes, 17 had one orthologue in zebrafish; 11 had two orthologues; 2 had more than two orthologues; and 10 did not have any annotated orthologue. More details about orthologues of Alzheimer's risk genes are provided in Supplementary file 1 (source: Ensembl).
b, Expression of Alzheimer's risk genes during early development in zebrafish. Genes were marked as "expressed" (green) if at least three cells had detectable transcripts in the single-cell RNA-seq dataset from Raj et al., 2020. *CABZ01076737.1vv* is the orthologue of *TSPOAP1*; *cd247l* is the orthologue of *FCER1G*; *si:ch211-260p9.3* is an orthologue of *PLCG2*; *zgc:174164* is an orthologue of *ADAM10*. Other genes have the same name as their human orthologue. The orthologues of *MS4A6E* were not included. hpf, hours post-fertilisation; dpf, days post-fertilisation.
c, Expression of *apoeb* in cells of the nervous system at 5 dpf. Each dot represents one cell. Cells are grouped by cluster identity, which are provided in Supplementary file 1. Single-cell RNA-seq data and clustering from Raj et al., 2020.
d, *In situ* hybridization chain reactions labelling *psen2*, *apoeb*, or *clu* mRNA in the brains of 6-dpf larvae. The images are maximum Z-projections of dorsal (top) and sagittal (bottom) views of three larvae. A, anterior; P, posterior; R, rightwards; L, leftwards; D, dorsal; V, ventral. Larva # labels individual animals across this figure and Fig. 1–supplement 3 and 4. See also Fig. 1–supplemental videos 1–9.

Fig. 1–suppl. 1: Expression of zebrafish orthologues of early-onset Alzheimer's risk genes from single-cell RNA-seq data.

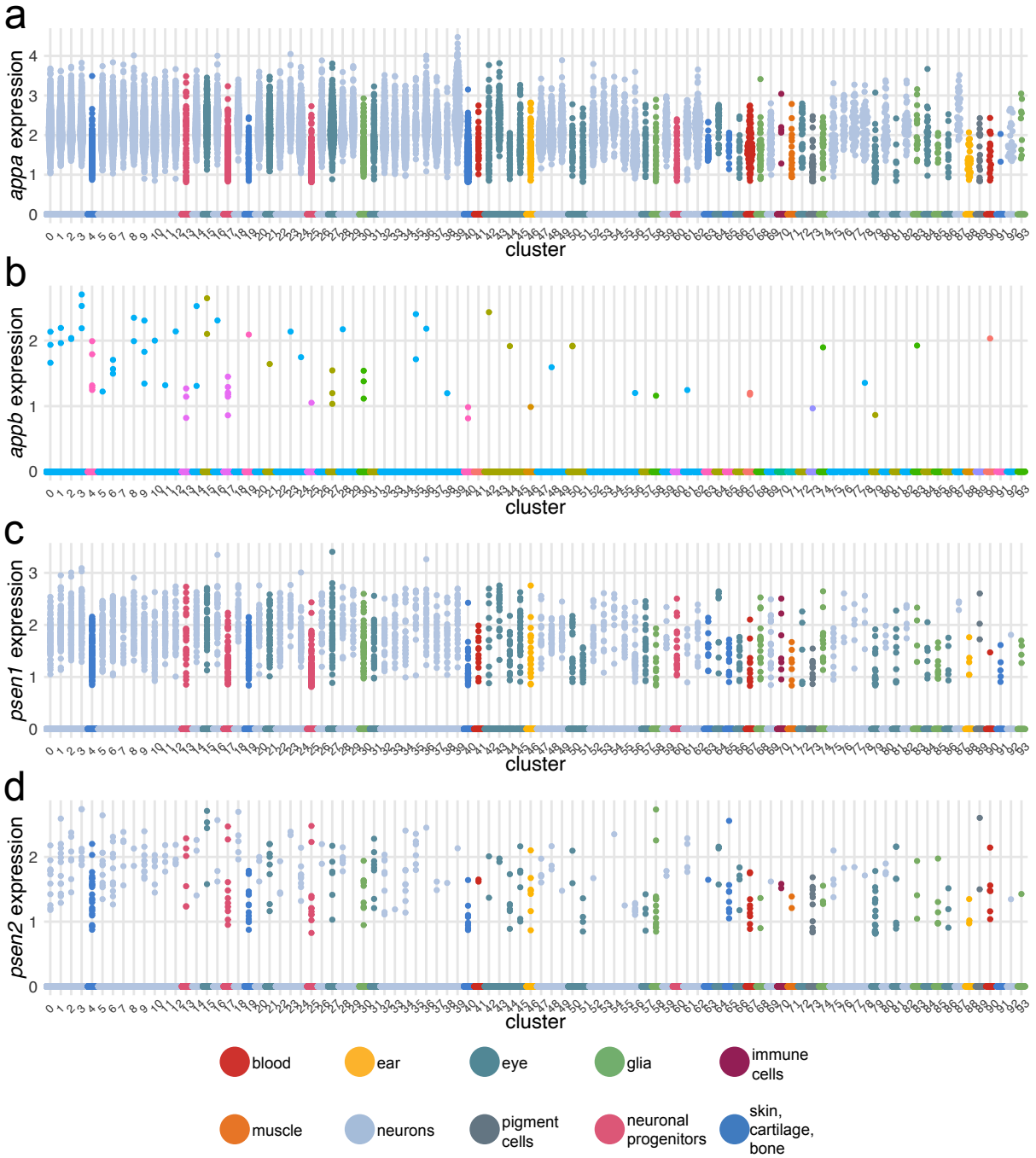

Expression of *appa* (**a**); *appb* (**b**); *psen1* (**c**); *psen2* (**d**) in brain cells of the larval zebrafish at 5 dpf. Each dot represents one cell. Cells are grouped by clusters, which are coloured by broad categories. Cluster identities are provided in Supplementary file 1. Single-cell RNA-seq data and clustering from Raj et al., 2020.

Fig. 1–suppl. 2: Expression of zebrafish orthologues of four late-onset Alzheimer's risk genes from single-cell RNA-seq data.

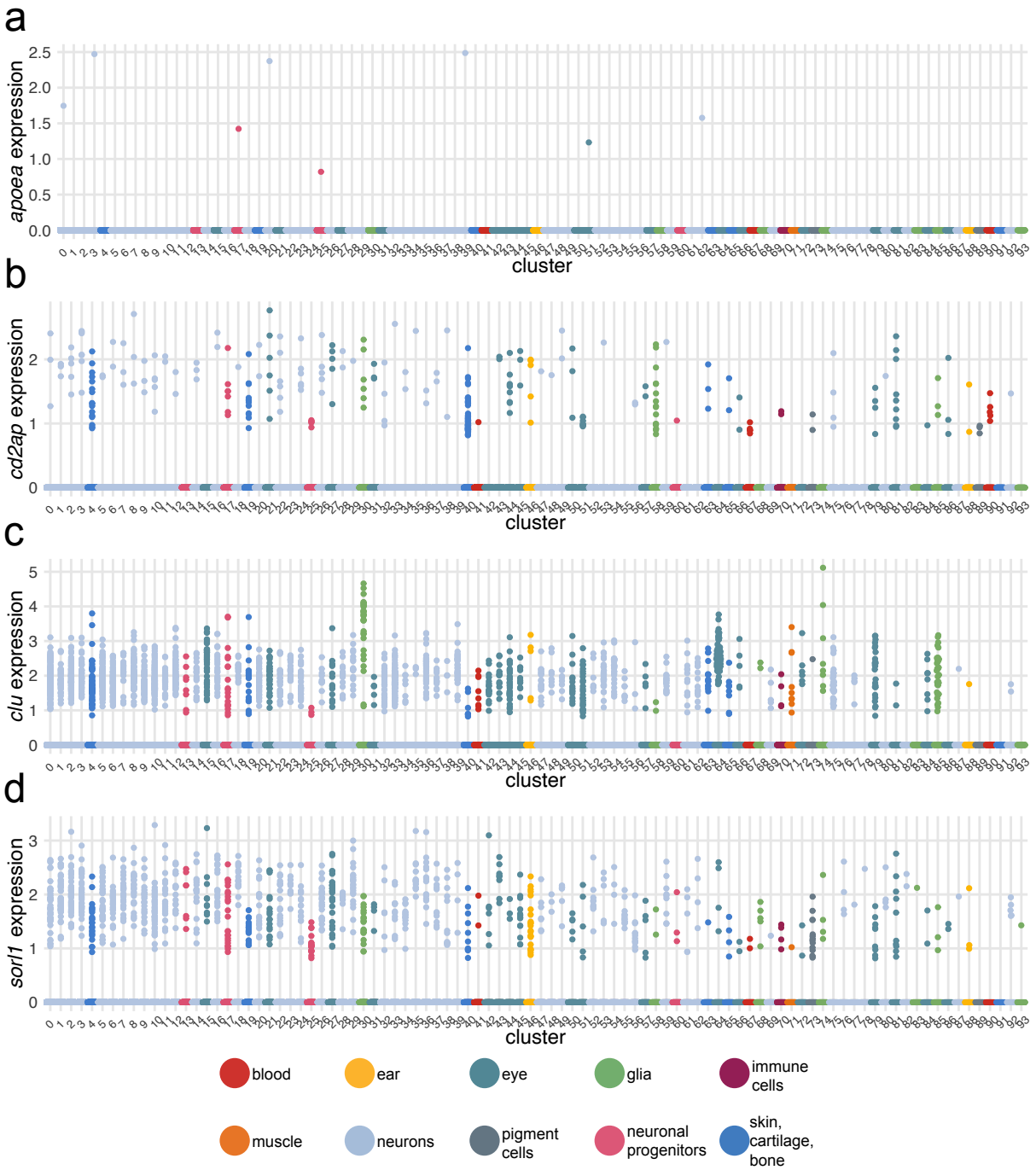

Expression of *apoea* (**a**); *cd2ap* (**b**); *clu* (**c**); *sorl1* (**d**) in brain cells of the larval zebrafish at 5 dpf. Each dot represents one cell. Cells are grouped by clusters, which are coloured by broad categories. Cluster identities are provided in Supplementary file 1. Single-cell RNA-seq data and clustering from Raj et al., 2020.

Fig. 1–suppl. 3: Expression of zebrafish orthologues of early-onset Alzheimer's risk genes in the zebrafish brain.

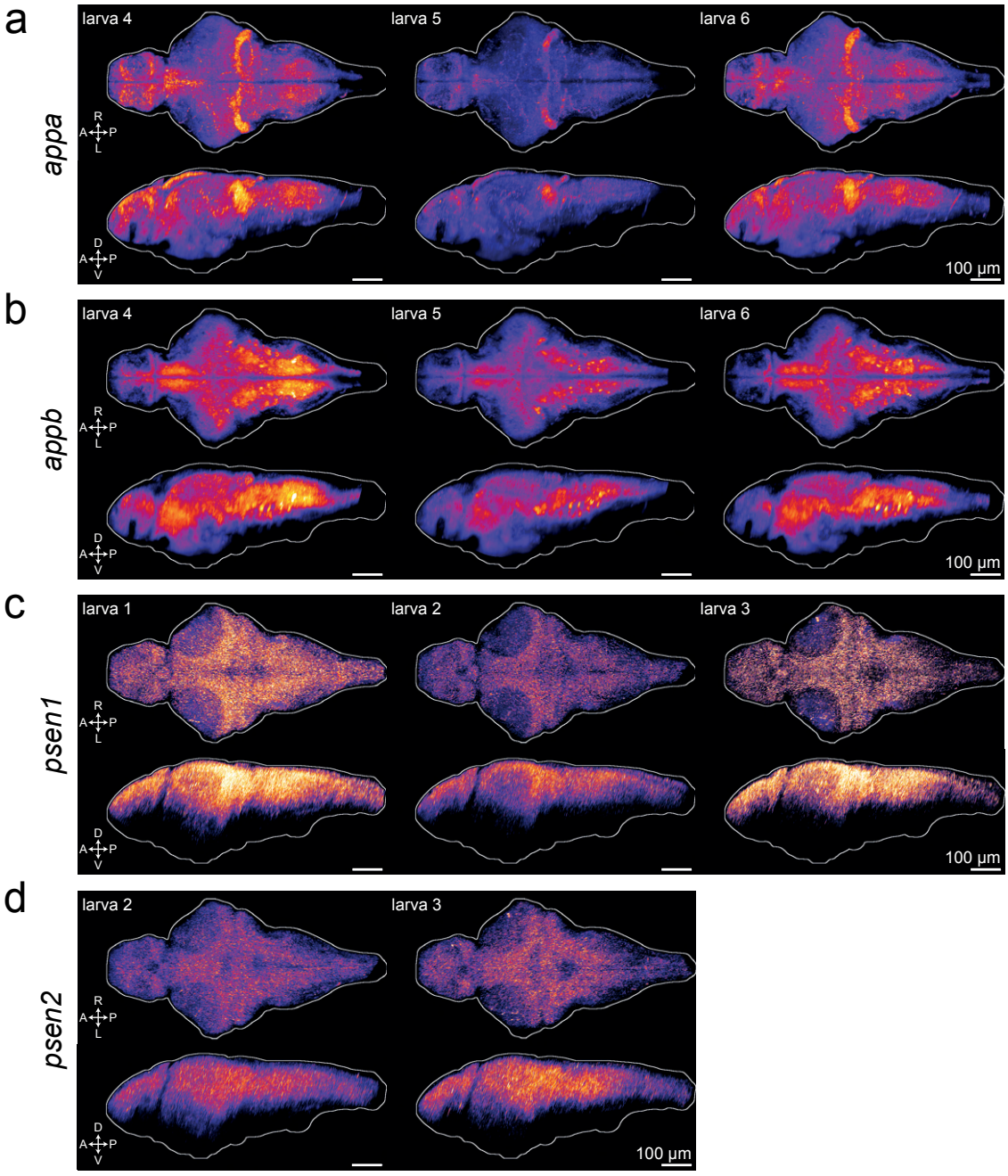

In situ hybridization chain reaction labelling *appa* (**a**); *appb* (**b**); *psen1* (**c**); *psen2* (**d**) mRNA in the brains of 6-dpf larvae. Maximum Z-projections of dorsal (top) and sagittal (bottom) views. A, anterior; P, posterior; R, rightwards; L, leftwards; D, dorsal; V, ventral. Larva # labels individual animals across this figure, Fig. 1d, and Fig. 1–supplement 4. See also Fig. 1–supplemental videos 1–9.

Fig. 1–suppl. 4: Expression of zebrafish orthologues of four late-onset Alzheimer's risk genes in the zebrafish brain.

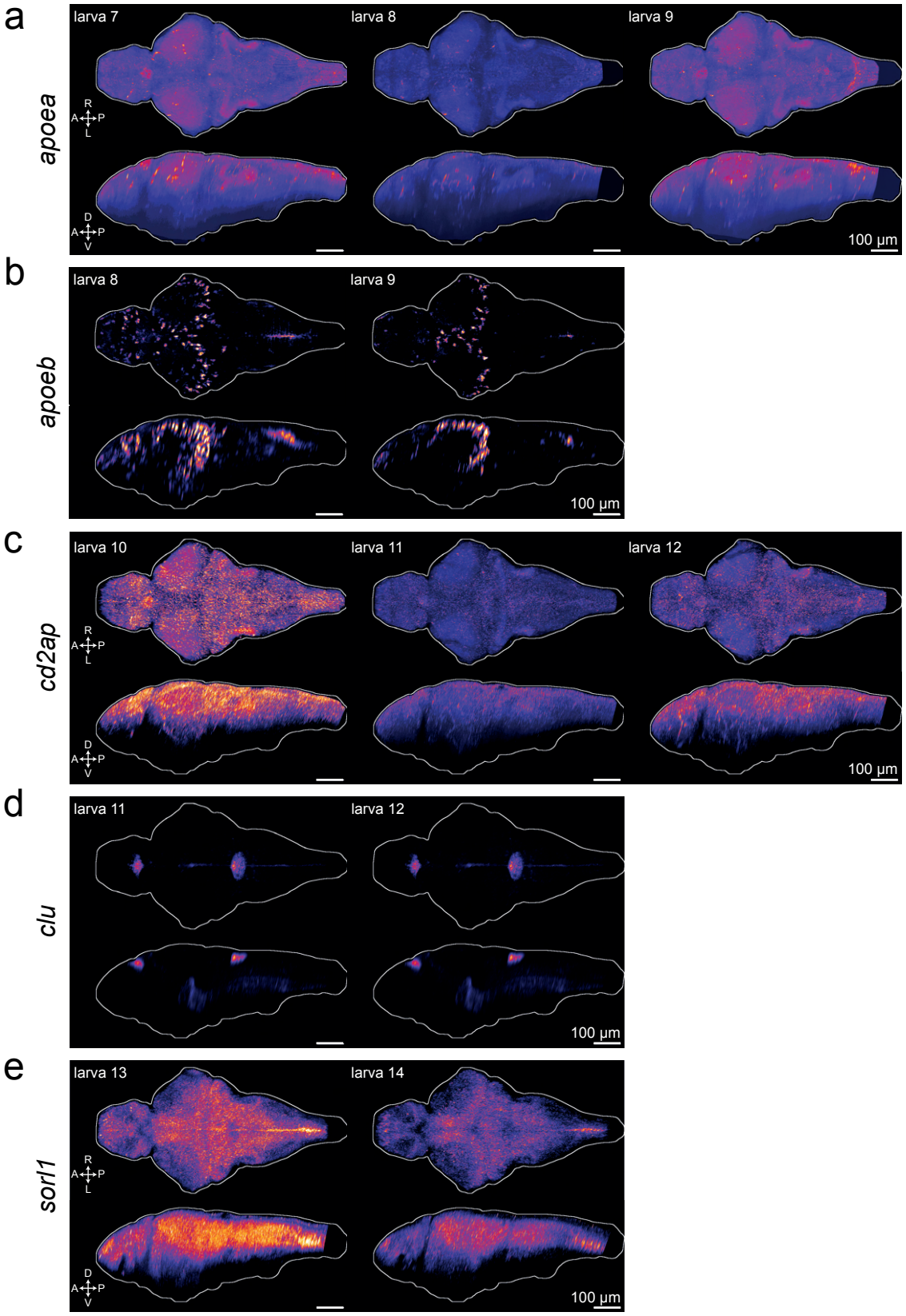

In situ hybridization chain reaction labelling *apoea* (**a**); *apoeb* (**b**); *cd2ap* (**c**); *clu* (**d**); *sorl1* (**e**) mRNA in the brains of 6-dpf larvae. Maximum Z-projections of dorsal (top) and sagittal (bottom) views. A, anterior; P, posterior; R, rightwards; L, leftwards; D, dorsal; V, ventral. Larva # labels individual animals across this figure, Fig. 1d, and Fig. 1–supplement 3. See also Fig. 1–supplemental videos 1–9.

Fig. 1–suppl. video 1: Expression of appa in the larval zebrafish brain.

Average stack (n = 3 larvae), from dorsal to ventral, of the brain of 6-dpf wild-type larvae stained for *appa* mRNA by *in situ* hybridization chain reaction. *gad1db* mRNA was also stained as background channel (grey scale).

Fig. 1–suppl. video 2: Expression of appb in the larval zebrafish brain.

Average stack (n = 3 larvae), from dorsal to ventral, of the brain of 6-dpf wild-type larvae stained for *appb* mRNA by *in situ* hybridization chain reaction. *gad1db* mRNA was also stained as background channel (grey scale).

Fig. 1–suppl. video 3: Expression of psen1 in the larval zebrafish brain.

Average stack (n = 3 larvae), from dorsal to ventral, of the brain of 6-dpf *elavl3:H2b-GCaMP6s* larvae stained for *psen1* mRNA by *in situ* hybridization chain reaction.

Fig. 1–suppl. video 4: Expression of psen2 in the larval zebrafish brain.

Average stack (n = 3 larvae), from dorsal to ventral, of the brain of 6-dpf *elavl3:H2b-GCaMP6s* larvae stained for *psen2* mRNA by *in situ* hybridization chain reaction.

Fig. 1–suppl. video 5: Expression of apoea in the larval zebrafish brain.

Average stack (n = 3 larvae), from dorsal to ventral, of the brain of 6-dpf *elavl3:H2b-GCaMP6s* larvae stained for *apoea* mRNA by *in situ* hybridization chain reaction.

Fig. 1–suppl. video 6: Expression of apoeb in the larval zebrafish brain.

Average stack (n = 3 larvae), from dorsal to ventral, of the brain of 6-dpf *elavl3:H2b-GCaMP6s* larvae stained for *apoeb* mRNA by *in situ* hybridization chain reaction.

Fig. 1–suppl. video 7: Expression of cd2ap in the larval zebrafish brain.

Average stack (n = 3 larvae), from dorsal to ventral, of the brain of 6-dpf *elavl3:H2b-GCaMP6s* larvae stained for *cd2ap* mRNA by *in situ* hybridization chain reaction.

Fig. 1–suppl. video 8: Expression of clu in the larval zebrafish brain.

Average stack (n = 3 larvae), from dorsal to ventral, of the brain of 6-dpf *elavl3:H2b-GCaMP6s* larvae stained for *clu* mRNA by *in situ* hybridization chain reaction.

Fig. 1–suppl. video 9: Expression of sorl1 in the larval zebrafish brain.

Average stack (n = 2 larvae), from dorsal to ventral, of the brain of 6-dpf *elavl3:H2b-GCaMP6s* larvae stained for *sorl1* mRNA by *in situ* hybridization chain reaction.

The FramebyFrame R package for analysis of sleep/wake behaviour from high-throughput video-tracking data

The next stage in our behavioural pharmacology strategy is to measure sleep/wake behaviour of F0 knockout larvae for the genes under study. To uncover even subtle behavioural phenotypes caused by the loss of Alzheimer's risk genes, we developed a high-throughput sleep/wake tracking assay for zebrafish larvae capable of analysing behaviour at the sub-second resolution over multiple days and nights. To achieve this, we combined previous sleep/wake analysis methods[41–43] with some aspects of the frame-by-frame analysis developed by Ghosh and Rihel (2020)[44] into a single software tool, the FramebyFrame R package (github.com/francoiskroll/FramebyFrame). We also designed a 3D-printed mesh-bottom plate that supports long-term (up to 8.5 days tested) tracking of larvae with minimal intervention by regulating the water level with a small pump and delivering paramecia for feeding through the mesh from the water bath below (Fig. 2a,b).

The FramebyFrame package extracts and analyses 17 behavioural parameters from frame-by-frame Δ pixel data, which represent the number of pixels that changed intensity at each frame-to-frame transition. These parameters capture both behaviours that unfold over multiple minutes or hours, such as sleep (Fig. 2c), and actions at smaller time scales (< 1 sec), such as individual swimming bouts (Fig. 2d). The parameters are grouped into three categories: activity parameters (Fig. 2–supplement 1a), which describe the overall activity of each larva during a complete day or night; active bout parameters (Fig. 2–supplement 1b), which describe the structure of individual swimming bouts; and sleep parameters (Fig. 2c) such as sleep latency (Fig. 2–supplement 2d). In zebrafish larvae, sleep is defined as any period of inactivity (Δ pixel = 0) lasting longer than one minute, a definition based on increases in arousal threshold and homeostatic rebound following deprivation[43,45]. This frame-by-frame analysis has several advantages over previous methods that analysed activity data at the one-minute resolution. First, individual swimming bouts could not be resolved by these methods as single bouts last ~0.2 sec on average. Second, the one-minute methods missed around one third of all sleep bouts because of how the Δ pixel data is binned in one-minute epochs (Fig. 2–supplement 2a). At the frame-by-frame resolution, the start and end frame of each sleep bout can be precisely determined, which also improves the measurement accuracy of sleep bout duration and sleep latency, the delay from lights-off to first sleep bout. For example, during a sample 10-hr night (Fig. 2–supplement 2b), the frame-by-frame analysis detected 35 ± 14 more sleep bouts, longer average sleep bout lengths (+0.2 ± 0.2 min), and shorter sleep latencies (1.6 ± 2.3 min earlier), resulting in a 42% increase in total sleep time (+2.3 ± 0.4 hr). During the day, the FramebyFrame analysis also detected more sleep and more sleep bouts (Fig. 2–supplement 2c). Most behaviour plots

included in this study were created using the FramebyFrame package in just a few commands from the raw frame-by-frame data.

Fig. 2: Analysis of zebrafish sleep/wake behaviour at the frame-by-frame resolution with the FramebyFrame R package.

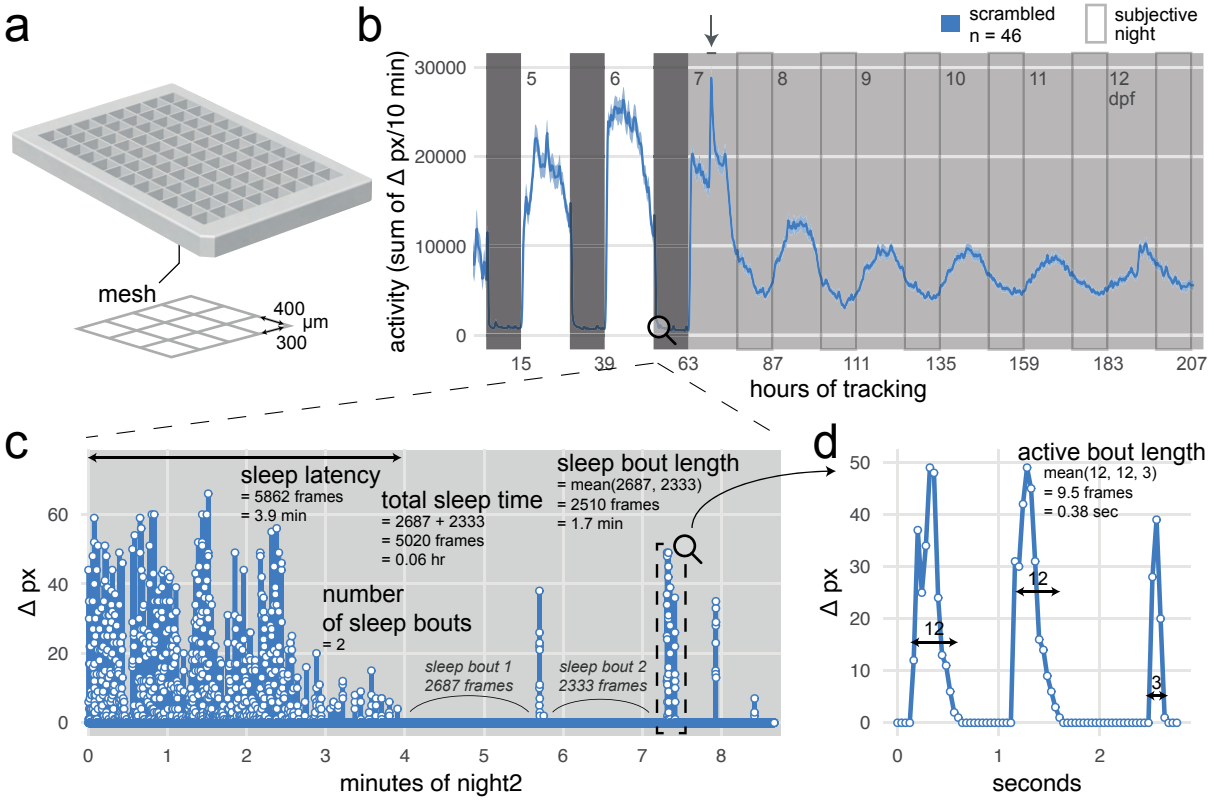

a, 3D model of the 96-square well mesh-bottom plate. Available at github.com/francoiskroll/FramebyFrame.
b, Example of an 8-day (208 hr total) video tracking experiment. scrambled-injected control larvae were in a mesh-bottom plate placed in a water bath containing paramecia. Larvae were tracked for 63 hr on a 14 hr:10 hr light:dark cycle (white and dark grey backgrounds, respectively), then switched to constant dim light (30 lux) for 145 hr (subjective nights are framed). The larvae were tracked from 4 to 13 dpf and all appeared healthy at the end of the experiment. The trace is the mean ± SEM across larvae of the activity (sum of Δ pixels/10 minutes). The arrow indicates when the water in the bath was replaced and fresh paramecia were supplemented, causing a spike in activity.
c, The FramebyFrame R package calculates 17 parameters from the Δ pixel timeseries of each larva. The parameters are grouped in three categories: activity parameters, active bout parameters, and sleep parameters. Here, sleep parameters calculated by the FramebyFrame R package are annotated on the first ~9 min of the Δ pixel timeseries for one wild-type larva starting at lights off. These parameters describe the sleep behaviour of each larva during each day or night. Sleep parameters are also calculated for days, except for sleep latency. This plot is connected to b) for illustrative purposes only; the data was not from the same experiment.
d, Example of an active bout parameter—active bout length—annotated on the sample data from c). For all the activity and active bout parameters calculated by the FramebyFrame R package, see Fig. 2–supplement 1.

Fig. 2–suppl. 1: Behavioural parameters calculated by the FramebyFrame R package on the Δ pixel timeseries.

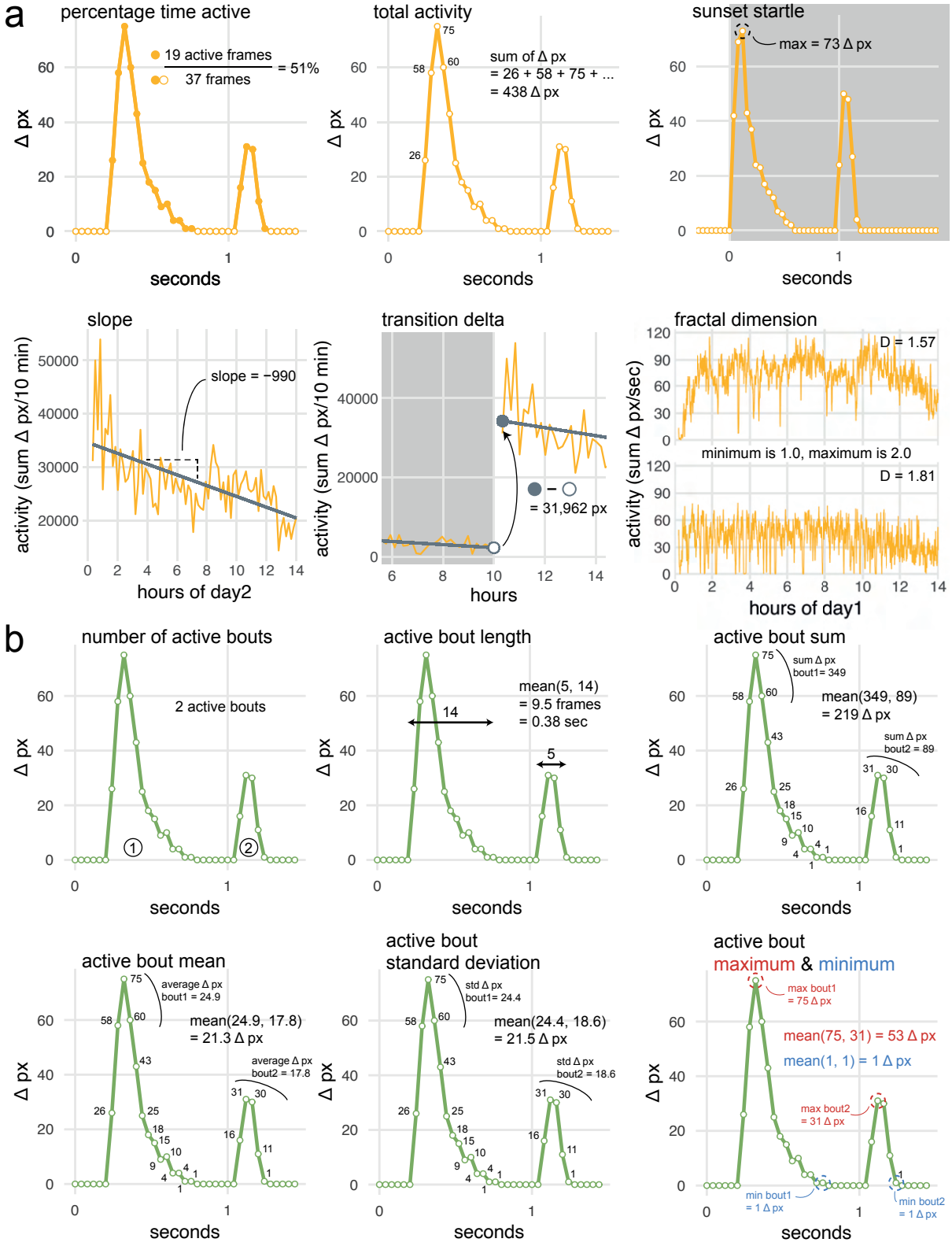

a, Activity parameters calculated by the FramebyFrame R package annotated on sample data from a single larva. These parameters describe the overall activity of each larva during each day or night and are calculated directly on the Δ pixel timeseries. Sunset startle describes the larva's startle response when lights abruptly switch off at the day-to-night transition, and therefore is only defined for nights.

b, Active bout parameters calculated by the FramebyFrame R package annotated on sample data from a single larva. These parameters describe the average swimming bout of each larva during each day or night.

Fig. 2–suppl. 2: Sleep detection by the FramebyFrame R package.

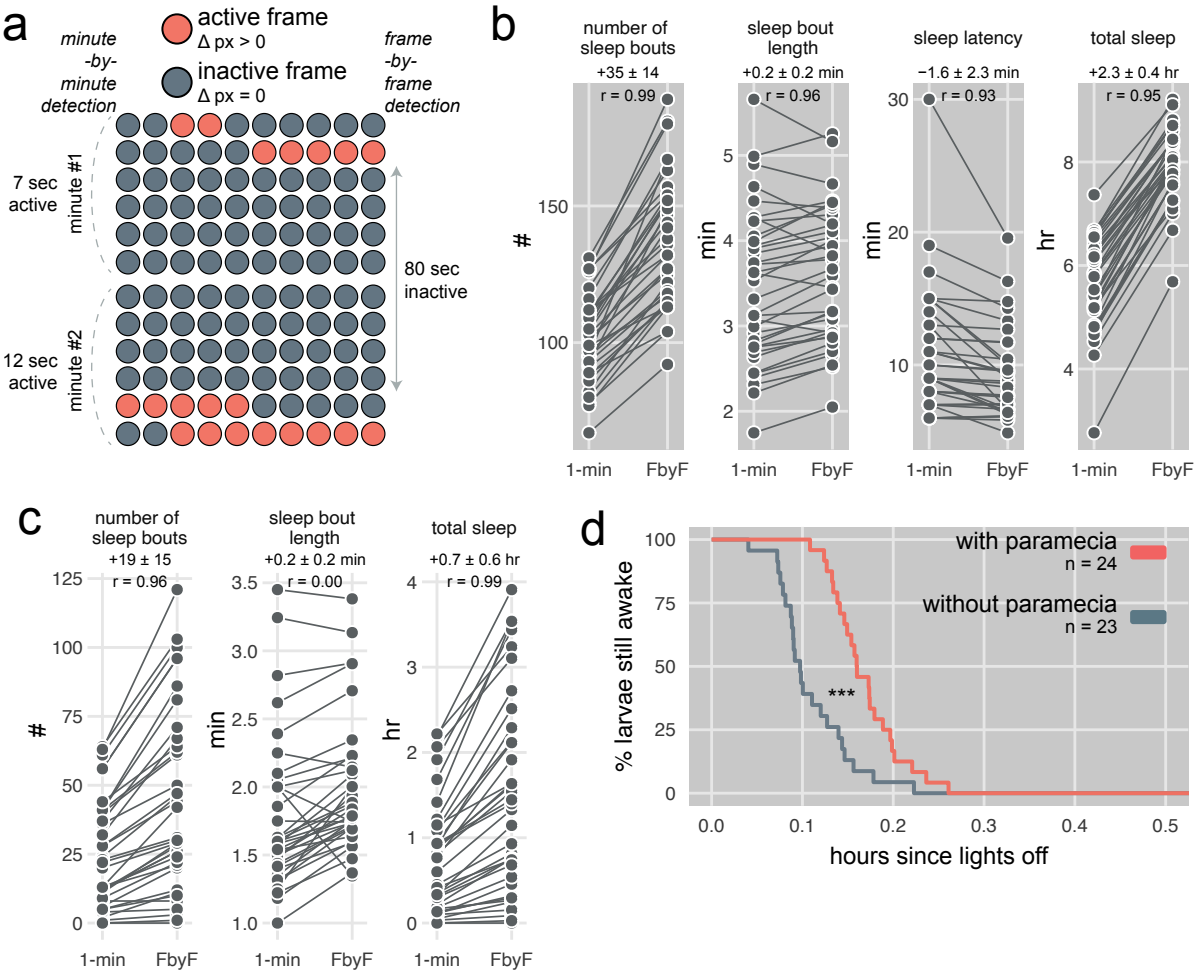

a, Example of a sleep bout detected by the FramebyFrame R package that is missed by analysis done on one-minute epochs. In this example, the larva was inactive for 80 consecutive seconds, which represents a sleep bout as per the one-minute inactivity criterion for sleep (Rihel, Prober, and Schier 2010). Binning in one-minute epochs misses the sleep bout as it returns two active minutes with 7 and 12 sec of activity per minute, while the FramebyFrame package detects the 80-sec sleep bout.
b, Difference in sleep parameters measurements between the one-minute analysis and the frame-by-frame analysis performed on the same dataset. One line represents one wild-type larva during one night. *1-min*, results obtained with the minute-by-minute detection; *FbyF*, results obtained with the FramebyFrame R package; *r*, Pearson correlation.
c, Difference in sleep parameters measurements between the one-minute analysis and the frame-by-frame analysis, as in b). One line represents one wild-type larva during one day.
d, Example of a sleep latency survival plot generated with the FramebyFrame R package. Starting at lights-off, larvae that experienced their first sleep bout were gradually removed from the survival curve. At any timepoint, the larvae with paramecia in the well were 68 ± 31% less likely to fall asleep for the first time than larvae housed without paramecia: hazard ratio for larvae with paramecia = 0.32 ± 0.31, *** $p < 0.001$ by likelihood-ratio test.

psen2 knockouts sleep more during the day

Next, we used CRISPR-Cas9 to generate F0 knockouts for the zebrafish orthologues of the three genes that can cause early-onset AD when mutated in humans—*psen1*, *psen2*, *appa*/*appb*—and tested these mutants for behavioural and other phenotypes. We focused first on *psen1* and *psen2*.

Zebrafish Psen1 and Psen2 are highly similar to their human counterparts (~70% identical amino acid sequence, Fig. 3a,b), with the same critical amino acid at the four annotated active sites (two per presenilin). Mismatches between the human and zebrafish proteins were largely clustered into disordered domains, suggesting that the zebrafish presenilins have the same catalytic activity as in humans. The Cas9/guide RNA ribonucleoproteins (RNPs) used to generate F0 knockouts mutated virtually every copy of the genome at each of the three targeted sites. At each targeted locus of *psen1*, 99.0 ± 2.7% of reads were mutated and 78.6 ± 29.7% of all reads had a frameshift mutation (Fig. 3c). At each targeted locus of *psen2*, 99.9 ± 0.1% reads were mutated and 82.0 ± 33.6% of all reads had a frameshift mutation (Fig. 3d). As each gene is mutated at three loci, the biallelic knockout probability, that is, the probability of having at least one frameshift mutation on both alleles, cumulatively reached > 98% (francoiskroll.shinyapps.io/frameshiftmodel/), indicating that most *psen1* and *psen2* F0 knockout larvae were complete loss-of-function mutants.

In humans, PSEN1 or PSEN2 acts as the catalytic subunit of the γ-secretase protein complex, which is responsible for the cleavage of more than 90 substrates, such as Notch. It also performs the last cleavage of APP to release Aβ, which aggregates in the brains of patients with AD[7,9,46,47]. Do presenilins also cleave zebrafish Appa/Appb into Aβ? Using a sensitive ELISA-based assay, Aβ40 and Aβ42 were detectable in control (uninjected and scrambled-injected) larvae but not in two clutches of *psen1* F0 knockouts (Fig. 3e), confirming that zebrafish Psen1 is required for the cleavage of Appa/Appb into Aβ. In contrast, Aβ40 and Aβ42 were detectable in *psen2* F0 knockouts, suggesting that most Aβ is generated by Psen1 in zebrafish and that Psen2 alone cannot compensate. This result extends previous findings that Aβ production in zebrafish is blocked by the γ-secretase inhibitor DAPT[48] and matches closely observations in mice, in which loss of PSEN2 had no measurable effect on Aβ40/42 production[49].

In mice, knockout of *Psen1*, but not of *Psen2*, causes severe skeletal malformations and brain haemorrhages, likely because of impaired Notch signalling[50]. Homozygous animals die within minutes after birth[51]. Morphologically, our *psen1* F0 knockout larvae developed normally (tested up to 16 dpf) and were indistinguishable from their wild-type siblings, as

observed in a *psen1* stable knockout line[52]. *psen2* F0 knockout larvae had a mild pigmentation defect (Fig. 3f and Fig. 3–supplement 2a), which has been previously reported in a *psen2* stable knockout line[53]. This difference suggests a specific function of Psen2 in melanophores which cannot be fulfilled by Psen1. We also generated *psen1*/*psen2* double F0 knockouts but most were lethal early in development (~5 dpf) with severe defects in eye development (Fig. 3–supplement 1a), in which the retinal pigment epithelium appeared patchy and some larvae developed oedema around the eye. The tail was severely curved outwards, in exactly the same way as larvae treated with a high dose of the γ-secretase inhibitor DAPT[54]. Incidentally, *Psen1* knockout mice also display defects in the axial skeleton[51]. Overall, these results suggest that zebrafish presenilins are more readily capable of compensating each other during development than in mice, as only double *psen1*/*psen2* knockout larvae showed a severe morphological phenotype.

We next video-tracked two clutches of *psen1* and *psen2* F0 knockout larvae over multiple day-night cycles and applied our frame-by-frame analysis to detect behavioural phenotypes over long and short time scales. The loss of *psen1* only had mild effects on behaviour. At night, *psen1* F0 knockout larvae slept slightly less (−8% vs. scrambled, Fig. 3–supplement 1b) and instead spent more time active than control injected siblings (+22%), mainly because they performed more swimming bouts (+20%). The *psen1* knockouts also showed a slightly reduced startle response at lights-off (−4%), in line with some data obtained from stable *psen1* knockout larvae[52]. Behaviour during the day was not affected (Fig. 3–supplement 1c). In contrast, *psen2* F0 knockouts of both cutches were substantially less active than controls during the day (total activity: −26% vs. scrambled, Fig. 3g,h and Fig. 3–supplement 1d), performing both fewer (−17%) and more subdued swimming bouts (active bout mean: −12%). *psen2* F0 knockouts also slept more during the day than controls (Fig. 3g,h, Fig. 3–supplement 1d), both spending more time asleep (+178%) and initiating more frequent sleep bouts (+150%). Loss of Psen2 did not strongly affect night-time behaviour. In summary, *psen2* F0 knockout larvae were substantially less active and sleeping more than controls during the day.

Since *psen2* knockout larvae were less pigmented (Fig. 3–supplement 2a), we tested whether the reduction in activity could be an artefact due to fainter detection by the camera. We extracted the maximum Δ pixel value each larva reached during the startle response at lights off (Fig. 3–supplement 2b). These vigorous swimming bouts can displace the whole larva in a tenth of a second, providing a measure of how many dark pixels are detectable for each larva. *psen2* F0 knockout larvae indeed displaced fewer pixels during the startle response than scrambled-injected controls (Fig. 3–supplement 2c, clutch 1: *psen2* knockouts displaced 78 ± 10 pixels vs 82 ± 8 pixels for scrambled-injected controls, clutch

2: 71 ± 8 pixels vs 80 ± 8 pixels). We then downscaled the Δ pixel values of the scrambled-injected larvae proportionally to the ratio of the startle response means (Fig. 3–supplement 2c,d), akin to artificially making the scrambled-injected larvae appear less dark. Even after this adjustment, *psen2* F0 knockouts were measurably less active and sleeping more during the day, although the parameter effect sizes were somewhat reduced (Fig. 3–supplement 2e). In summary, the *psen2* behavioural phenotype reflects a genuine difference in behaviour.

Finally, we examined the impact of loss of both Appa and Appb. As described previously[48,55], zebrafish Appa and Appb are highly similar to human APP (64–68% identical amino acid sequence, Fig. 3–supplement 3a,b). We generated *appa*/*appb* double F0 knockout larvae by mutating each gene at two loci, rather than three, to limit unviability[19]. The CRISPR-Cas9 RNPs were highly mutagenic (across all four loci: 95.8 ± 7.0% mutated reads, 76.5 ± 21.7 of all reads had a frameshift mutation, Fig. 3–supplement 3c,d). The *appa*/*appb* double F0 knockout larvae looked morphologically normal. Behaviourally, *appa*/*appb* double knockouts were less active during the day than control siblings (–14% vs. scrambled, Fig. 3–supplement 3e) and showed shorter swimming bouts across the day/night cycle (active bout duration during the day: –4%; at night: –3%). Sleep was not consistently affected by the loss of *appa*/*appb* (Fig. 3–supplement 3f).

In summary, knockout larvae for the three genes associated with early-onset AD had distinct morphological and behavioural phenotypes, with the strongest behavioural changes observed for *psen2* knockouts. Since both presenilins are broadly expressed in the larval brain (Fig. 1d and Fig. 1–supplement 3c,d), these results indicate that zebrafish Psen1- and Psen2-γ-secretases likely cleave different substrates, such as Appa/Appb which is primarily cleaved into Aβ by Psen1-γ-secretase. Moreover, the behavioural phenotypes of *appa*/*appb* and *psen1* knockout larvae had little overlap while they presumably both resulted in the loss of Aβ. The *appa*/*appb* day phenotype could be primarily caused by loss of some Appa/Appb cleavage product not relying on γ-secretase. Alternatively, the net effect of loss of all other Psen1-γ-secretase products could have masked the effect of loss of Aβ.

Fig. 3: *psen2* F0 knockouts initiate more sleep bouts during the day

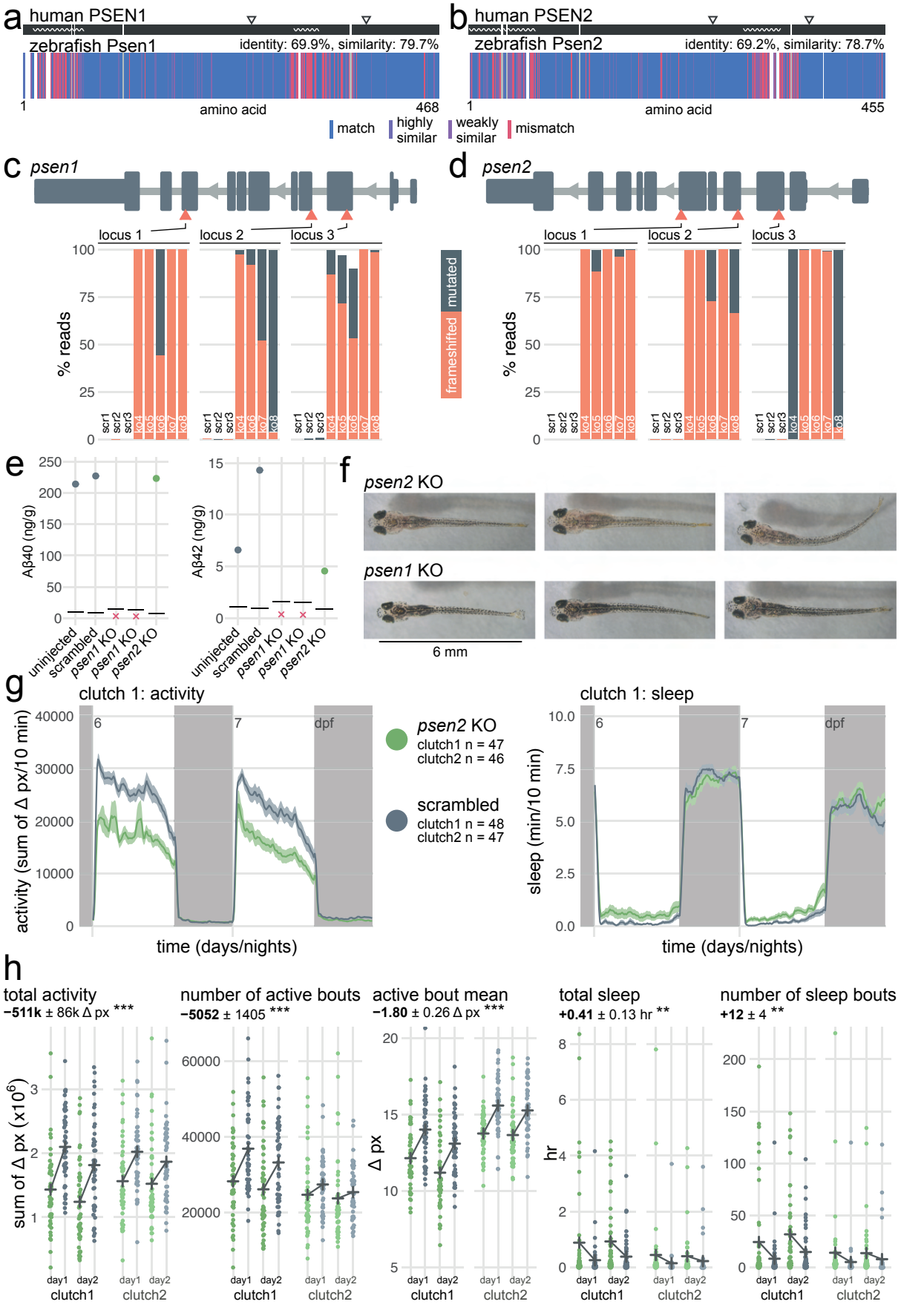

Legend on next page.

a, Human PSEN1 amino acid sequence (top) aligned to zebrafish Psen1 amino acid sequence (bottom). In the zebrafish protein, each amino acid (vertical bar) is coloured based on its similarity with the human protein. In the human protein, wavy lines represent disordered domains and arrowheads point to the two active sites at residues 257 and 385 (source: UniProt). White gaps are added when additional residues are present in the other sequence.
b, Human PSEN2 amino acid sequence (top) aligned to zebrafish Psen2 amino acid sequence (bottom), as in a). Active sites are at residues 263 and 366 (source: UniProt and AlphaFold).
c, (above) Schematic of *psen1* in the 5'–3' genome direction. Exons are in dark grey; tall exons are protein-coding, small are 5'- or 3'-UTR. Light grey lines are introns, and grey arrows represent the direction of transcription. Orange arrowheads mark the target loci. Exons and introns are on different scales. (below) Percentage of reads mutated (height of each bar, with orange representing percentage with a frameshift mutation) at each targeted locus of *psen1*. *scr*, scrambled-injected control larva; *ko*, *psen1* F0 knockout larva. The numbers refer to individual animals. For example, ko4 refers to an individual *psen1* F0 knockout larva for which mutations at each targeted locus are plotted. Across F0 knockout samples: 99.0 ± 2.7% mutated reads, 78.6 ± 29.7% of all reads had a frameshift mutation. One locus-2 sample was excluded because of low sequencing coverage.
d, (above) Schematic of *psen2* in the 5'–3' genome direction, as in c). (below) Percentage of reads mutated (height of each bar, with orange representing percentage with a frameshift mutation) at each targeted locus of *psen2*, as in c). Across F0 knockout samples: 99.9 ± 0.1% mutated reads, 82.0 ± 33.6% of all reads had a frameshift mutation.
e, Concentration of Aβ40 and Aβ42 in pools of n = 16–22 uninjected, scrambled-injected, *psen1* F0 knockout, and *psen2* F0 knockout 16-dpf larvae. Each datapoint is the mean of four technical replicates. Concentration unit is ng of Aβ40/42 per g of total protein extracted. Horizontal black line represents the limit of detection. Red crosses indicate samples for which all technical replicates were below the limit of detection. All Aβ38 measurements were below the limit of detection and are not plotted.
f, Top row: pictures of *psen2* F0 knockout larvae (16 dpf). Bottom row: pictures of *psen1* F0 knockout larvae (16 dpf). Note the fainter pigmentation of *psen2* F0 knockout larvae.
g, (left) Activity (sum of Δ pixels/10 minutes) of *psen2* F0 knockout larvae and scrambled-injected siblings during 48 hr on a 14 hr:10 hr light:dark cycle (white background for days, dark grey background for nights). (right) Sleep (minutes per 10-minute epoch) during the same experiment. Traces are mean ± SEM across larvae. See also Fig. 3–supplement 1d for results from replicate clutch 2.
h, Parameter plots for two clutches of *psen2* F0 knockout larvae and scrambled-injected siblings. Each dot represents one larva during one day. Black crosses mark the group means. Compared to scrambled-injected siblings, *psen2* F0 knockouts displaced fewer pixels (total activity, *** $p < 0.001$) and initiated fewer swimming bouts (number of active bouts, *** $p < 0.001$), each displacing fewer pixels in average (active bout mean, *** $p < 0.001$). They also spent more time asleep (total sleep, ** $p = 0.002$) and initiated more sleep bouts (number of sleep bouts, ** $p = 0.002$) than scrambled-injected siblings. Statistics by likelihood-ratio test on linear mixed effects models.

Fig. 3–suppl. 1: *psen1* F0 knockouts are slightly hyperactive at night

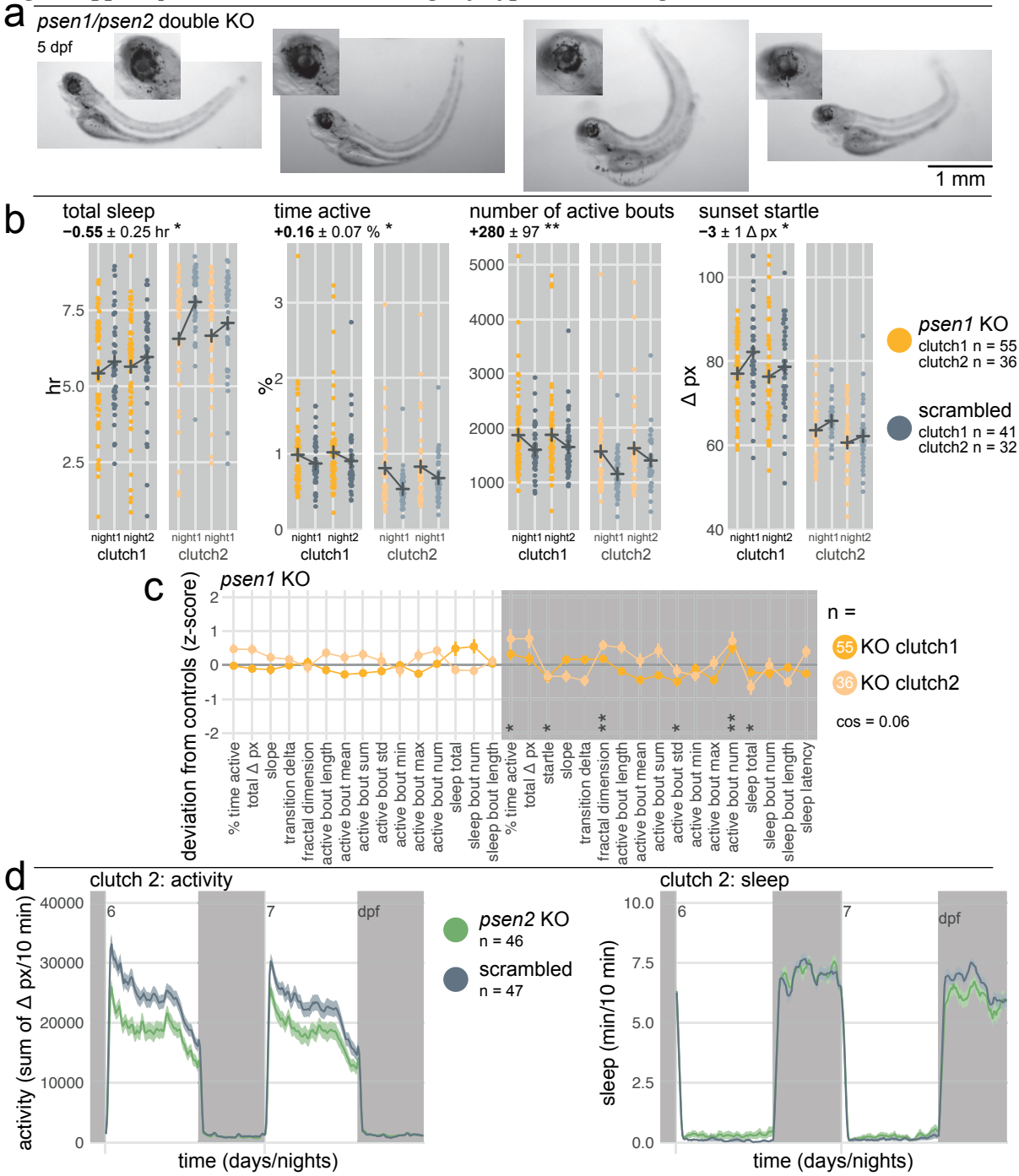

a, Pictures of *psen1/psen2* double F0 knockout larvae (5 dpf). Note patchy retinal pigment epithelium and eye oedema (insets).

b, Parameter plots for two clutches of *psen1* F0 knockout larvae and scrambled-injected siblings. Each dot represents one larva during one night. Black crosses mark the group means. At night, *psen1* F0 knockouts slept less (total sleep, * p = 0.030), spent more time active (time active, * p = 0.018), and initiated more swimming bouts (number of active bouts, ** p = 0.004) than scrambled-injected siblings. The startle response of *psen1* F0 knockouts was also slightly suppressed (sunset startle, * p = 0.015). Statistics by likelihood-ratio test on linear mixed effects models.

c, Behavioural fingerprints of two clutches of *psen1* F0 knockout larvae. Each dot represents the mean deviation from the same-clutch scrambled-injected mean for that parameter (z-score, mean ± SEM). Asterisks represent the p-values by likelihood-ratio test on linear mixed effects models calculated on the raw parameter values. *cos*, cosine similarity between the two clutch fingerprints.

d, (left) Activity (sum of Δ pixels/10 minutes) of *psen2* F0 knockout larvae and scrambled-injected siblings during 48 hr on a 14 hr:10 hr light:dark cycle (white background for days, dark grey background for nights). (right) Sleep (minutes per 10-minute epoch) during the same experiment. Traces are mean ± SEM across larvae. This replicate experiment is called clutch 2 in Fig. 3h.

Fig. 3–suppl. 2: The behavioural phenotype of *psen2* F0 knockouts is not an artefact caused by their fainter pigmentation.

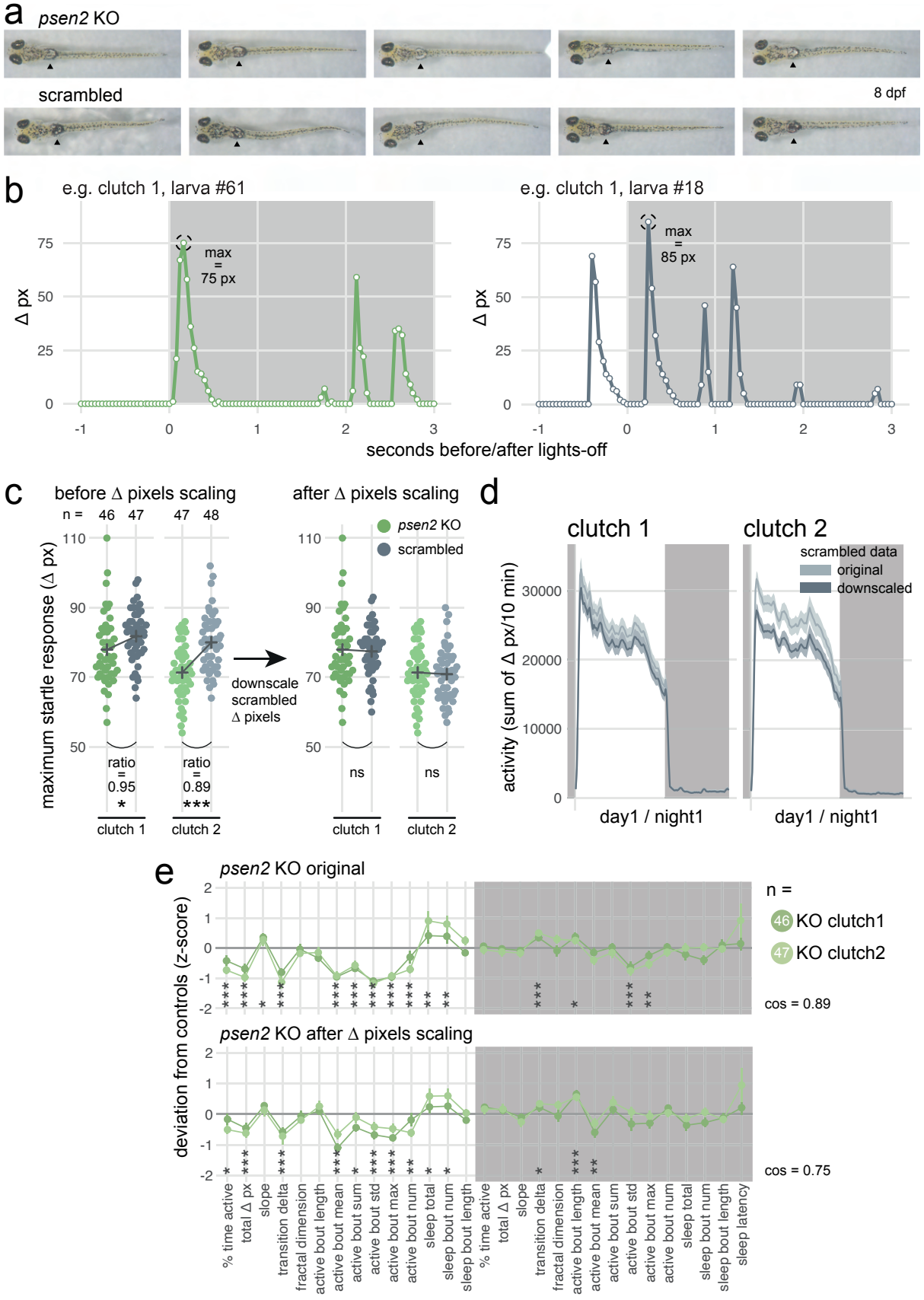

Legend on next page.

a, Pictures of *psen2* F0 knockout larvae (top row) and scrambled-injected control larvae at the end of the behavioural tracking (8 dpf). Note the fainter pigmentation of *psen2* F0 knockout larvae, particularly over the swim bladder (marked by black arrowheads).
b, Frame-by-frame Δ pixel timeseries of two individual larvae showing the startle response shortly after the lights turn off. (left) Startle response of a *psen2* F0 knockout larva. During the 3 seconds after lights-off, the most vigorous bout reached a maximum Δ pixel value of 75 px. (right) Startle response of a scrambled-injected larva. During the 3 seconds after lights-off, the most vigorous bout reached a maximum Δ pixel value of 85 px.
c, Maximum startle responses over the three consecutive lights-off transitions, by clutch (clutch 1 and clutch 2) and group (*psen2* KO or scrambled). Each dot represents one larva. The startle response was defined as the maximum Δ pixel during the 3 seconds directly after lights-off (see b). There were three lights-off transitions during the experiment; plotted for each larva is the largest of the three startle responses (maximum startle response). (left) Unprocessed data. scrambled-injected larvae displaced more pixels during the startle response at lights-off compared to *psen2* F0 knockout larvae, presumably because they appeared darker to the camera (clutch 1: * $p = 0.042$; clutch 2: *** $p < 0.001$, by Welch's t-test). The ratio of the means estimated how much darker *psen2* knockout larvae were compared to scrambled-injected larvae; that is, *psen2* knockout larvae were 0.95 and 0.89× as dark as scrambled-injected larvae. (right) The ratios were then used to downscale the frame-by-frame Δ pixel data of the scrambled-injected larvae, in a sense artificially making them as faint as *psen2* knockout larvae. As intended, the downscaling rendered the differences in startle response non-significant (clutch 1: ns $p = 0.78$; clutch 2: ns $p = 0.77$, by Welch's t-test).
d, The original activity trace (sum Δ pixels/10 minutes, mean ± SEM) of scrambled-injected larvae (lighter grey) compared to the downscaled one (darker grey), during the first day and night as illustration. The data of *psen2* F0 knockouts is not shown as it is not modified during the downscaling.
e, Behavioural fingerprints of two clutches of *psen2* F0 knockout larvae, before and after downscaling the Δ pixel data of the scrambled-injected larvae. Each dot represents the mean deviation from the same-clutch scrambled-injected mean for that parameter (z-score, mean ± SEM). Two parameters were excluded from the fingerprints: sunset startle, as the difference between knockouts and controls was artificially nullified by the pixel scaling procedure; and active bout minimum, because the pixel scaling procedure artefactually raised this parameter for scrambled-injected larvae. Asterisks represent the p-values by likelihood-ratio test on linear mixed effects models calculated on the raw parameter values. *cos*, cosine similarity between the two clutch fingerprints.
The pixel scaling procedure is available as a function (*pixelAdjust(...)*) in the FramebyFrame R package.

Fig. 3–suppl. 3: *appa/appb* F0 knockouts have subdued swimming bouts throughout the day/night cycle.

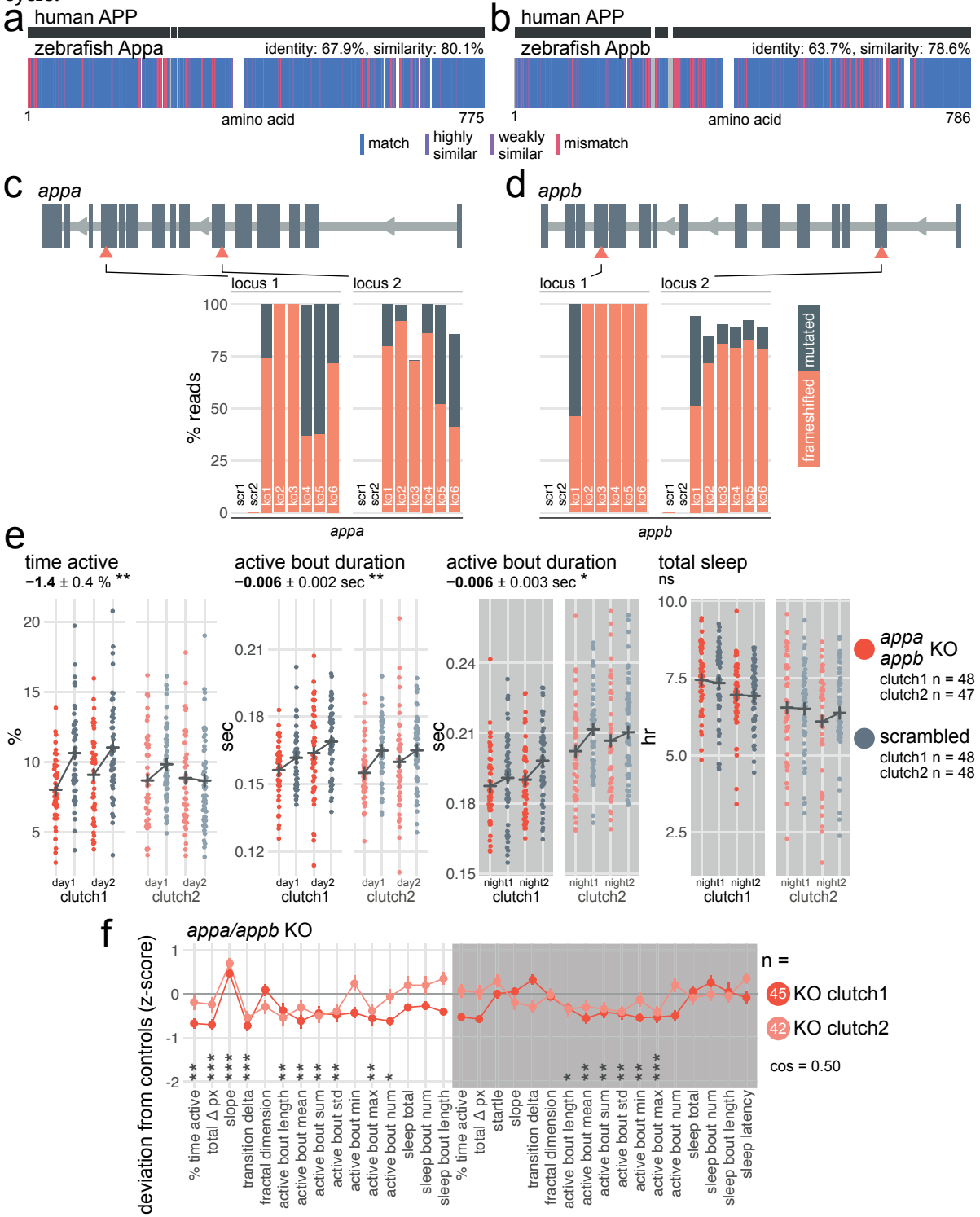

a, Human APP amino acid sequence (top) aligned to zebrafish Appa amino acid sequence (bottom). In the zebrafish protein, each amino acid (vertical bar) is coloured based on its similarity with the human protein. White gaps are added when additional residues are present in the other sequence.

b, Human APP amino acid sequence (top) aligned to zebrafish Appb amino acid sequence (bottom), as in a).

c, (top) Schematic of *appa* in the 5'–3' genome direction. Exons are in dark grey; tall exons are protein-coding, small are 5'- or 3'-UTR. Light grey lines are introns, and grey arrows represent the direction of transcription. Orange arrowheads mark the target loci. Exons and introns are on different scales. (bottom) Percentage of reads mutated (height of each bar, with orange representing percentage with a frameshift mutation) at each targeted locus of *appa*. *scr*, scrambled-injected control larva; *ko*, *appa* F0 knockout larva. Across F0 knockout samples: 96.6 ± 8.4% mutated reads, 70.4 ± 23.2% of all reads had a frameshift mutation.

Legend continued on next page.

d, (top) Schematic of *appb*, as in c). (bottom) Percentage of reads mutated (height of each bar, with orange representing percentage with a frameshift mutation) at each targeted locus of *appb*. *scr*, scrambled-injected control larva; *ko*, *appb* F0 knockout larva. Across F0 knockout samples: 95.0 ± 5.6% mutated reads, 82.6 ± 19.0% of all reads had a frameshift mutation. In c) and d), the numbers refer to individual animals. For example, ko5 refers to an individual *appa/appb* double F0 knockout larva for which mutations at the four targeted loci are plotted.
e, Parameter plots for two clutches of *appa/appb* F0 knockout larvae and scrambled-injected siblings. Each dot represents one larva during one day (left) or night (right). Black crosses mark the group means. Compared to scrambled-injected controls, *appa/appb* F0 knockouts spent less time active during the day (time active, ** p = 0.002) and had shorter swimming bouts across the day/night cycle (active bout duration, day: ** p = 0.003; night: * p = 0.018). Sleep was not affected (sleep total, ns p = 0.71). Statistics by likelihood-ratio test on linear mixed effects models.
g, Behavioural fingerprints of two clutches of *appa/appb* double F0 knockout larvae. Each dot represents the mean deviation from the same-clutch scrambled-injected mean for that parameter (z-score, mean ± SEM). Asterisks represent the p-values by likelihood-ratio test on linear mixed effects models calculated on the raw parameter values. *cos*, cosine similarity between the two clutch fingerprints.

sorl1 knockouts are less active during the day and sleep less at night

To test whether knockout of genes associated with late-onset AD also impacted behaviour in larvae, we then generated F0 knockouts for the zebrafish orthologues of *APOE* (*apoea*/*apoeb*), *CD2AP* (*cd2ap*), *CLU* (*clu*), and *SORL1* (*sorl1*).

APOE shares 22–25% amino acid identity with its two zebrafish orthologues, *apoea* and *apoeb* (Fig. 4–supplement 2a,b). To make *apoea*/*apoeb* double F0 knockouts, we targeted each gene at two loci in separate exons with highly mutagenic CRISPR-Cas9 RNPs (Fig. 4–supplement 2c,d). Consistently across three clutches, double *apoea*/*apoeb* F0 knockout larvae performed slightly more subdued swimming bouts during the day than scrambled-injected siblings (active bout mean: −4%; active bout maximum: −5% vs. scrambled; Fig. 4–supplement 2e). This slight hypoactivity is unlikely to reflect a motor defect because at night, *apoea*/*apoeb* knockouts performed more swimming bouts (+31%) and had less sleep (−7%, Fig. 4–supplement 2e) than controls.

Knockout of other early-onset AD risk genes also impacted behaviour, especially at night. We mutated zebrafish *cd2ap* (44% identical amino acid sequence vs. human CD2AP; Fig. 4–supplement 3a), at three loci on distinct exons (Fig. 4–supplement 3b). While the two clutches of *cd2ap* F0 knockouts gave generally inconsistent results, knockout larvae of both clutches were more active (time active: +38%; total activity: +44% vs. scrambled) and slept less at night than control siblings (−13%), mainly because they performed more swimming bouts (+34%, Fig. 4–supplement 3c). Similarly, knockout of *clu* (39% identical amino acid sequence vs. human CLU, Fig. 4–supplement 4a) did not strongly affect behaviour during the day (Fig. 4–supplement 4c), despite a particularly high rate of frameshift mutations at all three targeted loci (Fig. 4–supplement 4b). At night, *clu* F0 knockouts were slightly more active (time active: +12% vs. scrambled) and slept less than control siblings (−7%, Fig. 4–supplement 4c). Finally, we generated F0 knockouts for *sorl1* (63% identical amino acid sequence vs. human SORL1, Fig. 4a) by mutating three exons (Fig. 4b). *sorl1* F0 knockout larvae were less active during the day but slept less at night (Fig. 4c and Fig. 4–supplement 1). Specifically, during the day (Fig. 4d), *sorl1* F0 knockouts spent less time active than scrambled-injected larvae (−15% vs. scrambled), performing fewer swimming bouts (−15%) of approximately the same duration and intensity as controls. Sleep during the day was unaffected. At night (Fig. 4d), *sorl1* F0 knockouts spent more time active than control siblings (+20%), largely because their swimming bouts tended to last longer (+6%). They also slept less (−5%), initiating fewer sleep bouts (−9%) of roughly the same duration.

In summary, we video-tracked the sleep/wake behaviours of F0 knockout larvae in four genes associated with late-onset AD: *apoea*/*apoeb*, *cd2ap*, *clu*, and *sorl1*. Remarkably, loss of

all four genes produced a fairly consistent phenotype at night (Fig. 4–supplement 5), with all knockout larvae spending 5–13% less time asleep and instead spending 12–38% more time active because they were moving 13–34% more often. In contrast, each mutant had distinct day-time behavioural alterations. Comparing with early-onset genes, *psen1* knockouts had similar night-time phenotypes, but loss of *psen2* or *appa*/*appb* had no effect on night-time sleep. Therefore, at least some late-onset (and one early-onset) Alzheimer's risk genes have common effects on sleep from an early age, despite being expressed in different tissues and having distinct biochemical properties.

Fig. 4: *sorl1* F0 knockouts are hypoactive during the day but hyperactive at night.

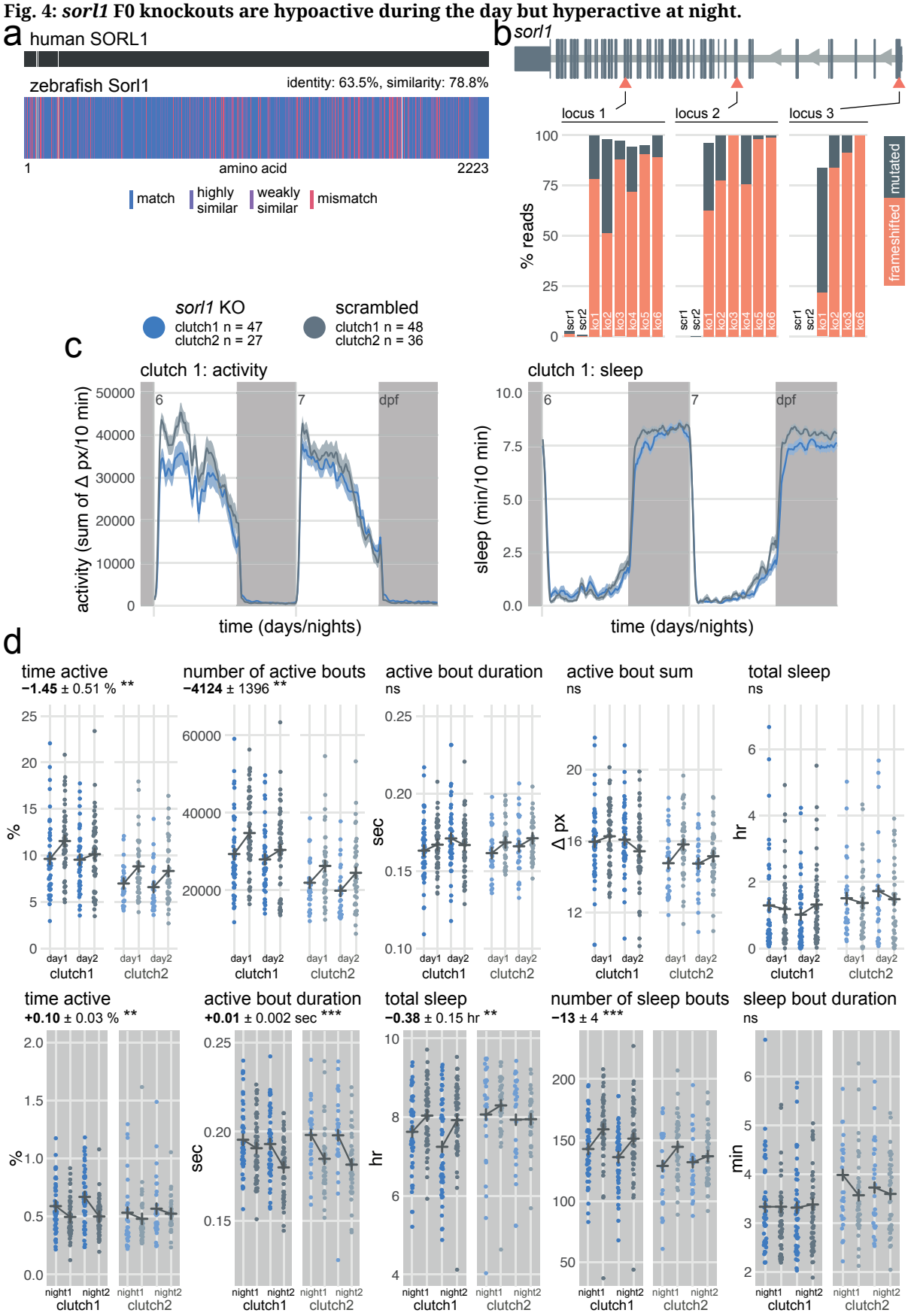

Legend on next page.

a, Human SORL1 amino acid sequence (top) aligned to zebrafish Sorl1 amino acid sequence (bottom). In the zebrafish protein, each amino acid (vertical bar) is coloured based on its similarity with the human protein. White gaps are added when additional residues are present in the other sequence.
b, (top) Schematic of *sorl1* in the 5'–3' genome direction. Exons are in dark grey; tall exons are protein-coding, small are 5'- or 3'-UTR. Light grey lines are introns, and grey arrows represent the direction of transcription. Orange arrowheads mark the target loci. Exons and introns are on different scales. (bottom) Percentage of reads mutated (height of each bar, with orange representing percentage with a frameshift mutation) at each targeted locus of *sorl1*. *scr*, scrambled-injected control larva; *ko*, *sorl1* F0 knockout larva. The numbers refer to individual animals. For example, ko6 refers to an individual *sorl1* F0 knockout larva for which mutations at each targeted locus are plotted. Across F0 knockout samples: 97.7 ± 4.2% mutated reads, 80.1 ± 20.8% of all reads had a frameshift mutation. Two locus-3 samples were excluded because of low sequencing coverage.
c, (left) Activity (sum of Δ pixels/10 minutes) of *sorl1* F0 knockout larvae and scrambled-injected siblings during 48 hr on a 14 hr:10 hr light:dark cycle (white background for days, dark grey background for nights). (right) Sleep (minutes per 10-minute epoch) during the same experiment. Traces are mean ± SEM across larvae. See also Fig. 4–supplement 1 for results from replicate clutch 2.
d, Parameter plots for two clutches of *sorl1* F0 knockout larvae and scrambled-injected siblings. Each dot represents one larva during one day (top row) or night (bottom row). Black crosses mark the group means. (top row) During the day, *sorl1* F0 knockouts spent less time active (time active, ** $p = 0.005$) and initiated fewer swimming bouts (number of active bouts, ** $p = 0.004$) than scrambled-injected controls. The average duration and number of pixels each swimming bout displaced were not affected by the loss of Sorl1 (active bout duration, ns $p = 0.40$; active bout sum, ns $p = 0.84$). Sleep was also not affected (total sleep, ns $p = 0.98$). (bottom row) During the night, *sorl1* F0 knockouts spent more time active (time active, ** $p = 0.002$) and their swimming bouts lasted longer on average (active bout duration, *** $p < 0.001$) than scrambled-injected siblings. *sorl1* F0 knockouts also slept less (total sleep, ** $p = 0.001$), mainly because they initiated fewer sleep bouts (number of sleep bouts, *** $p < 0.001$), while the duration of each sleep bout remained broadly unchanged (sleep bout duration, ns $p = 0.69$). One scrambled-injected larva from clutch 2 falls outside the Y axis limit of sleep bout duration (night1: 16.1 min, night2: 12.3 min). Statistics by likelihood-ratio test on linear mixed effects models.

Fig. 4–suppl. 1: Replicate clutch of *sorl1* F0 knockouts.

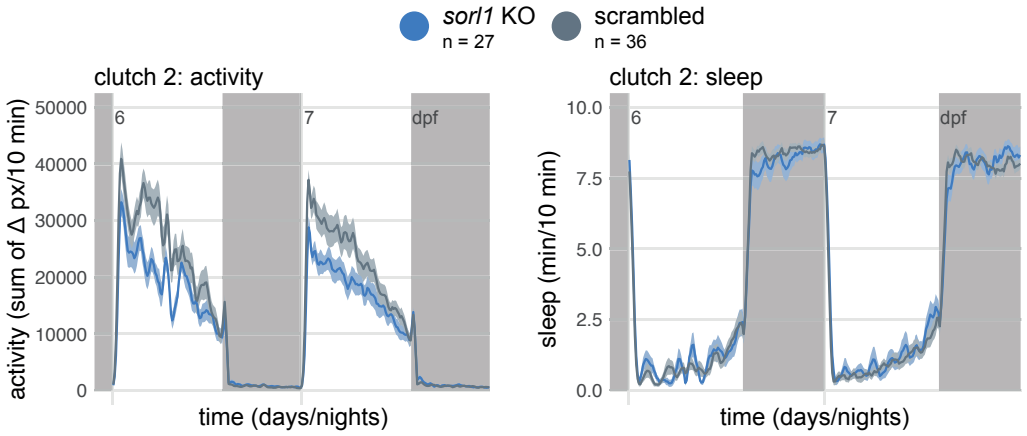

(left) Activity (sum of Δ pixels/10 minutes) of *sorl1* F0 knockout larvae and scrambled-injected siblings during 48 hr on a 14 hr:10 hr light:dark cycle (white background for days, dark grey background for nights). Traces are mean ± SEM across larvae. (right) Sleep (minutes per 10-minute epoch) during the same experiment. Traces are mean ± SEM across larvae. This replicate experiment is called clutch 2 in Fig. 4d.

Fig. 4–suppl. 2: *apoea/apoeb* double F0 knockouts have subdued swimming bouts during the day and sleep less at night.

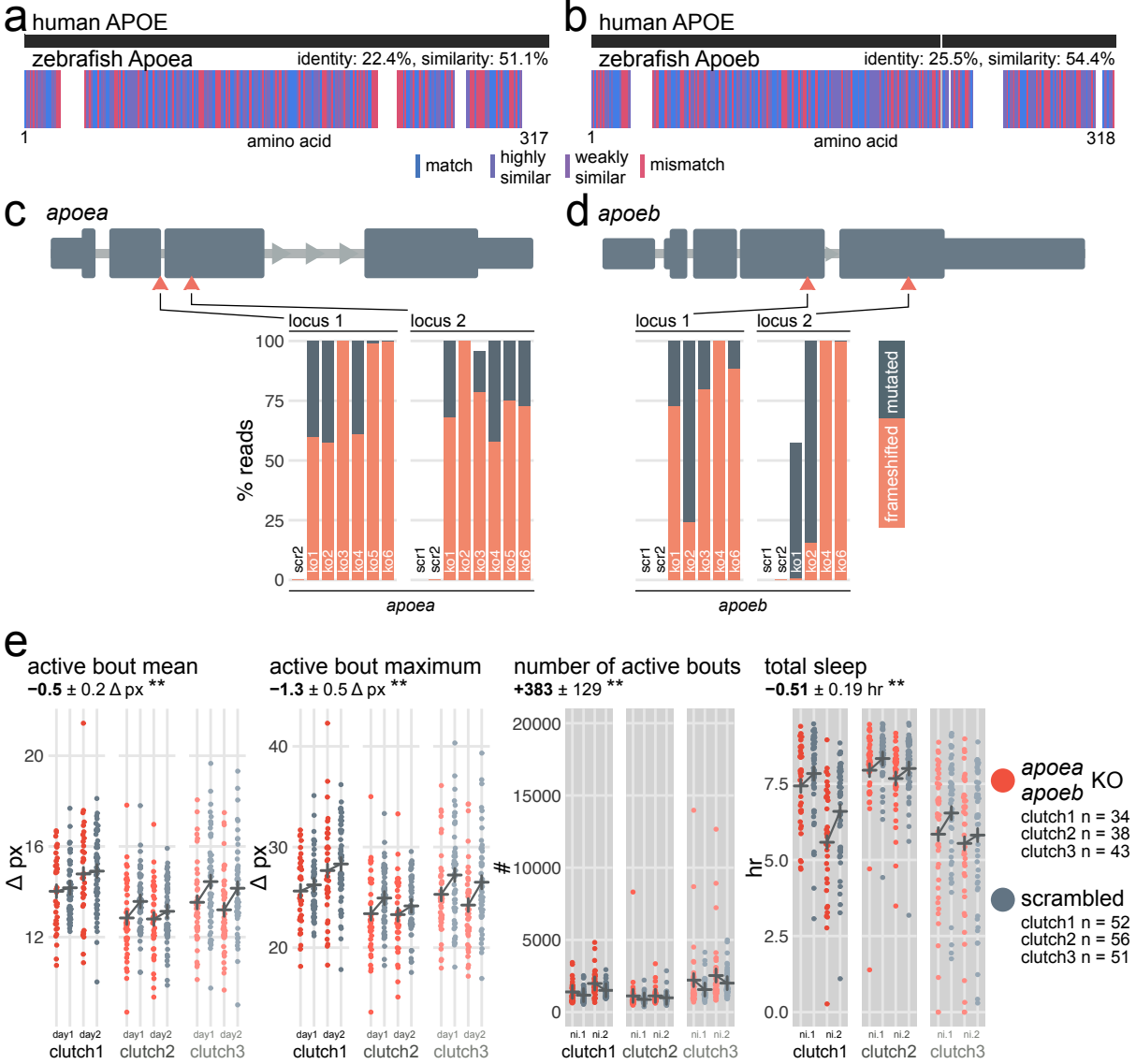

a, Human APOE amino acid sequence (top) aligned to zebrafish Apoea amino acid sequence (bottom). In the zebrafish protein, each amino acid (vertical bar) is coloured based on its similarity with the human protein. White gaps are added when additional residues are present in the other sequence.

b, Human APOE amino acid sequence (top) aligned to zebrafish Apoeb amino acid sequence (bottom), as in a).

c, (top) Schematic of *apoea* in the 5'–3' genome direction. Exons are in dark grey; tall exons are protein-coding, small are 5'- or 3'-UTR. Light grey lines are introns, and grey arrows represent the direction of transcription. Orange arrowheads mark the target loci. Exons and introns are on different scales. (bottom) Percentage of reads mutated (height of each bar, with orange representing percentage with a frameshift mutation) at each targeted locus of *apoea*. *scr*, scrambled-injected control larva; *ko*, *apoea* F0 knockout larva. Across F0 knockout samples: 99.6 ± 1.2% mutated reads, 77.5 ± 17.8% of all reads had a frameshift mutation. One locus-1 sample was excluded because of low sequencing coverage.

d, (top) Schematic of *apoeb*, as in c). (bottom) Percentage of reads mutated (height of each bar, with orange representing percentage with a frameshift mutation) at each targeted locus of *apoeb*. *scr*, scrambled-injected control larva; *ko*, *apoeb* F0 knockout larva. Across F0 knockout samples: 95.2 ± 14.2% mutated reads, 64.6 ± 39.9% of all reads had a frameshift mutation. One locus-1 and two locus-3 samples were excluded because of low sequencing coverage. In c) and d), the numbers refer to individual animals. For example, ko6 refers to an individual *apoea/apoeb* double F0 knockout larva for which mutations at the four targeted loci are plotted.

Legend continued on next page.

e, Parameter plots for three clutches of *apoea/apoeb* double F0 knockout larvae and scrambled-injected siblings. Each dot represents one larva during one day (left) or night (right). Black crosses mark the group means. (left) During the day, *apoea/apoeb* double F0 knockout larvae had more subdued swimming bouts than scrambled-injected siblings (active bout mean, ** p = 0.006; active bout maximum, ** p = 0.004). (right) At night, *apoea/apoeb* double F0 knockout larvae were performing more swimming bouts (number of active bouts, ** p = 0.003) and sleeping less (total sleep, ** p = 0.009) than scrambled-injected siblings. Six datapoints from four *apoea/apoeb* F0 knockout larvae fall outside the Y axis limit of the number of active bouts (7,229–13,975 bouts). Statistics by likelihood-ratio test on linear mixed effects models. *ni.*, night.

Fig. 4–suppl. 3: *cd2ap* F0 knockouts are hyperactive at night.

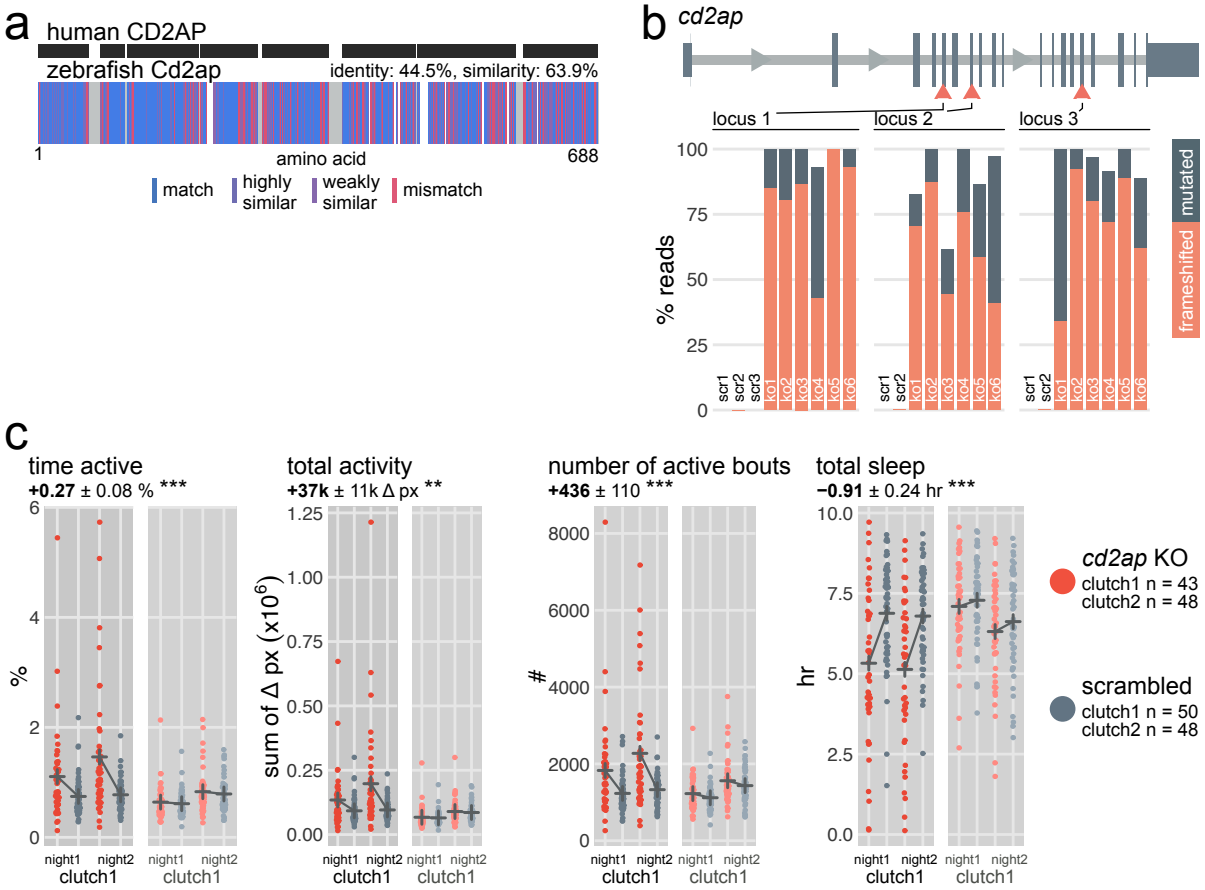

a, Human CD2AP amino acid sequence (top) aligned to zebrafish Cd2ap amino acid sequence (bottom). In the zebrafish protein, each amino acid (vertical bar) is coloured based on its similarity with the human protein. White gaps are added when additional residues are present in the other sequence.
b, (top) Schematic of *cd2ap* in the 5'–3' genome direction. Exons are in dark grey; tall exons are protein-coding, small are 5'- or 3'-UTR. Light grey lines are introns, and grey arrows represent the direction of transcription. Orange arrowheads mark the target loci. Exons and introns are on different scales. (bottom) Percentage of reads mutated (height of each bar, with orange representing percentage with a frameshift mutation) at each targeted locus of *cd2ap*. *scr*, scrambled-injected control larva; *ko*, *cd2ap* F0 knockout larva. The numbers refer to individual animals. For example, ko1 refers to an individual *cd2ap* F0 knockout larva for which mutations at each targeted locus are plotted. Across F0 knockout samples: 94.3 ± 9.8% mutated reads, 72.1 ± 20.3% of all reads had a frameshift mutation.
c, Parameter plots for two clutches of *cd2ap* F0 knockout larvae and scrambled-injected siblings. Each dot represents one larva during one night. Black crosses mark the group means. At night, *cd2ap* F0 knockouts spent more time active (time active, *** p < 0.001), displaced more pixels in total (total activity, ** p = 0.001), initiated more swimming bouts (number of active bouts, *** p < 0.001), and slept less (total sleep, *** p < 0.001) than scrambled-injected siblings.

Fig. 4–suppl. 4: *clu* F0 knockouts sleep slightly less at night.

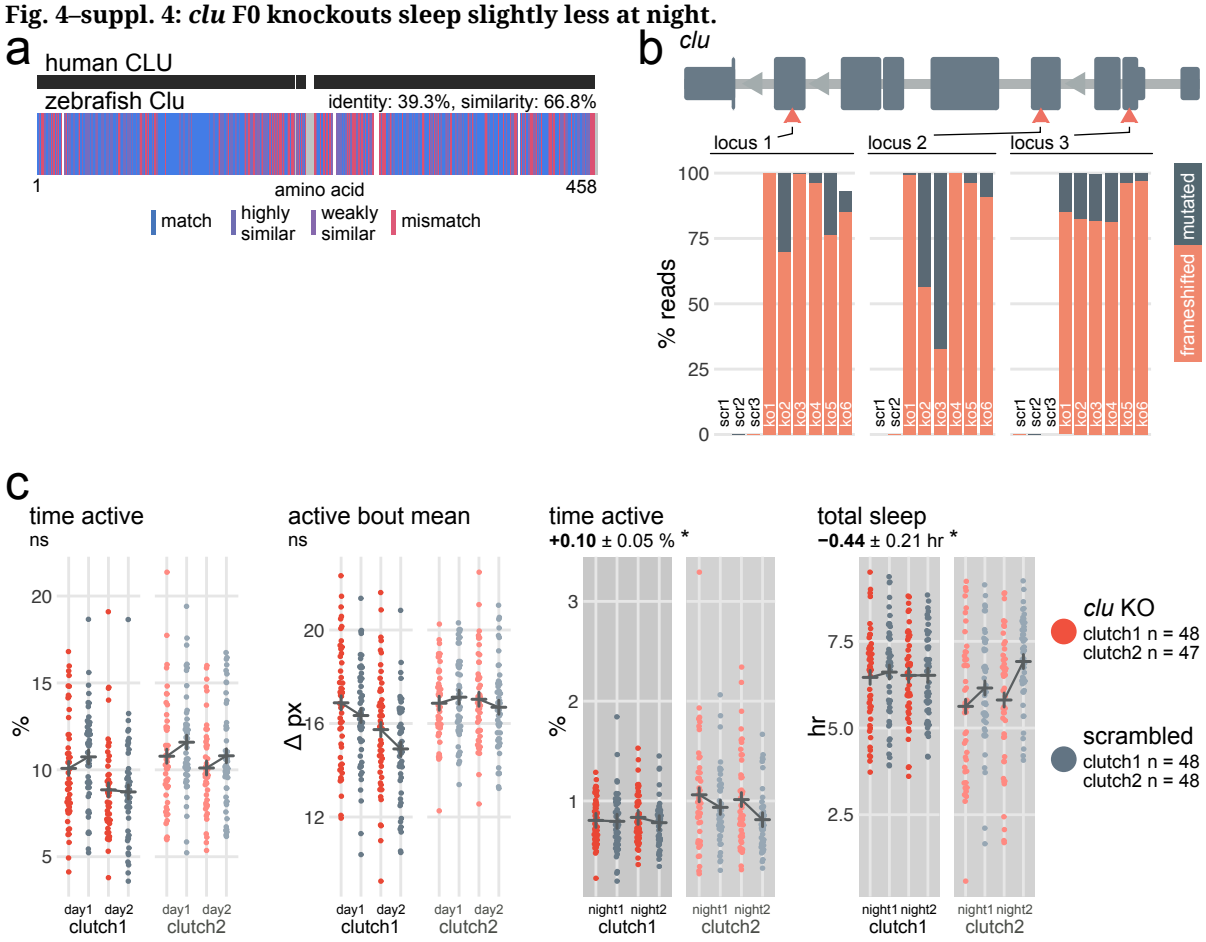

a, Human CLU amino acid sequence (top) aligned to zebrafish Clu amino acid sequence (bottom). In the zebrafish protein, each amino acid (vertical bar) is coloured based on its similarity with the human protein. White gaps are added when additional residues are present in the other sequence.

b, (top) Schematic of *clu* in the 5'–3' genome direction. Exons are in dark grey; tall exons are protein-coding, small are 5'- or 3'-UTR. Light grey lines are introns, and grey arrows represent the direction of transcription. Orange arrowheads mark the target loci. Exons and introns are on different scales. (bottom) Percentage of reads mutated (height of each bar, with orange representing percentage with a frameshift mutation) at each targeted locus of *clu*. *scr*, scrambled-injected control larva; *ko*, *clu* F0 knockout larva. The numbers refer to individual animals. For example, ko2 refers to an individual *clu* F0 knockout larva for which mutations at each targeted locus are plotted. Across F0 knockout samples: 99.6 ± 1.6% mutated reads, 84.9 ± 17.7% of all reads had a frameshift mutation.

c, Parameter plots for two clutches of *clu* F0 knockout larvae and scrambled-injected siblings. Each dot represents one larva during one day (left) or night (right). Black crosses mark the group means. Loss of Clu did not consistently affect locomotor activity during the day (time active, ns p = 0.18; active bout mean, ns p = 0.21). At night, *clu* F0 knockouts were slightly more active (time active, * p = 0.047) and slept less (total sleep, * p = 0.033) than scrambled-injected siblings, although the effect sizes were not well replicated across clutches.

Fig. 4–suppl. 5: F0 knockout larvae in genes associated with late-onset Alzheimer's disease slept less at night.

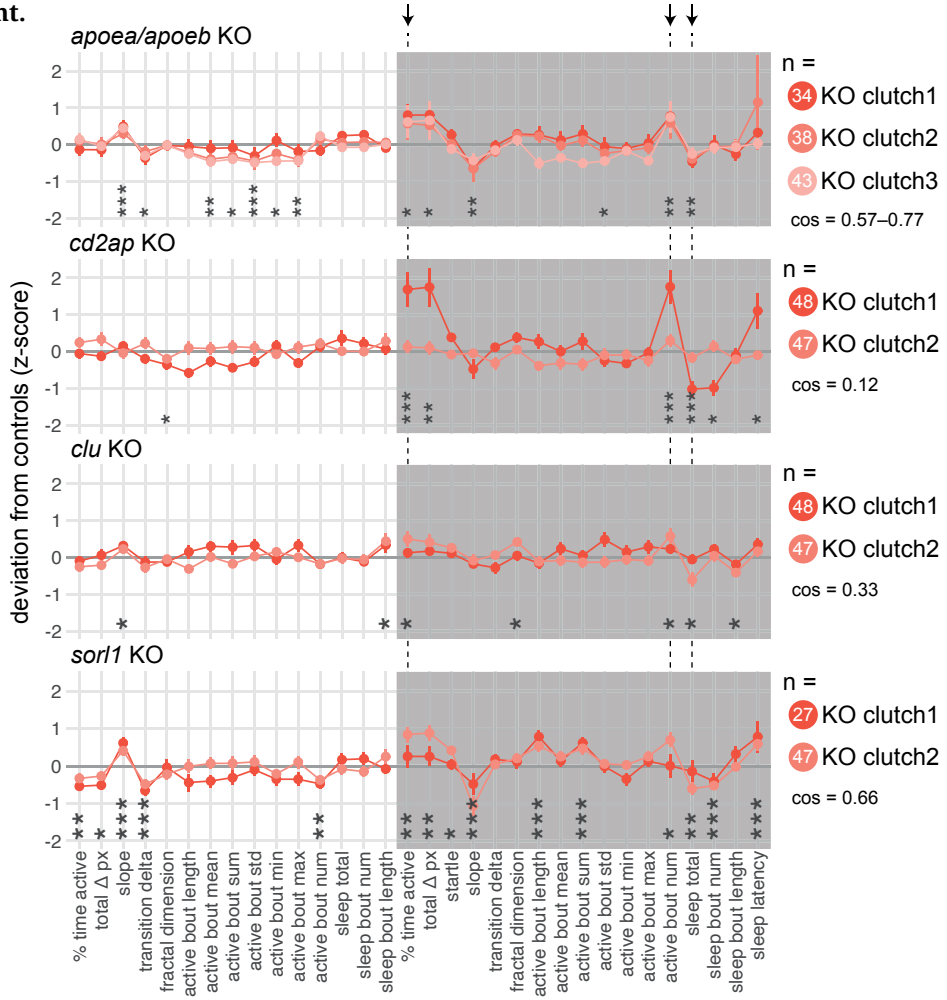

For each gene: behavioural fingerprints of N = 2–3 clutches of F0 knockout larvae. Each dot represents the mean deviation from the same-clutch scrambled-injected mean for that parameter (z-score, mean ± SEM). Asterisks represent the p-values by likelihood-ratio test on linear mixed effects models calculated on the raw parameter values. *cos*, cosine similarities between fingerprints. Arrows and dashed lines mark the three parameters which are significant for all four late-onset Alzheimer's risk genes tested.

From behavioural fingerprint to causal process: serotonin signalling disruption by the loss of Sorl1

From genomic studies of AD, we know that mutations in genes such as *SORL1* modify risk by disrupting some biological processes. Presumably, the same processes are disrupted in zebrafish *sorl1* knockouts, and some caused the behavioural alterations we observed. Can we now follow the thread backwards and predict some of the biological processes in which Sorl1 is involved based on the behavioural profile of *sorl1* knockouts?

To predict disrupted biological processes from the *sorl1* knockout behavioural profile, we developed a behavioural pharmacology approach based on a database of 5,756 small molecule behavioural fingerprints (3,674 unique compounds) obtained in wild-type larvae[42]. First, we used information from the Therapeutic Target Database[56] to annotate each compound with its indications (e.g. triprolidine is used to treat hay fever), targets (e.g. triprolidine targets the histamine H1 receptor), and the pathways it affects through its targets (e.g. triprolidine affects the “inflammatory mediator regulation of TRP channels”). Second, we converted the frame-by-frame behavioural fingerprint of *sorl1* knockouts to the one-minute format used by the database. We then compared the mean *sorl1* knockout fingerprint with each small molecule behavioural fingerprint, creating a ranked list from the small molecule fingerprint most similar to the *sorl1* fingerprint (SU6656: cosine similarity = 0.83) to the small molecule fingerprint most opposite to the *sorl1* fingerprint (flumazenil: cos = −0.80). Third, we tested using a custom permutation test whether specific indication, target, or pathway annotations were significantly enriched at the top and/or the bottom of the ranked list. More present among the small molecules most (anti-)correlating with the *sorl1* fingerprint were drugs used to treat depression (Fig. 5–supplement 1a, simulated p-value = 0.0129), targeting the serotonin transporter SLC6A4 (Fig. 5a,b, simulated p-value = 0.0112), and affecting the “serotonergic synapse” pathway (Fig. 5–supplement 1b, simulated p-value = 0.0003). Thus, *sorl1* knockout larvae behaved similarly to larvae treated with small molecules targeting serotonin signalling, suggesting that the loss of Sorl1 disrupted serotonin signalling.

If serotonin signalling is disrupted in *sorl1* knockouts, they should react differently to serotonergic drugs than wild-type animals. To test this hypothesis, we treated *sorl1* F0 knockouts and controls with citalopram, a selective serotonin reuptake inhibitor used to treat depression[57]. Citalopram binds the serotonin transporter SLC6A4, preventing the reuptake of serotonin from the synaptic cleft. At a low dose of citalopram (1 µM, added directly to the fish water), *sorl1* F0 knockouts and scrambled-injected controls reacted similarly, sleeping about 1.1 hr more during both day and night (Fig. 5c). In contrast, at a higher dose of citalopram (10 µM) *sorl1* F0 knockouts had a stronger reaction than their

control siblings. For example, sleep during the day increased 2.5× in *sorl1* knockouts, while it only increased 2.2× in controls. The heightened sensitivity of *sorl1* knockouts to citalopram was also apparent when taking all parameters into account by measuring each larva's Euclidean distance from the average H_2O-treated sibling of same genotype (Fig. 5d). Indeed, 10 µM citalopram displaced the *sorl1* knockout larvae further from their behavioural baseline than it pushed controls from theirs. Thus, our behavioural pharmacology approach correctly predicted from behaviour alone that serotonin signalling was disrupted in *sorl1* knockouts.

There are at least two ways *sorl1* knockouts could be more sensitive to citalopram. First, compared to wild types, *sorl1* knockouts could undergo a larger spike of serotonin in the synaptic cleft when reuptake is blocked. This may be because *sorl1* knockouts synthesise more serotonin, either because they have more serotonergic neurons or a higher expression of the enzymes required to make serotonin, or because they produce less of the serotonin transporter, making them more sensitive to citalopram as a given dose would inhibit a larger proportion of the transporter than in wild-type animals. Second, *sorl1* knockouts may be overly sensitive to serotonin itself because post-synaptic neurons have higher levels of serotonin receptors.

To distinguish between these two hypotheses, we used HCR to label serotonergic neurons by tagging mRNA coding for tryptophan hydroxylases (in zebrafish: *tph1a*, *tph1b*, *tph2*; Fig. 5e), an enzyme required for the synthesis of serotonin, and serotonin transporters by tagging *slc6a4a* and *slc6a4b* mRNA[58] (Fig. 5–supplement 1c). We registered the brain stacks to a common atlas (Zebrafish Brain Browser) and segmented them into 168 anatomical regions. In each region with expression, we counted the number of positive voxels and measured the total signal intensity in each channel (channel 1: *tph1a* + *tph1b* + *tph2*; channel 2: *slc6a4a* + *slc6a4b*). *sorl1* F0 knockouts had slightly more (+2%) *slc6a4a*/*b* positive voxels than controls across regions, but this difference was not definite for any one region and not replicated when looking at total signal intensity (Fig. 5–supplement 1d). *sorl1* F0 knockouts had on average 18% lower *tph1a*/*1b*/*2* signal intensities across regions, particularly in the hypothalamus (hypothalamus – caudal zone 1: –24%, Fig. 5e,f). Therefore, although we see small differences in the levels of serotonin transporters or synthesis enzymes, these were opposite to our hypotheses so do not readily explain the heightened sensitivity of *sorl1* to citalopram. Additionally, at least one study did not find changes in serotonin levels in the striatum of *SORL1* knockout mice[59], and we did not find genes related to serotonin signalling to be differentially expressed in a bulk RNA-seq dataset of *sorl1* knockout zebrafish brains[60]. Ruling out the first hypothesis, *sorl1* knockouts may react excessively to a given spike in serotonin.

Fig. 5: Predictive behavioural pharmacology identifies impaired serotonin signalling in *sorl1* knockouts.

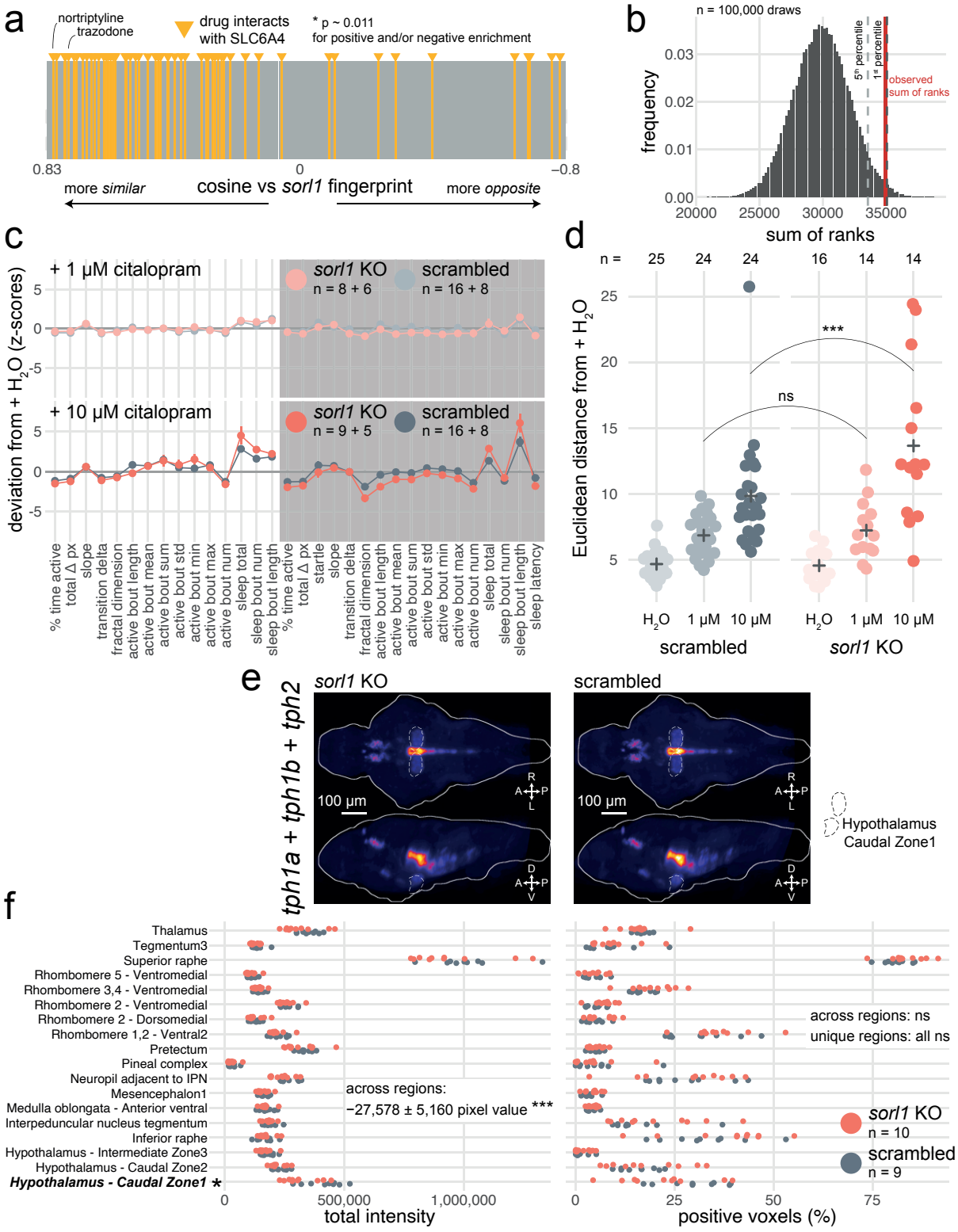

a, Compounds interacting with the serotonin transporter SLC6A4 tend to generate behavioural phenotypes similar to the *sorl1* F0 knockout fingerprint. 5,756 small molecule fingerprints (vertical bars) are ranked from the fingerprint with the most positive cosine to the fingerprint with the most negative cosine in comparison with the mean *sorl1* F0 knockout fingerprint. Fingerprints of drugs that interact with SLC6A4 are coloured in yellow (source: Therapeutic Target Database). Simulated p-value = 0.011 for enrichment of drugs interacting with SLC6A4 at the top (positive cosine) and/or bottom (negative cosine) of the ranked list by a custom permutation test.

Legend continued on next page.

b, Result of the permutation test for top and/or bottom enrichment of drugs interacting with SLC6A4 in the ranked list. In the ranked list, fingerprints were assigned ranks starting from the centre of the list (cos ~ 0 position) and counting in both directions, in such a way that the most similar fingerprint (SU6656: cos = 0.83) and the most opposite fingerprint (flumazenil: cos = −0.80) both had rank #1000. The ranks of the fingerprints of drugs interacting with SLC6A4 (n = 59) were summed, giving sum of ranks = 34,958. To simulate a null distribution, 59 fingerprints were randomly drawn 100,000 times, generating a distribution of 100,000 random sum of ranks. Here, only 1,127 random draws gave a larger sum of ranks than the observed one, so the simulated p-value was p = 1,127/100,000 = 0.011 *.
c, (top) Behavioural fingerprints of *sorl1* F0 knockouts and scrambled-injected siblings treated with 1 µM citalopram. (bottom) Behavioural fingerprints of *sorl1* F0 knockouts and scrambled-injected siblings treated with 10 µM citalopram. In both plots, each dot represents the mean deviation from the mean of the same-group (F0 knockout or scrambled-injected) untreated (H_2O) siblings (z-score, mean ± SEM), therefore the baseline (z-scores = 0) does not represent the same larvae for *sorl1* F0 knockouts and scrambled-injected controls. Z-scores from two clutches were averaged.
d, Euclidean distance from same-group controls' mean across the 32 parameters. ns p = 0.71, *** p < 0.001 by Welch's t-test.
e, HCRs labelling transcripts encoding tryptophan hydroxylases (*tph1a*, *tph1b*, *tph2*) in 6-dpf *sorl1* F0 knockouts and scrambled-injected controls. The images are maximum Z-projections of dorsal (top) and sagittal (bottom) views of the median stack of all larvae in each group. A, anterior; P, posterior; R, rightwards; L, leftwards; D, dorsal; V, ventral.
f, Quantification of HCRs from e). (left) Total grey pixel intensity per anatomical region in *sorl1* F0 knockouts and scrambled-injected controls. *** p < 0.001, * p = 0.012. (right) Number of voxels with positive signal per anatomical region in *sorl1* F0 knockouts and scrambled-injected controls. Across regions: ns p = 0.08; unique regions: ns p > 0.07. Statistics across regions by likelihood-ratio test on linear mixed effects models; statistics on unique regions by Welch's t-test without p-value adjustment. The same larvae are plotted in Fig. 5–supplement 1c,d.

Fig. 5–suppl. 1: Predictions of disrupted processes in *sorl1* knockouts based on indications and KEGG pathways.

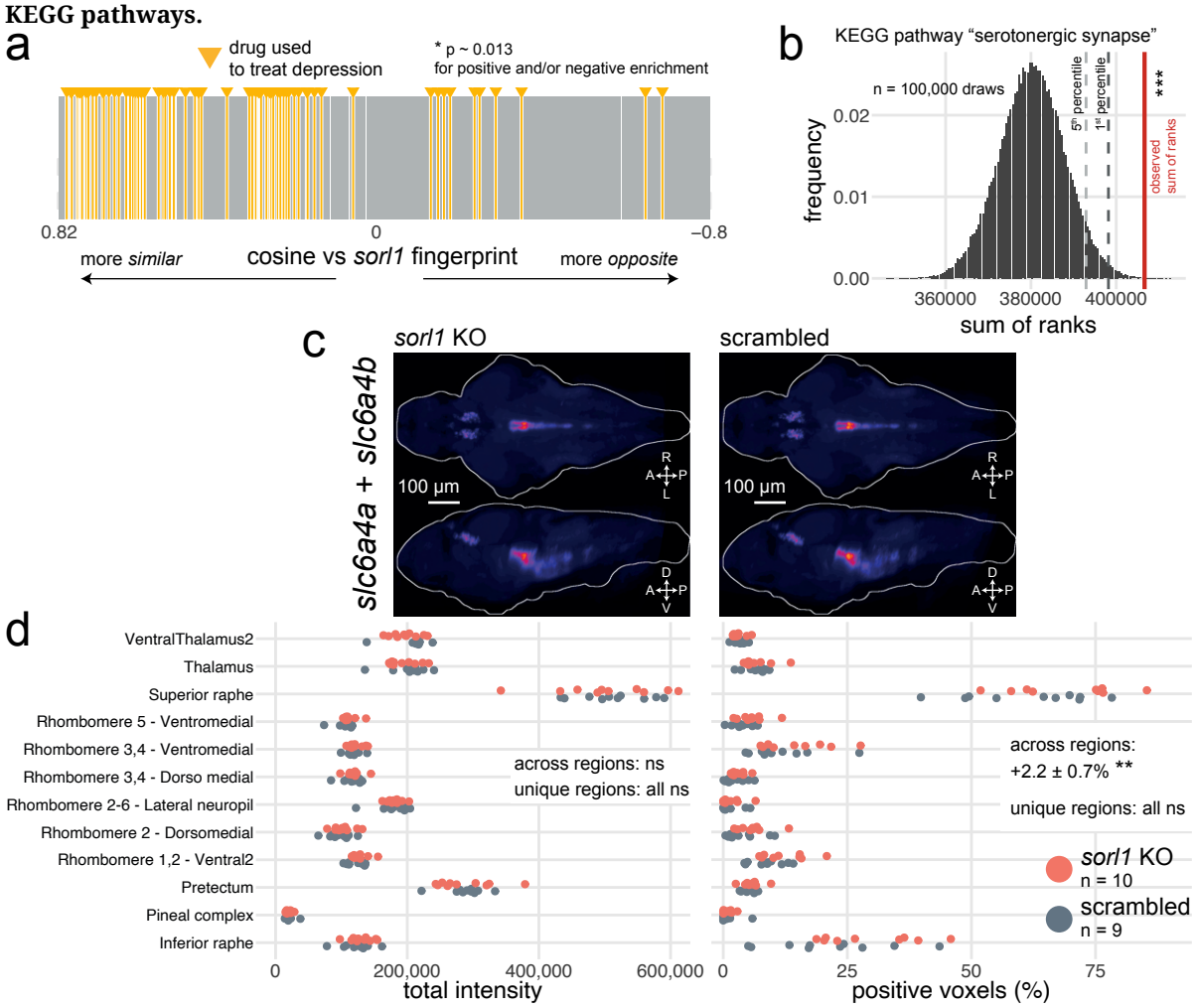

a, Drugs used to treat depression tend to generate behavioural phenotypes similar to the *sorl1* F0 knockout fingerprint. 5,756 small molecule fingerprints (vertical bars) are ranked from the fingerprint with the most positive cosine to the fingerprint with the most negative cosine in comparison with the mean *sorl1* F0 knockout fingerprint. Fingerprints of drugs used to treat depression are coloured in yellow (source: Therapeutic Target Database). Simulated p-value = 0.013 for enrichment of drugs used to treat depression at the top (positive cosine) and/or bottom (negative cosine) of the ranked list by a custom permutation test.

b, Result of the permutation test for top and/or bottom enrichment of drugs affecting the "serotonergic synapse" KEGG pathway. In the ranked list, fingerprints were assigned ranks starting from the centre of the list (cos ~ 0 position) and counting in both directions, in such a way that the most similar fingerprint (SU6656: cos = 0.83) and the most opposite fingerprint (flumazenil: cos = −0.80) both had rank #1000. The ranks of the fingerprints of drugs which affect the "serotonergic synapse" KEGG pathway (n = 744) were summed, giving sum of ranks = 406,646. To simulate a null distribution, 744 fingerprints were randomly drawn 100,000 times, generating a distribution of 100,000 random sum of ranks. Here, only 30 random draws gave a larger sum of ranks than the observed one, so the simulated p-value was p = 30/100,000 = 0.0003 ***.

c, HCRs labelling transcripts encoding serotonin transporters *(slc6a4a* and *slc6a4b*) in 6-dpf *sorl1* F0 knockouts and scrambled-injected controls. The images are maximum Z-projections of dorsal (top) and sagittal (bottom) views of the median stack of all larvae in each group. A, anterior; P, posterior; R, rightwards; L, leftwards; D, dorsal; V, ventral.

d, Quantification of HCRs from c). (left) Total grey pixel intensity per anatomical region in *sorl1* F0 knockouts and scrambled-injected controls. Across regions: ns p = 0.98; unique regions: ns p > 0.25. (right) Number of voxels with positive signal per anatomical region in *sorl1* F0 knockouts and scrambled-injected controls. ** p = 0.001, unique regions: ns p > 0.07. Statistics across regions by likelihood-ratio test on linear mixed effects models; statistics on unique regions by Welch's t-test without p-value adjustment. The same larvae are plotted in Fig. 5e,f.

From behavioural fingerprint to candidate therapeutic: betamethasone rescues the *psen2* behavioural phenotype

In addition to pointing to the disrupted pathways, behavioural pharmacology can also predict small molecules that may normalise mutant behavioural phenotypes by pointing to compounds that generate the opposite behavioural fingerprint in wild-type larvae.

Using this approach, we sought to identify compounds capable of normalising the behavioural alterations of *psen2* knockouts, such as the increased day-time sleep. We ranked the 5,756 small molecule behavioural fingerprints in comparison with the mean *psen2* F0 knockout fingerprint and focused on compounds that generated the most opposite (anti-correlating) fingerprint when applied on wild-type larvae. This identified three compounds with a high negative cosine compared to *psen2* knockouts (Fig. 6a and Fig. 6–supplement 1a): tinidazole (minimum cos = −0.85), fenoprofen (minimum cos = −0.74), and betamethasone (minimum cos = −0.74). These compounds were also selected because they were each replicated at least once in the database, lending confidence to the prediction. We then applied the three compounds on *psen2* F0 knockouts and measured their effects on sleep/wake parameters. For each treatment, we grouped the behavioural parameters into four categories: “rescue” if the parameter was significantly altered in DMSO-treated *psen2* knockout larvae but got normalised by the drug; “missed rescue” if the *psen2* knockout parameter remained altered after drug treatment; “side effect” if a parameter was unaffected in *psen2* knockouts but got altered by the drug; and “no effect” if the parameter was unaffected in *psen2* knockouts and remained unchanged by the drug.

All three compounds normalised at least some aspects of the *psen2* knockout behavioural phenotype. Tinidazole did not reduce the abnormally high day-time sleep characteristic of *psen2* knockouts (Fig. 6c left). It rescued the swimming bout alterations (active bout parameters) during the day but not at night. Overall, the compound barely caused any side effect but only rescued a small aspect of the *psen2* knockout phenotype (9/18 altered parameters rescued). Fenoprofen performed worse (Fig. 6c middle, 8/18 altered parameters rescued), rescuing some of the swimming bout alterations during the day but aggravating them at night. Furthermore, fenoprofen made *psen2* knockout larvae drowsier than they were during the day, causing sleep to increase further and activity to decrease. Strikingly, betamethasone completely resolved the excess day-time sleep without causing hyperactivity (Fig. 6b and Fig. 6–supplement 1b). Betamethasone rescued most, but not all, of the swimming bout alterations during both the day and night (Fig. 6c right, 14/18 altered parameters rescued). Betamethasone did cause a few side effects, likely by making *psen2* knockout larvae overly aroused at the start of the night, extending sleep latency and decreasing the slope in activity and the startle response. Therefore, of the three drugs we

selected using behavioural pharmacology, one almost completely normalised the *psen2* knockout phenotype, albeit with a few side effects.

Fig. 6: Betamethasone normalises the *psen2* knockout behavioural phenotype.

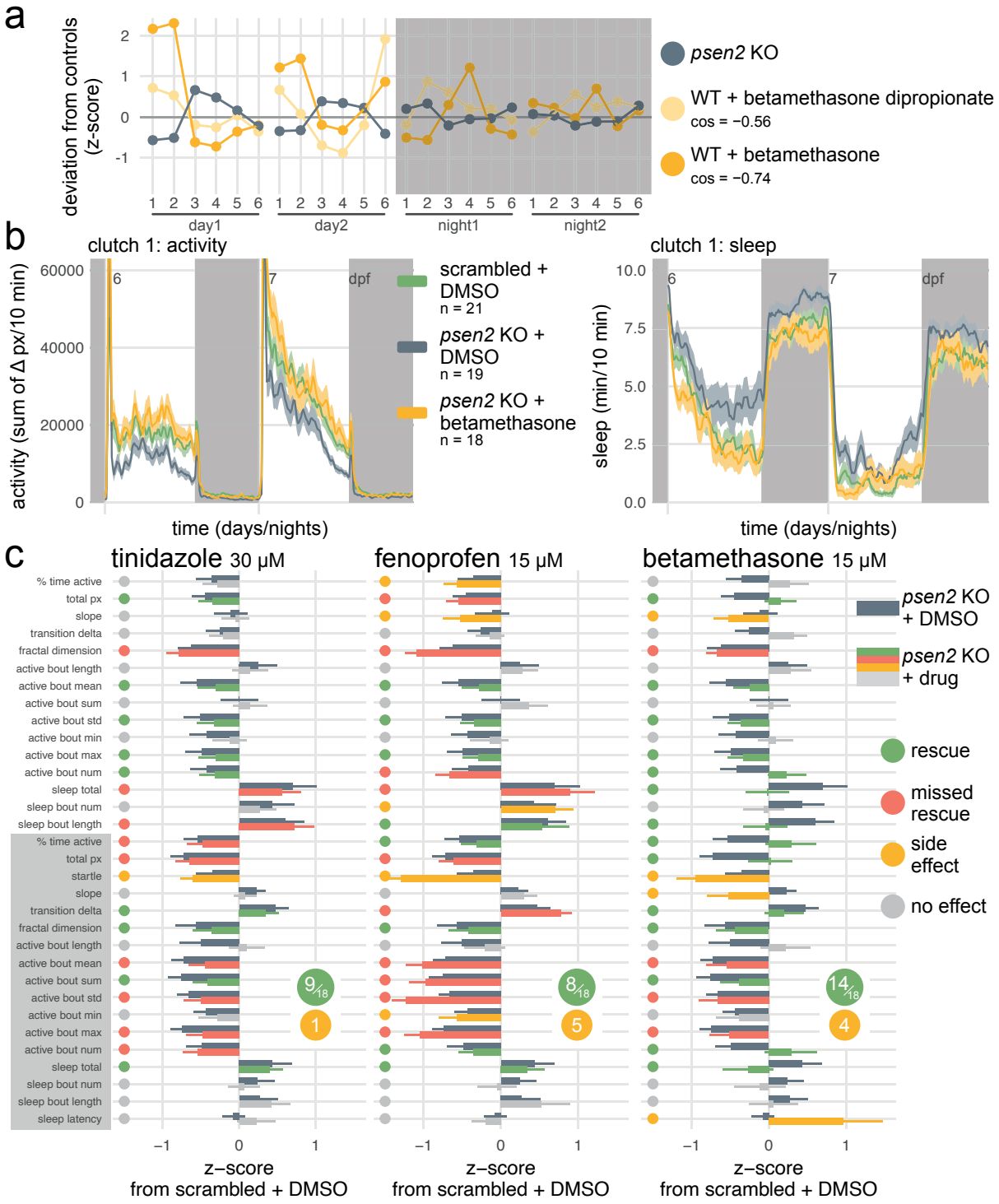

a, The *psen2* F0 knockout fingerprint was used as query to identify small molecules that generate the opposite behavioural phenotype when applied on wild-type larvae, returning betamethasone as candidate therapeutic. Plotted are the query *psen2* fingerprint (mean of two clutches, dark grey) and the two betamethasone fingerprints from the drug database with the largest negative cosine similarities (yellow). Parameters: 1, average activity (sec active/min); 2, average waking activity (sec active/min, excluding inactive minutes); 3, total sleep (hr); 4, number of sleep bouts; 5, sleep bout length (min); 6, sleep latency (min until first sleep bout). *cos*, cosine similarity between each betamethasone fingerprint and the *psen2* F0 knockout fingerprint.

Legend continued on next page.

b, (left) Activity (sum of Δ pixels/10 minutes) of scrambled-injected larvae treated with DMSO and *psen2* F0 knockout larvae treated with DMSO or 15 µM betamethasone during 48 hr on a 14 hr:10 hr light:dark cycle (white background for days, dark grey background for nights). (right) Sleep (minutes per 10-minute epoch) during the same experiment. Traces are mean ± SEM across larvae. See also Fig. 6—supplement 1 for results from replicate clutch 2.
c, Survey of behavioural parameters for each drug treatment. Bars represent the mean deviation from scrambled-injected siblings treated with DMSO (z-score, mean ± SEM). Dark grey bars represent the *psen2* knockouts treated with DMSO, i.e. the phenotype to be treated (same population of *psen2* knockouts treated with DMSO for the all drug treatments). Other bars are colour-coded by the effect of each drug on *psen2* knockouts: "rescue" (green) if the drug normalised the parameter; "missed rescue" (red) if the drug failed to normalise the parameter; "side effect" (yellow) if the drug significantly altered a parameter which was unaffected in *psen2* knockouts; and "no effect" (grey). Calls were decided based on significance by likelihood-ratio test on linear mixed effects models calculated on the raw parameter values from both clutches.

Fig. 6–suppl. 1: Selection of candidate therapeutics to normalise the *psen2* behavioural phenotype by predictive behavioural pharmacology.

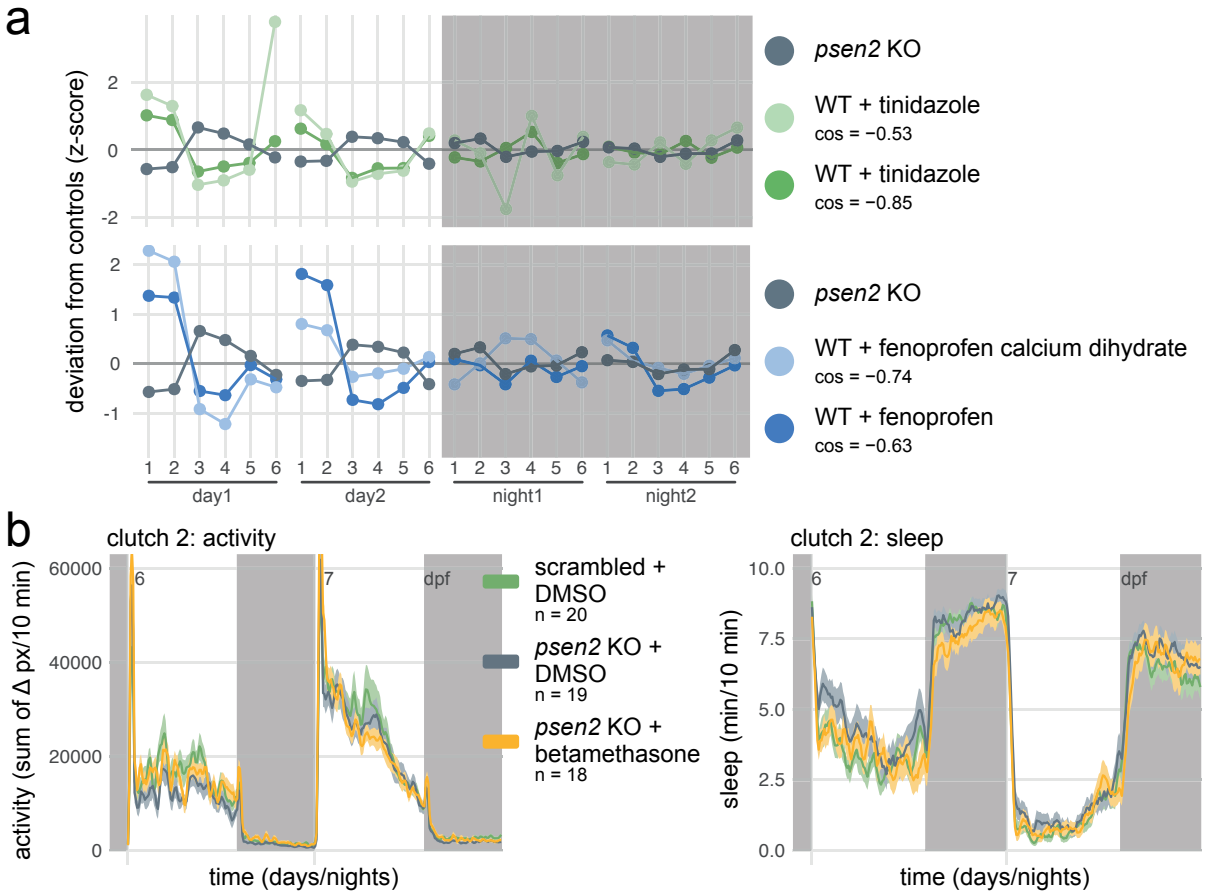

a, The *psen2* F0 knockout fingerprint was used as query to identify small molecules that generate the opposite behavioural phenotype when applied on wild-type larvae, returning tinidazole and fenoprofen as candidate therapeutics. Plotted are the query *psen2* fingerprint (mean of two clutches, dark grey) and the tinidazole (green) and fenoprofen (blue) fingerprints from the drug database. Parameters: 1, average activity (sec active/min); 2, average waking activity (sec active/min, excluding inactive minutes); 3, total sleep (hr); 4, number of sleep bouts; 5, sleep bout length (min); 6, sleep latency (min until first sleep bout). *cos*, cosine similarity between the drug fingerprint and the *psen2* F0 knockout fingerprint.
b, (left) Activity (sum of Δ pixels/10 minutes) of scrambled-injected larvae treated with DMSO and *psen2* F0 knockout larvae treated with DMSO or 15 µM betamethasone during 48 hr on a 14 hr:10 hr light:dark cycle (white background for days, dark grey background for nights). (right) Sleep (minutes per 10-minute epoch) during the same experiment. Traces are mean ± SEM across larvae.

Discussion

The F0 knockout and behavioural pharmacology approach was able to successfully predict a signalling pathway that was disrupted by knockout of the Alzheimer's risk gene *sorl1* and identify a drug capable of normalising the *psen2* knockout behavioural phenotype. To allow researchers to generate pharmacological predictions from their own sleep/wake datasets, we built an online app (francoiskroll.shinyapps.io/zoltar/) that can plot behavioural fingerprints, rank all 5,756 small molecule fingerprints in the database in comparison to the query fingerprint, and perform permutation tests for enrichment of indications, drug targets, and KEGG pathways (Fig. 7–supplement 1a,b). While we used genes associated with AD as a case study, predictive behavioural pharmacology provides a generalisable framework that can be applied to any set of disease risk genes.

Disrupted sleep and serotonin signalling—causal processes of Alzheimer's disease?

Of the seven genes tested, *psen1* and all four late-onset Alzheimer's risk genes tested decreased sleep duration at night when mutated in zebrafish larvae. Could disrupted sleep itself be a causal process in AD? AD patients often take longer to fall asleep, have higher sleep fragmentation, and spend sharply less time in NREM sleep[61,62]. Sleep disruption can be present before the onset of cognitive deficits. For example, very high sleep fragmentation in elderly people is associated with subsequent diagnosis of AD[63]. Experiments on humans and animal models also point to disrupted sleep being a causal process in some cases. In healthy adults, one night of sleep deprivation was sufficient to cause a 25–30% increase in Aβ signal on PET scans[64], a ~30% increase in CSF concentrations of Aβ[65], and a ~50% increase in CSF concentrations of tau[66]. In wild-type rats and mice overexpressing mutated human *APP* and *PSEN1*, restricting sleep for 21 days increased Aβ deposits in the cortex[67,68]. Conversely, pharmaceutically or chemogenetically consolidating sleep in AD mouse models for 1–2 months delayed Aβ plaque formation[67,69]. Disrupted sleep is therefore likely to be a causal process in AD. Can it become a therapeutic target? An ongoing clinical trial (NCT04629547) is underway to test whether suvorexant, an orexin receptor antagonist that increases sleep, can reduce Aβ accumulation by consolidating sleep in older adults without dementia[70]. Our observation that disruption of genes associated with AD diagnosis after 65 years reduces sleep in 7-day zebrafish larvae suggest that disrupted sleep may be a common mechanism through which these genes exert an effect on risk. Impaired sleep early in life may be especially deleterious as it is likely essential for brain development: infants spend most of their time asleep during the first year of life[71]. Incidentally, infants who are *APOE ε4* carriers show differences in grey matter volume and myelin content in multiple brain regions[72]. Differences are also present in children 9–17 years old who carry the disease-causing *PSEN1* E280A mutation[73]. Future

work should assess whether sleep is impaired in infants at higher genetic risk of AD and whether it is related to these structural differences.

Fig. 7–suppl. 1: The ZOLTAR online app for prediction of therapeutics and disrupted processes from behavioural fingerprints.

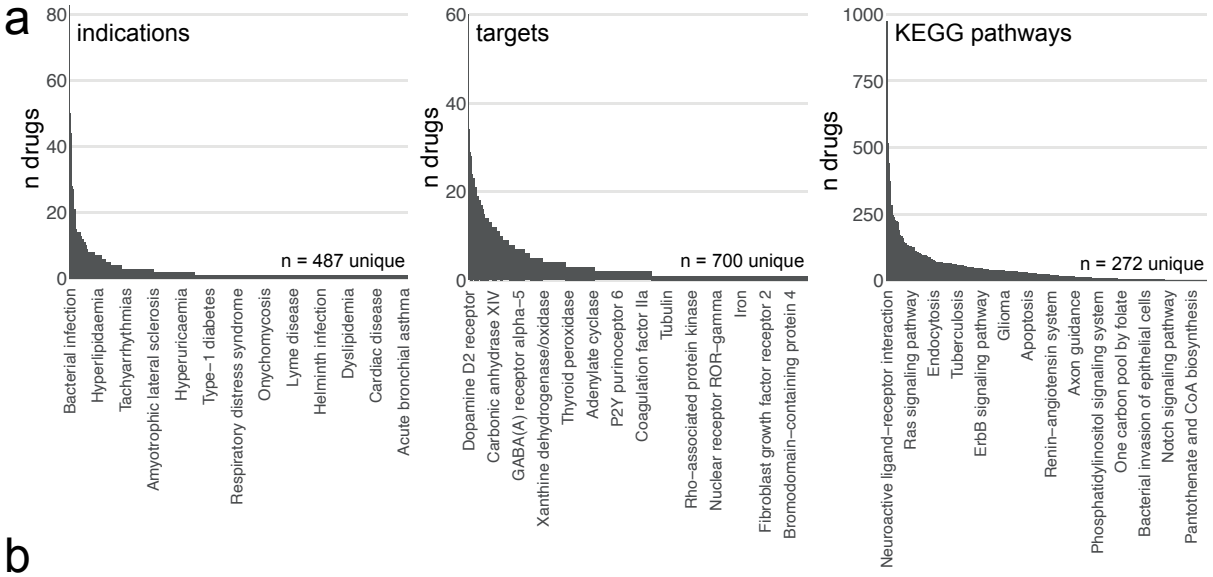

b

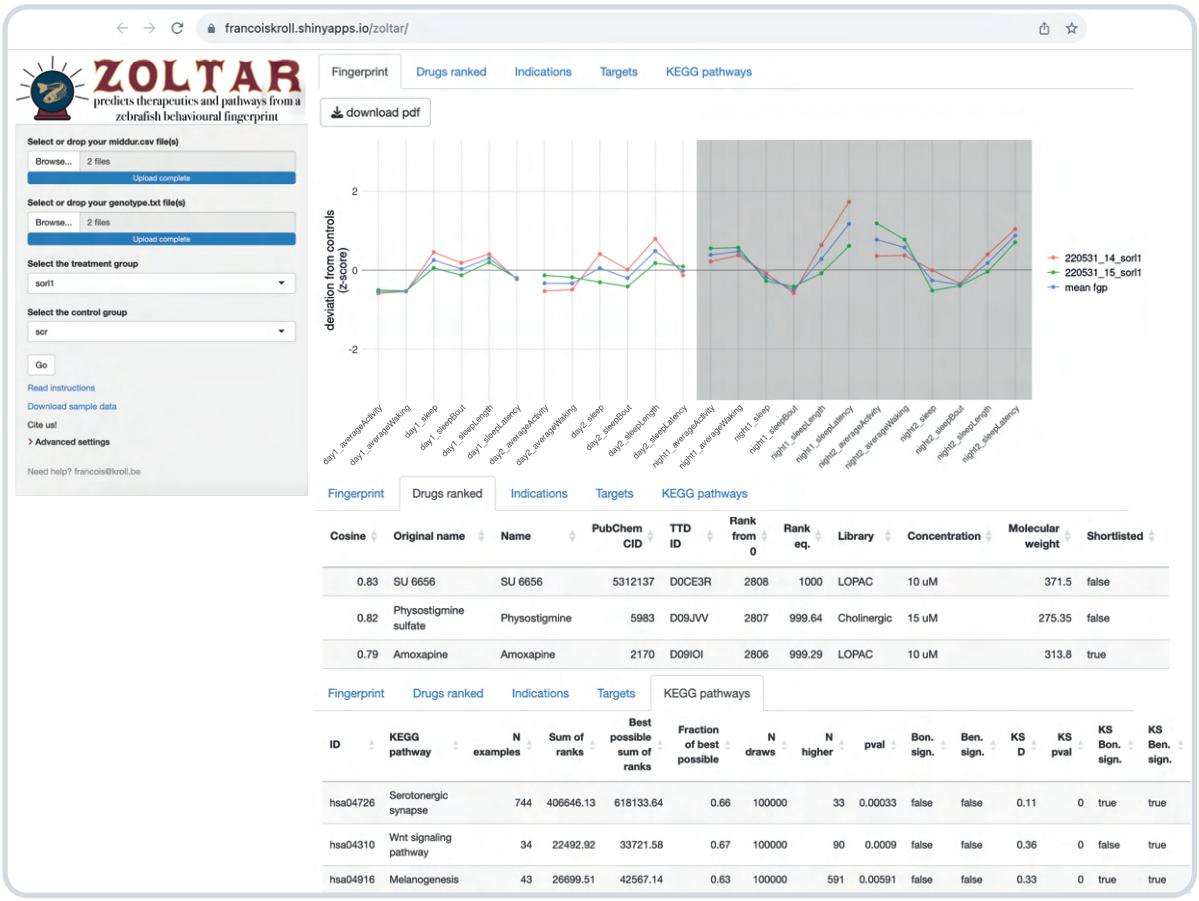

a, Datasets currently available to the ZOLTAR online app for predictions. The height of each bar represents the number of unique compounds with this annotation. Some annotations are labelled as examples. Of 3,674 unique compounds labelled with a PubChem ID, 1,122 were annotated with one or more indications; 1,551 were annotated with one or more targets; and 1,140 were annotated with one or more KEGG pathways through their targets. Source of annotations: Therapeutic Target Database.

Legend continued on next page.

b, Screenshot showing some of the features of the ZOLTAR online app. User drags and drops data file(s) (*middur* = sec active/min for each larva) and file(s) labelling each well with a condition (called "genotype file", but can be any group assignments). The app reads the groups from the genotype file(s) and the user selects the treatment and control groups in a dropdown menu. The app calculates and plots the fingerprint(s) (tab *Fingerprint*), then ranks the 5,756 small molecule fingerprints (tab *Drugs ranked*) from maximum positive cosine to maximum negative cosine. Clicking on a row in the table of ranked compounds plots all the fingerprints of this compound (all fingerprints with the same PubChem ID) in comparison with the query fingerprint, as in Fig. 6a. The app tests, for each annotation, enrichment towards the top and/or bottom of the ranked list with a custom permutation test. Current annotations are clinical indications (tab *Indications*), target proteins (tab *Targets*), and the KEGG pathways each target protein is associated with (tab *KEGG pathways*). Clicking on a row in a table of annotation results generates the "barcode plot" for this annotation, as in Fig. 5a. The tables can be downloaded as .csv files and the plots as .pdf files.

Our behavioural pharmacology approach also predicted that loss of Sorl1 impaired serotonin signalling, which was confirmed by increased sensitivity of *sorl1* knockouts to citalopram. SORL1 acts as an adaptor protein between retromer and several cargo proteins, such as APP[74], GDNF receptor α1[59], and glutamate receptor 1 (GLUA1)[75]. Retromer is a large protein complex which 'rescues' proteins from endosomes, targeting them to recycling instead of lysosomal digestion[76]. By disrupting retromer function, mutations in SORL1 disrupt endosomal recycling, which appears as swelling of early endosomes[77]. As a result, APP remains in endosomes for longer, where it is more likely to be cleaved by β-secretase, the first step towards production of Aβ[78]. Similarly, retromer dysfunction also lowers the level of GLUA1 receptors on the neuron membrane, likely because endocytosed receptors are not recycled back to the membrane, which can result in both increased or decreased firing rates *in vitro*[75]. We speculate that some serotonin (5-hydroxytryptamine, 5-HT) receptors are also recycled via retromer and SORL1. Consequently, *sorl1* knockouts would react differently to a large spike in serotonin (citalopram treatment) as they have different levels of 5-HT receptors on the synaptic membrane. In support for this idea, both 5-HT type 4 receptor[79] and SORL1[80] interact with sorting nexin 27, a subunit of retromer. Furthermore, the 5-HT receptor type 2 was also an enriched target for *sorl1* (simulated p-value = 0.046). Other observations are consistent with serotonin signalling being a causal process of AD. For example, treatment of an AD mouse model with the serotonin reuptake inhibitor (SSRI) citalopram caused a rapid decrease in Aβ concentrations in the ISF and eventually reduced amyloid plaque load. Additionally, humans treated with SSRIs within the past 5 years had significantly lower cortical amyloid plaque load on PET scans, suggesting a causal relationship[81]. While much work remains to be done, SSRIs can generally be used continuously with no adverse effects, so modulating serotonin signalling may be an attractive approach to reduce Aβ levels for years before the onset of cognitive symptoms[81].

Limitations and future directions for predictive behavioural pharmacology

Currently, the hypotheses that our behavioural pharmacology approach can test are limited by the small molecule screen dataset[42], which was biased towards specific themes and targets. For example, of 1,551 compounds with an annotated target, 60 (3.8%) target

the dopamine D2 receptor but only 1 (0.06%) targets mitochondrial uncoupling proteins (UCP1, 2, 3). Consequently, the approach presumably has high sensitivity for disruptions in dopamine signalling, while some hypotheses, such as impairment in mitochondrial coupling, are never formally tested. Broadly, this means that a negative (non-significant) result may not be meaningful if the biological process in question is underrepresented. Additionally, about 30% of the annotated compounds in the database have more than one target. While this is not necessarily an issue when the goal is to find any small molecule which rescues the phenotype, this lack of specificity likely blurs the signal from modulation of a specific target to effect on behaviour. For example, all five compounds which target the histamine H4 receptor also target the histamine H3 receptor, so if the H3 receptor is detected as significantly enriched, the H4 receptor is certain to be significant too, regardless of whether the H4 receptor is indeed specifically disrupted. To develop the biological process prediction, future work should focus on selecting specific agonists and antagonists for a set list of targets, such as the compound VUF-6002 to selectively target the histamine H4 receptor without also activating H3[82].

A way to improve the specificity of the approach is to enhance the resolution of the behaviour tracking so that targets which give similar but unique effects on behaviour can be distinguished. We introduced the FramebyFrame R package to enable analysis at sub-second resolution, but the original small molecule screen dataset was collected at the one-minute resolution[42], so comparing a new behavioural profile to the small molecule database first involves losing resolution to make the fingerprints comparable. During a new small molecule screen, one could use SLEAP[83] or DeepLabCut[84] to extract additional behavioural parameters from video recordings such as speed or position in the well. A faster and higher definition camera could be introduced to allow fine tracking of tail and eye movements. Exposing the larvae to various stimuli is also a way to increase the number of parameters while avoiding redundancy[85]. With more behavioural parameters, the prediction of therapeutics using behavioural pharmacology would also be more precise and the detection of possible behavioural side effects more thorough. Analytically, an improvement could be to represent larval behaviour as a sequence of movements, rather than parameter averages. For example, the Δ pixel time course from our experiments can be encoded as a sequence of bout types termed modules, themselves organised in motifs which are 2–20-module long[44]. Alternatively, behaviour could be represented as sequences of known types of swimming bouts[86] or automatically discovered ‘syllables’[87]. In mouse, this sequence representation was better than a fingerprint one at differentiating similar compounds or even doses[87], so should also improve the predictive power of the behavioural pharmacology approach.

This leads to a thought experiment: assuming absolute resolution in behaviour tracking, does every knockout give a unique effect on behaviour? In other words, are there ~26,000 distinct knockout fingerprints or do multiple genes converge on a smaller set of possible fingerprints? How much resolution is required to distinguish every possible fingerprint?

Conclusion

In summary, we present a behavioural pharmacology approach which uses the sleep/wake behaviour of zebrafish larvae as a tool to translate genomic findings into druggable biological processes and candidate therapeutics. We used Alzheimer's risk genes, especially *SORL1* and *PSEN2*, as case studies and correctly predicted mutant-drug interactions from behaviour alone. Our strategy is both scalable thanks to the F0 knockout method and the FramebyFrame analysis package and generalisable beyond AD through the ZOLTAR app. Other neurological conditions for which many risk genes are known, such as autism, epilepsy, or schizophrenia, are prime candidates for the application of the strategy.

Methods

Animals

Adult zebrafish were reared by University College London's Fish Facility on a 14 hr:10 hr light:dark cycle. To obtain eggs, pairs of one female and one male were isolated in breeding boxes overnight, separated by a divider. Around 9 AM (lights on) the next day, the dividers were removed and eggs were collected 7–10 min later. The embryos were then raised in 10-cm Petri dishes filled with fish water (0.3 g/L Instant Ocean) in a 28.5˚C incubator on a 14 hr:10 hr light:dark cycle. Debris and dead or dysmorphic embryos were removed every other day with a Pasteur pipette under a bright-field microscope and the fish water replaced. At the end of the experiments, larvae were euthanised with an overdose of 2-phenoxyethanol (ACROS Organics). Experimental procedures were in accordance with the Animals (Scientific Procedures) Act 1986 under Home Office project licences PA8D4D0E5 and PP6325955 awarded to Jason Rihel. Adult zebrafish were kept according to FELASA guidelines[88].

Wild types refer to AB × Tup LF fish. Throughout, F0 knockouts refer to wild-type embryos that were injected with gRNA/Cas9 RNPs at the single-cell stage.

Generation of F0 knockout larvae

crRNA selection

The crRNA was the only component of the Cas9/gRNA RNP specific to the target locus.

In previous work[19], we selected predesigned crRNAs from the Integrated DNA Technologies (IDT) database (eu.idtdna.com) based on predicted on-target and off-target scores calculated by a proprietary IDT algorithm. Subsequent benchmarking in zebrafish of various crRNA design algorithms revealed that the IDT on-target scores did not predict mutagenesis rates *in vivo*[89]. All crRNAs used in F0 knockout experiments were therefore designed using CHOPCHOP (chopchop.cbu.uib.no)[90] implementing both the on-target score calculation by CRISPRScan[91], which benchmarking determined was the best predictor of mutagenesis[89], and inDelphi[92], which predicts to some extent the generated mutations in zebrafish embryos[93].

We prioritised targeting asymmetrical exons and only selected crRNAs without any off-targets with 0, 1, 2, or 3 mismatches, as off-targets with up to 3 mismatches may undergo mutation[19,94]. We then selected the crRNAs based on their on-target score and the prediction of frameshift mutations by inDelphi (crRNAs used had 82.8 ± 5.7% predicted frameshift mutation rate). We also used SNPfisher, an online database of common single-nucleotide polymorphisms (SNP) in zebrafish wild-type strains, to check that putative target sites did not contain any SNP[95].

A protocol describing how to select crRNAs based on these developments is available at dx.doi.org/10.17504/protocols.io.81wgb6r5qlpk/v1. Sequences of the crRNAs and information about the targeted loci are provided in Supplementary file 1.

Cas9/gRNA preparation

A protocol describing how to generate F0 knockout larvae is available at dx.doi.org/10.17504/protocols.io.5qpvo52wdl4o/v3.

The CRISPR-Cas9 RNP was made of three components bought from IDT: the crRNA (Alt-R® CRISPR-Cas9 crRNA) and tracrRNA (Alt-R® CRISPR-Cas9 tracrRNA), together forming the gRNA, and the Cas9 (Alt-R® S.p. Cas9 Nuclease V3). The crRNA and tracrRNA were received as pellets, which were individually resuspended in Duplex buffer (IDT, received with the tracrRNA) to form 200 µM stocks. Stocks of crRNA and tracrRNA were stored at −70˚C before use. Cas9 was stored at –20˚C before use. Each crRNA was annealed separately with the tracrRNA by mixing 1 µL crRNA 200 µM; 1 µL tracrRNA 200 µM; 1.28 µL Duplex buffer. The mix was heated to 95˚C for 5 min, then cooled on ice, to obtain a 61 µM gRNA solution. The gRNA solutions were then mixed in equal volumes with Cas9 (1 µL gRNA 61 µM; 1 µL Cas9 61 µM directly from the IDT vial), incubated at 37˚C for 5 min then cooled on ice, generating three 30.5 µM RNP solutions. The three RNP solutions were pooled; the final concentration of each RNP in the pool was thus 10.2 µM and the total RNP concentration 30.5 µM.

The RNPs were usually kept overnight in a 4˚C fridge on ice before injections the following day. Some experiments used RNPs stored at –70˚C for a few weeks.

For experiments targeting two genes simultaneously (*appa*/*appb*, *psen1*/*psen2*, *apoea*/*apoeb*), we targeted each gene at two loci to potentially reduce unviability[19]. While mutating two loci instead of three is predicted to reduce rates of complete biallelic knockout animals, given the high rate of frameshift mutations achieved with the RNPs that were used, ~90% of injected animals were still expected to be complete biallelic knockouts. Across loci that were mutated during double F0 knockout experiments, 97.5 ± 7.0% of the reads were mutated, and 78.9 ± 24.0% of all reads had a frameshift mutation; see francoiskroll.shinyapps.io/frameshiftmodel/ for the theoretical knockout rate prediction. The preparation followed the same steps as above. The four RNP solutions were pooled, so the final concentration of each RNP in the pool was 7.6 µM and the total RNP concentration was 30.5 µM.

Injections

Approximately 1 nL of the three-RNP pool was injected into the yolk at the single-cell stage before cell inflation. This amounts to ~30.5 fmol of RNP (30.5 fmol [5029 pg] of Cas9 and 30.5 fmol [1070 pg] of total gRNA). Each unique RNP was present in equal amounts in the pool. Therefore, in the case of three RNPs, ~10.2 fmol of each RNP were co-injected.

When targeting two genes simultaneously, approximately 1.3 nL of the four-RNP mix were injected so the amount of RNP per gene would remain equal to when a single gene is targeted at three loci.

The injected eggs were kept at ~20˚C for ~50 min after injection before transfer to a 28.5˚C incubator, as delaying the first cell division by lowering the temperature was tentatively shown to increase mutagenesis and reduce the diversity of alleles[96].

Scrambled RNPs

In all F0 knockout experiments, three or four non-targeting, 'scrambled', crRNAs were prepared into RNPs and injected following the same steps as above. These were created by shuffling the spacer sequence of existing crRNAs until the only predicted targets had 4 or more mismatches in protein-coding sequences, or 3 or more in non-coding sequences. Sequences of the scrambled crRNAs are available in Supplementary file 1.

Preparation of samples for Illumina MiSeq

We sequenced every targeted locus in samples of F0 knockout larvae using Illumina MiSeq. For *psen1*, *psen2*, *apoea*, and *apoeb*, the samples were from video-tracked larvae. For *appa*, *appb*, *cd2ap*, *clu*, and *sorl1*, we generated F0 knockout larvae expressly to be sequenced. For each locus, we prepared 5–6 F0 knockout samples and 2–3 scrambled-injected samples. Individual larvae were sequenced at the three or four mutated loci.

The larvae were anaesthetised and their genomic DNA extracted by HotSHOT[97] as follows. Individual larvae were transferred to a 96-well PCR plate or strips of 12 tubes. Excess liquid was removed from each well before adding 50 µl of 1× base solution (25 mM KOH, 0.2 mM EDTA in water). Plates were sealed and incubated at 95°C for 30 min then cooled to room temperature before the addition of 50 µL of 1× neutralisation solution (40 mM Tris-HCl in water). Genomic DNA was then stored at –20˚C.

PCR primers were designed for each target locus using Primer-BLAST (NCBI) to amplify a window of 150–200 bp with at least 30 bp between each primer binding site and the predicted double-strand break site, as this is where most deletions are found[19]. PCR primers were ordered with a Nextera overhang at the 5'-end of each primer to allow indexing (see Supplementary file 1).

Each PCR well contained: 7.98 µL PCR mix (2 mM $MgCl_2$, 14 mM pH 8.4 Tris-HCl, 68 mM KCl, 0.14% gelatine in water, autoclaved for 20 min, cooled to room temperature, chilled on ice, then added 1.8% 100 mg/mL BSA and 0.14% 100 mM d[A, C, G, T]TP), 3 µL 5× Phusion HF buffer (New England Biolabs), 2.7 µL dH_2O, 0.3 µL forward primer (100 µM), 0.3 µL reverse primer (100 µM),

0.12 µL Phusion High-Fidelity DNA Polymerase (New England Biolabs), 1.0 µL genomic DNA; for a total of 15.4 µL. The PCR plate was sealed and placed into a thermocycler. The PCR program was: 95˚C – 5 min, then 40 cycles of: 95˚C – 30 sec, 60˚C – 30 sec, 72˚C – 30 sec, then 72˚C – 10 min, then cooled to 10˚C until collection. The PCR product's concentration was quantified with Qubit (dsDNA High Sensitivity or Broad Range Assay) and its length was verified on a 2.5% agarose gel with GelRed (Biotium). Excess primers and dNTPs were removed by ExoSAP-IT (ThermoFisher) following the manufacturer's instructions. The samples were then sent for Illumina MiSeq, which used MiSeq Reagent Nano Kit v2 (300 Cycles).

Illumina MiSeq data analysis

Illumina MiSeq data was received as two fastq files for each well, one forward and one reverse. The paired-end reads were aligned to the reference amplicon with bwa v0.7.17 and the resulting bam alignment file was sorted and indexed with samtools v1.11[98]. Alignments were then filtered to keep only reads with less than 20% of its length soft-clipped and spanning at least 20 bp on each side of the predicted Cas9 double-strand break site, 4 bp upstream of the 'N' of the NGG protospacer adjacent motif. Whenever necessary, bam alignment files were visualised with IGV v2.16.0. The resulting filtered bam file was converted back to a forward and a reverse fastq file using bedtools v2.30.0[99]. The filtered fastq files were used as input to the R package ampliCan v1.20.0[100], together with a csv configuration file containing metadata information about the samples. AmpliCan was run with settings min_freq = 0.005 (any mutation at a frequency below this threshold was considered as a sequencing error), cut_buffer = 12 (any insertion/deletion starting within ±12 bp of the PAM may be Cas9-generated), and event_filter = FALSE (no filtering of reads), as the reads were already filtered. AmpliCan can normalise mutation counts by ignoring any insertion/deletion found in control samples. On rare occasions, this could artefactually decrease mutation counts in F0 knockout samples because of low-level contamination in control samples (e.g. Fig. 4b, locus 1, sample scr1) so we turned this feature off. Instead, we manually checked the scrambled-injected samples in IGV to confirm that there were no insertions or deletions already present in the wild-type background. AmpliCan detected and counted mutations in the reads and wrote results files that were used for subsequent analysis. Any sample with less than 20× paired-end (40× single-read) coverage were excluded from plots and subsequent analysis. Figures like Fig. 3c,d plot the proportion of mutated reads and the proportion of reads with a frameshift mutation at each locus, as computed by ampliCan. If a read contained multiple indels, ampliCan summed them to conclude whether the read had a frameshift mutation or not.

3D-printed 96-well mesh-bottom plate

The 96-square well mesh-bottom plate (Fig. 2a) was designed using Fusion 360 and PrusaSlicer. Multiple copies were 3D-printed in clear polylactic acid (PLA) with a Creality Ender-3 3D printer. The 3D model is available at github.com/francoiskroll/FramebyFrame.

Behavioural video-tracking

In F0 knockout experiments, wild-type embryos from separate clutches were injected at the single-cell stage with CRISPR-Cas9 RNPs. Each clutch was from a unique pair of parents allowed to mate for 7–10 min. For each clutch, about half of the embryos were injected with non-targeting 'scrambled' RNPs to generate control siblings. Clutch-to-clutch variability in locomotor activity is substantial in zebrafish larvae, even between wild-type clutches of the same strain[101]. Therefore, keeping clutches from different parents/mating events separate is predicted to increase sensitivity of the assay by reducing variability. More generally, it is crucial never to perform comparisons where treatment larvae (e.g. mutant, transgenic, drug-treated) are from one clutch and the control larvae are from another (i.e. controls are not siblings), as any difference discovered with such an experimental design could be caused by clutch-to-clutch variability.

At 5 dpf, individual larvae were transferred to the wells of 3D-printed mesh-bottom plates (see *3D-printed 96-well mesh-bottom plate*), each sitting in the water bath of a ZebraBox (ViewPoint Behavior Technology). To avoid any potential localisation bias during the tracking, F0 knockout and scrambled-injected larvae were plated in alternating columns of the 96-well plate. From each well, the video-tracking software (ZebraLab, ViewPoint Behavior Technology) recorded the number of pixels that changed intensity between successive frames. To be counted, a pixel must have changed grey value above a sensitivity threshold, which was set at 20. The metric, termed Δ pixel, describes each animal's behaviour over time as a sequence of zeros and positive values, denoting if the larva was still or moving. In ZebraLab, the *freeze* setting was set to 3 and the *burst* setting was set to 200. However, note that these settings determine how the Δ pixel data is summarised into number of seconds active per minute by the software (*middur* parameter, see *One-minute vs. frame-by-frame*); therefore, their values are irrelevant when analysing the data using the FramebyFrame package. Tracking was performed at 25 frames per second on a 14 hr:10 hr light:dark cycle for ~65 hours, generating sequences of roughly 5,850,000 Δ pixel values per animal. During the experiment, a pump on a timer (Kollea Automatic Watering System, Amazon UK) injected fish water from a reservoir to the bath every morning around 9 AM (lights on) to counteract water evaporation. Water could overflow through an exit pipe, whose height was adjusted to set the water level in the bath. The day light level was calibrated at 555 lux with a RS PRO RS-92 light meter (RS Components). Night was in complete darkness with infrared lighting for video recording. Temperature and light transitions were recorded with a HOBO Pendant (Onset Data Loggers) immersed in the water bath. Temperature throughout the experiment was 23–26˚C.

At the end of the tracking, we inspected the larvae under a bright-field microscope and excluded from analysis any larva that did not appear healthy or was not responsive to a light touch with a P10 tip. We then randomly selected 2–3 scrambled-injected and 5–6 F0 knockout larvae for sequencing of the targeted loci (see *Preparation of samples for Illumina MiSeq*).

Behavioural video-tracking with drug treatment

This refers to the experiment treating *sorl1* F0 knockouts with citalopram (Fig. 5c,d) and the experiment treating *psen2* F0 knockouts with tinidazole, fenoprofen, and betamethasone (Fig. 6 and Fig. 6–supplement 1b). Broadly, video-tracking was performed as above (see *Behavioural video-tracking*) but larvae were housed in standard 96-square well plates (Whatman) in fish water with drug. Water was topped up every morning shortly after 9 AM (lights on).

Citalopram hydrobromide (Fisher Scientific, #15732987) was stored at room temperature before use. We chose the treatment concentrations (1 µM and 10 µM) based on previous work in zebrafish larvae[102] that found that the minimum dose which had a discernible effect on locomotor activity was 373 µg/L (0.92 µM). A 500× stock (5 mM) for the 10 µM treatment was prepared by diluting 0.0203 g in 10 mL dH_2O (molecular weight = 405.3 g/mol). The 5 mM solution was then diluted 1:10 (100 µL citalopram 5 mM + 900 µL dH_2O) to obtain a 500× stock (500 µM) for the 1 µM treatment. Using a P1000 pipet with a tip whose end was cut-off, individual 5-dpf larvae were transferred in 650 µL fish water to the wells of clear 96-square well plates (Whatman). 1.3 µL of each 500× stock was added on top of each well, effectively diluting each stock 1:500 (5 mM stock diluted to 1 µM and 500 µM stock diluted to 10 µM). Control wells were topped-up with 1.3 µL dH_2O.

Tinidazole (Fisher Scientific, #16594384) was stored at room temperature before use. We chose the treatment concentration (30 µM) based on a preliminary experiment where we video-tracked wild-type larvae treated with 10 µM, 30 µM, 100 µM tinidazole (data not shown). A 50 mM solution was prepared by diluting 0.0247 g in 2 mL DMSO (molecular weight = 247.27 g/mol), then diluted this solution to 15 mM in DMSO as 500× stock.

Fenoprofen calcium salt hydrate (Sigma-Aldrich, #F1517) was stored at room temperature before use. We chose 15 µM as the treatment concentration based on the results from the Rihel et al., 2010 small molecule behavioural screen database[42]. A 200 mM solution was prepared by diluting 0.1114 g in 1065 µL DMSO (molecular weight = 522.6 g/mol), then diluting this solution to 7.5 mM in DMSO as 500× stock.

Betamethasone (Cayman Chemical, #20363) was stored at –20˚C before use. We chose 15 µM as the treatment concentration based on the results from the Rihel et al., 2010 small molecule behavioural screen database. A 33 mM solution was prepared by diluting 0.0204 g in 1,575 µL DMSO (molecular weight = 393.5 g/mol), then diluting this solution to 7.5 mM in DMSO as 500× stock.

For tinidazole, fenoprofen, and betamethasone, 100 µL of each 500× stock was then mixed in 20 mL fish water in a Falcon, and the solution transferred to one Petri dish per drug. A Petri dish

for control larvae was prepared by mixing 100 µL of DMSO in 20 mL fish water. Using a P1000 pipet with a tip whose end was cut-off, individual 5-dpf larvae were transferred in 500 µL fish water to the Petri dishes. Each Petri dish was then topped-up with fish water to 50 mL final volume, which effectively diluted each drug to the final treatment concentration (100 µL 500× stock in 50 mL fish water). The final DMSO concentration was 0.002% (100 µL 100% DMSO in 50 mL fish water). Using a P1000 pipet with a tip whose end was cut-off, individual larvae were then transferred in 650 µL to the 96-square well plates. This process was to avoid adding drug in DMSO directly to the well as the solution sinks in water and may not mix properly.

Video-tracking was then performed with the same settings as above (see *Behavioural video-tracking*). Both mornings shortly after 9 AM (lights on), the wells were manually topped-up with fish water (no drug), which assumes that the drug does not evaporate and was stable in fish water at 23–26˚C for a few days.

A protocol for behavioural video-tracking with drug treatment is available at dx.doi.org/10.17504/protocols.io.4r3l27p6pg1y/v1.

Behavioural data analysis

Behavioural data analysis was performed using the FramebyFrame R package v0.11.0. A tutorial and documentation are available at github.com/francoiskroll/FramebyFrame. The important steps of the analysis are summarised below.

The raw file generated by the ZebraLab software was exported into thousands of xls files each containing 1 million rows of data. Each row of data represented the Δ pixel of one larva at one frame transition. Using the `vpSorter(…)` function, these data were re-organised in a large csv file where each column was a well, each row was a frame transition, and each cell a Δ pixel value. To visualise activity over time, we smoothed the Δ pixel time course for each larva with a 60-min (~45,000 rows) rolling average and binned the data by summing Δ pixels in 10-min epochs. We generated the activity trace of individual larvae using `ggActivityTraceGrid(…)` and excluded from subsequent analysis any larva that had an obviously aberrant behaviour, defined as having missed entirely a day-night transition (no jump/drop in the activity trace) or having shown activity during a day lower than the previous night. Each well was assigned to a group using a metadata file generated by `genotypeGenerator(…)`. For each 10-min epoch, we calculated the mean and standard error of the mean (SEM) across larvae in each group to build the activity traces (e.g. Fig. 3g left).

Sleep was measured on the large csv file containing all the frame-by-frame Δ pixel data. A 60-second (~1,500 rows) rolling sum was applied on the Δ pixel time course of each larva, so that any data point that became zero indicated that the previous 60 seconds of Δ pixels were all zeros, that is, a sleep bout started exactly 60 seconds ago. The data after the rolling sum was converted

into a series of Booleans: *true* if the data point was 0 (i.e. that frame was part of a sleep bout); *false* if the data point was positive (i.e. that frame was not part of a sleep bout, as the larva moved at some point in the preceding 60 seconds). At this stage, the first 0 of each sleep bout marked the frame at the 60th second of each sleep bout. Therefore, a correction was then applied to extend each sleep bout 60 seconds in the past by switching the ~1,500 frames of *false* before each sleep bout start to *true*. The time spent asleep in 10-min epochs (~45,000 rows) was calculated by counting the number of *true* frames in each epoch and multiplying the counts by 1/frame rate (typically 1/25 frames per second), which was converted into minutes for the sleep trace. For example, if larva #3 had 10,000 out of 45,000 frames marked *true* (i.e. these frames are part of a sleep bout) from minute 20 to 30 of tracking, that represented $10{,}000 \times {}^{1}/_{25} \times {}^{1}/_{60} = 6.67\ minutes\ asleep$ for that epoch. As for the activity trace, the mean and SEM across larvae in each group were calculated for each 10-min epoch to build the sleep traces (e.g. Fig. 3g right).

15 behavioural parameters were then calculated for each larva and day/night. Two additional parameters, startle response at sunset and sleep latency, were only defined for nights, for a total of 32 unique parameters (15 day parameters and 17 night parameters). Full days/nights during the experiment were: night0, day1, night1, day2, night2. Larvae were 5 dpf during night0, 6 dpf during day1/night1, 7 dpf during day2/night2, and the experiment was stopped in the morning of 8 dpf. Night0 (5 dpf) was excluded from the analysis as a habituation period; therefore, two day data points and two night data points were calculated for each larva and behavioural parameter. Definitions of the behavioural parameters can be found in the documentation of the FramebyFrame package (github.com/francoiskroll/FramebyFrame).

To build the behavioural fingerprints, a z-score was calculated for each day/night, each larva, and each unique parameter. For example, to calculate the z-score for parameter active bout length of larva #5 for day1, we first calculated the mean and standard deviation of all active bout length data points for control larvae during day1. These were then used to calculate larva #5's z-score as:

$$z_{day1} = \frac{x - \mu_{con}}{\sigma_{con}}$$

Where x was larva #5's day1 data point, μ_{con} was the mean of control day1 data points, σ_{con} was the standard deviation of control day1 data points. The calculation was repeated for day2. The day1 and day2 z-scores were then averaged to produce a common day z-score for active bout length of larva #5. The process was repeated for each unique parameter, producing 32 z-scores for each larva, which we term each larva's behavioural fingerprint. To draw the fingerprint plots (e.g. Fig. 3–supplement 1c), the mean and SEM of all z-scores were calculated for each unique parameter and group of larvae. By definition of the z-score, the mean z-score for the control larvae was always 0 and the SEM constant for each experiment (dependent on the number of control larvae), so the controls' fingerprint was omitted from the plot.

In Fig. 6c, for each parameter, the mean and SEM of all z-scores from each clutch were calculated separately. The two z-score means and SEMs were then averaged to draw each bar. See *Statistics on behavioural parameters* for the definition of each category.

Each larva's fingerprint can be conceptualised as the coordinates of one data point in a 32-dimension space where each dimension represents one behavioural parameter. In Fig. 5d, the centre of the H_2O-treated scrambled-injected larvae or the centre of the H_2O-treated *sorl1* F0 knockout larvae was set as the origin of this 32-dimension space (point at coordinates 0, 0, 0, …) by the z-scoring procedure. We then measured the Euclidean distance between each larva's fingerprint and the origin.

Statistics on behavioural parameters

Each behavioural parameter was statistically compared between F0 knockout and scrambled-injected larvae using linear mixed effects (LME) modelling implemented in the `lmer` function of the R package lme4 v1.1.31[103]. The data were parameter values per larva per time window, for example larva #3 slept 4 hr during night2. We always tracked one unique clutch in each ZebraBox run; therefore, the replicate experiment(s) provided both technical and biological replication. The data collected during nights or during days were analysed separately. The fixed effect was the group assignment (genotype or treatment). Random effects were intercepts for clutch assignment (experiment), larva number, and the larva's age (dpf). Random effects of clutch assignment and larva number were modelled as nested, as data points between larvae of the same clutch were expected to be more similar than between larvae of different clutches; and within each clutch, the day 1 (or night 1) data point of one larva was expected to be similar to its day 2 (or night 2) data point. The command to create the day or night model was:

$$lmer(parameter \sim group + (1|experiment/larva) + (1|dpf), data = night\ or\ day)$$

The model provided the slope and its standard error reported on top of the parameter plots (e.g. Fig. 3h). A model without the fixed effect group was then created, as:

$$lmer(parameter \sim 1 + (1|experiment/larva) + (1|dpf), data = night\ or\ day)$$

This null model was compared with the full model created above with a likelihood-ratio test, which provided the p-value reported in the figures and legends.

The LME analysis was informed by a published tutorial[104]. The FramebyFrame R package performs the above LME analysis when generating parameter plots with `ggParameterGrid(…)` or writing a report of LME statistics using `LMEreport(…)`.

The main likelihood-ratio test (see above) tested the null hypothesis that group assignment had no effect on parameter values. In experiments with more than two groups, each group was also compared to the reference group using estimated marginal means implemented in the R package emmeans, which provided the p-value.

In Fig. 6c, the LME analysis was performed on data from both clutches, as described above. The colour for each parameter was based on two p-values obtained using estimated marginal means: the p-value when comparing DMSO-treated scrambled-injected controls with DMSO-treated *psen2* F0 knockouts ("knockout p-value"), and the p-value when comparing DMSO-treated scrambled-injected controls with drug-treated *psen2* F0 knockouts ("drug p-value"), such that:

- if knockout p-value < 0.05 and drug p-value > 0.05, parameter was a "rescue";
- if knockout p-value < 0.05 and drug p-value < 0.05, parameter was a "missed rescue";
- if knockout p-value > 0.05 and drug p-value < 0.05, parameter was a "side effect";
- if knockout p-value > 0.05 and drug p-value > 0.05, parameter was a "no effect".

One-minute vs. frame-by-frame

The one-minute analyses developed previously[41–43] use the *middur* parameter calculated by ZebraLab. The *middur* parameter reports, for each minute, the number of seconds each larva spent above the *freeze* threshold (set by the user, typically 3 Δ pixel) and below the *burst* threshold (set by the user, typically 200 Δ pixel). In Fig. 2–supplement 2b,c, to better focus the comparisons on the effect of the one-minute binning, we re-calculated the *middur* dataset of the experiment using the FramebyFrame R package (function `rawToMiddur(…)`) setting the *freeze* threshold to 0. Larvae plotted were the scrambled-injected larvae from *sorl1* F0 knockout clutch 2 (Fig. 4–supplement 1).

Pilot long-term video-tracking in 96-well plate

For the experiment in Fig. 2b, we placed 4-dpf scrambled-injected larvae in the wells of a mesh-bottom plate and added to the water bath 50 mL of paramecia culture filtered through a 40-µm cell strainer nylon mesh (Fisherbrand) to remove the large debris which may be detected by the camera of the ZebraBox. Larvae were video-tracked for a total of 208 hr, first on a 14 hr:10 hr light:dark cycle for 63 hr then in constant dim light at 30 lux for 145 hr for the free-running segment. In the afternoon of the first day in constant dim conditions, we removed most of the water from the bath using a 10 mL Pasteur pipette, replaced with fresh fish water, and added another 50 mL of filtered paramecia. As can be seen in Fig. 2b, this created a sharp rise in activity. We did not intervene for the rest of the experiment. The activity trace was generated as above (see *Behavioural data analysis*).

Sleep latency in presence of paramecia

We video-tracked wild-type 6-dpf larvae as described above (see *Behavioural video-tracking*) for 24 hr, including a 14-hr night. Larvae were in the wells of a standard 96-square well plate (Whatman), and we added two drops of filtered paramecia in half of the wells. There was no water bath and the light level at night was 0 lux.

Zebrafish orthologues of Alzheimer's risk genes

We used the GWAS meta-analysis and list of most likely causal genes from Schwartzentruber et al. (2021)[22]. We downloaded from Ensembl the list of all zebrafish orthologues of human genes (last updated 27/04/2023). More details about GWAS loci, causal genes, and zebrafish orthologues can be found in Supplementary file 1.

Single-cell RNA sequencing data

We downloaded single-cell RNA sequencing (scRNA-seq) data generated by Raj et al. (2020)[26] from GEO repository GSE158142 (.rds.gz files, Seurat data structure). In Fig. 1b, each gene was considered expressed if it was detected in at least three cells at this developmental stage. In Supplementary file 1, we manually grouped the clusters from Raj et al. (2020) in broad categories to add colours. The expression data plotted (e.g. Fig. 1c) were scaled from raw counts by the authors such that the mean expression across all cells was 0 and the variance was 1.

In situ hybridization chain reaction

In situ hybridization chain reaction (HCR) probes were designed as described by Choi et al. (2018)[105] using a custom Python script. HCR split initiator sequences B1, B3, and B5 were obtained from Choi et al. (2018). To generate probe sets, probe pairs were excluded if they fell below melting temperature and %GC thresholds. Probe pairs with strong sequence similarity to off-target transcripts were also excluded. For each target transcript, we generated sets of 15–25 probe pairs. Multiple transcripts were often stained in individual larvae. HCR probes were purchased as custom DNA oligos from Thermo Fisher Scientific. HCR amplifiers (B1-Alexa Fluor 488, B3-Alexa Fluor 546, and B5-Alexa Fluor 647) and buffers were purchased from Molecular Instruments. More details about HCR probes can be found in Supplementary file 1.

The HCR protocol we used was adapted from MI-Protocol-RNAFISH-Zebrafish (Rev10) (Molecular Instruments). Proteinase K and methanol permeabilisation steps from the protocol were skipped. HCR to label Alzheimer's risk genes was performed in *Tg(elavl3:H2b-GCaMP6s)* larvae homozygous for the *mitfa*^{w2} allele (*nacre*)[106,107]. 6-dpf larvae were euthanised and fixed in 4% paraformaldehyde (PFA)/Dulbecco's phosphate-buffered saline (DPBS) overnight at 4˚C. Following fixation, larvae were washed three times 5 min in phosphate-buffered saline (PBS). Larvae were then transferred to a SYLGARD-coated Petri dish and the eyes were removed using forceps. Sample preparation was completed by two brief PBST (1× DPBS + 0.1% Tween 20) washes. For the probe hybridization stage, larvae were first incubated in hybridization buffer at 37˚C for 30 min. Meanwhile, a probe solution was prepared by adding 4 µL of each 1 µM probe set (4 pmol) to 500 µL hybridization buffer. Hybridization buffer was replaced by the probe solution, and larvae were incubated at 37˚C overnight (12–16 hr).

The next day, excess probe solution was removed by washing larvae four times 15 min with 500 µL of probe wash buffer preheated to 37˚C. Larvae were then washed twice 5 min with 5× SSCT at room temperature. Samples were kept at room temperature for subsequent amplification steps. First, larvae were transferred to amplification buffer at room temperature for 30 min. 3 µM stocks of hairpin H1 and hairpin H2 were individually heated to 95˚C for 90 sec then left to cool at room temperature in the dark for 30 min. For HCR on up to 8 larvae together, a hairpin solution was prepared by adding 4 µL (12 pmol) of hairpin H1 and 4 µL of hairpin H2 (12 pmol) to 200 µL amplification buffer. Finally, amplification buffer was removed and the hairpin solution was added to the larvae which were incubated overnight (12–16 hr) in the dark at room temperature. After overnight incubation, excess hairpins were removed by washing in 5× SSCT for twice 5 min, then twice 30 min and finally once 5 min at room temperature. Larvae were transferred to PBS and kept at 4˚C protected from light for up to 3 days.

For a subset of transcripts (*appa*, *appb*, *slc6a4a*, *slc6a4b*, *tph1a*, *tph1b*, *tph2*), HCR was not carried out in *nacre*, *elavl3:H2b-GCaMP6s* larvae. Instead, *gad1b* was labelled as a reference channel. We proceeded as above, with some amendments at the sample preparation stage. Larvae were fixed in 4% PFA with 4% (w/v%) sucrose overnight at 4˚C. Brains were dissected with forceps, removing the eyes and the skin that covers the brain. After dissection, there was a 20-min postfix in 4% PFA with 4% (w/v%) sucrose followed by three washes in PBST to remove the fixative. When performing HCR on *sorl1* F0 knockout and scrambled-injected larvae (Fig. 5e and Fig. 5–supplement 1c), larvae from both conditions were pooled in a single Eppendorf tube prior to the hybridization steps. Using a scalpel, a portion of the tail was removed from the scrambled-injected larvae to differentiate the genotypes during imaging.

For imaging, larvae were mounted in 1% low melting point agarose (Sigma-Aldrich) in fish water and imaged with a ZEISS LSM 980 equipped with an Airyscan 2 detector (CO-8Y multiplex mode, confocal resolution) and a ZEISS C-Aprochromat 10×/0.45 W M27 objective. The whole brain was imaged without tiling. The image size was 844.29 µm (3188 pixels) × 846.41 µm (3196 pixels). Each pixel was 0.265 × 0.265 × 1.5 µm. The laser wavelength was 639 nm for B5-Alexa Fluor 647; 561 nm for B3-Alexa Fluor 546; 488 nm for GCaMP6s.

Samples in Fig. 1–supplement 3a,b, Fig. 5e,f, and Fig. 5–supplement 1c,d were imaged with a lightsheet ZEISS Z.1 microscope equipped with a W Plan-Aprochromat 10×/0.5 M27 75 mm objective. The image size was 889.56 µm (1920 pixels) × 889.56 µm (1920 pixels). Each pixel was 0.46 × 0.46 × 1.0 µm. The laser wavelength was 638 nm for B5-Alexa Fluor 647; 561 nm for B3-Alexa Fluor 546; 488 nm for GCaMP6s or B1-Alexa Fluor 488 to image *gad1db*.

Brains were registered to the reference brain from the Zebrafish Brain Browser[108,109] with *elavl3:H2B-GCaMP6s* or *gad1b* as reference channel using ANTs toolbox version 2.1.0[110], as described previously[111].

We prepared Fig. 1d, and Fig. 1–supplement 3 and 4 using Fiji[112]. The minimum/maximum and contrast of each stack/channel were adjusted before generating a maximum Z-projection. We created the sagittal views using Image > Stacks > Reslice before generating a maximum Z-projection. Whole-brain dorsal and sagittal outlines were from the Zebrafish Brain Browser.

In the *sorl1* experiments, masks for anatomical regions were from the Zebrafish Brain Browser. To measure total signal intensity in different anatomical regions (Fig. 5f left and Fig. 5–supplement 1d left), we summed the grey pixel values of every voxel within each mask on the stacks after registration. To count the number of positive voxels in different anatomical regions (Fig. 5f right and Fig. 5–supplement 1d right), we first rescaled each stack to the maximum grey value of the stack. We then applied a threshold at grey pixel value 15 (8bit image, so grey pixel value 0–255) so that the grey value of any voxel with signal below 15 was turned to 0. The threshold value was decided using the multi-Otsu algorithm with two classes implemented in the scikit-image Python package[113]. We then counted for each anatomical region the number of voxels with grey pixel value > 0.

To prepare Fig. 5e and Fig. 5–supplement 1c, we calculated each median stack using MATLAB. The maximum of all four median stacks were then adjusted to the same value in Fiji to keep intensities comparable. The dorsal and sagittal Z-projections were prepared as above.

Amyloid beta measurements on psen1 and psen2 F0 knockouts

psen1, *psen2*, and double *psen1*/*psen2* F0 knockout larvae were generated as described above (see *Generation of F0 knockout larvae*). Most double *psen1*/*psen2* F0 knockout larvae died or were severely dysmorphic by 5 dpf. The other larvae were raised until 16 dpf to increase the amount of tissue available for the assay. Larvae were euthanised by an overdose of tricaine then decapitated with a scalpel. Heads were snap-frozen in liquid nitrogen then homogenized using a mechanical homogenizer in 100 µL TBS (50mM Tris-HCl, pH 8.0) containing 1:200 protease inhibitor cocktail set III (Calbiochem). Homogenates were centrifuged at 16,000 g at 4°C for 30 min. The supernatant was then collected and stored at –70°C. We measured total protein concentration of each sample using the Pierce Detergent Compatible Bradford Assay Kit (ThermoFisher). Aβ38, Aβ40, and Aβ42 concentrations were measured on the Meso Scale Discovery platform (Meso Scale Diagnostics) using the V-PLEX Plus Aβ Peptide Panel 1 (4G8) kit.

Each pool of larvae was measured in four technical replicates: two at the original concentration and two diluted 1:1 in TBS. Meso Scale returned concentrations of Aβ38, Aβ40, Aβ42 in pg/mL. All Aβ38 measurements were below the detection limit. We converted the Aβ concentrations to pg Aβ/µg total protein using the total protein content measured with the Bradford assay. The limit of detection (LOD) for each Aβ species was the concentration of the most diluted standard in pg/mL. We calculated a sample-specific LOD by calculating the Aβ concentration (pg Aβ/µg

total protein) that would have given exactly the LOD in pg/mL. For example, the LOD for Aβ40 was 39.79 pg/mL. Therefore, for a sample whose total protein content was 3788 µg/mL, Aβ40 concentration should have been 0.0105 pg Aβ40/g total protein to give exactly the LOD (39.79 pg/mL). Each data point represents the mean of the four technical replicates, except if both diluted replicates were below the sample-specific LOD, in which case the data point represents the mean of the two undiluted technical replicates. If one undiluted sample was below the LOD but not the other, we replaced the below-LOD measurement by the sample-specific LOD itself. If all four technical replicates (undiluted and diluted) were below the sample-specific LOD, the sample was marked with a cross in the plot.

Annotation of the Rihel et al., 2010 small molecule behavioural database

From the Rihel et al., 2010 small molecule zebrafish behavioural database[42], we extracted the name of each compound tested and the 5,756 behavioural fingerprints, which are the mean z-score for each sleep/wake parameter (see Fig. 6a for the one-minute parameters). The same compound could have alternate database names (e.g. “Dopamine hydrochloride” and “Dopamine HCl”), and could vary by its stereochemistry or salts (e.g. atropine sulfate vs. atropine methyl nitrate). Therefore, we first simplified as much as possible each compound name by removing various stereochemistry and salt information. This reduced the number of unique compound names from 5,149 to 4,731. We then used the webchem R package[114] to automatically search each name in the PubChem database and return the PubChem CID. CID could be retrieved automatically for 4,365 (92%) of the names. We manually searched the remaining 366 compound names, eventually leaving only 12 of 4,731 compound names without a CID. The final number of unique CIDs was 3,674. The Therapeutic Target Database (TTD) uses a custom TTD Drug ID but provided a file for cross-matching PubChem CIDs to TTD Drug IDs (*P1-03-TTD_crossmatching.txt*). We found a TTD Drug ID for 1,738 of the 3,674 CIDs (47%). Using each TTD Drug ID as query, we then extracted indications and target proteins from databases provided by the TTD using TTD Drug IDs as queries (*P1-05-Drug_disease.txt* and *P1-01-TTD_target_download.txt*). Proteins are given a target ID by the TTD, which we then used as query to extract the KEGG pathways each protein was associated with (*P4-01-Target-KEGGpathway_all.txt*).

As TTD Drug IDs were used to extract annotations but that only 47% of compounds were assigned one, the ZOLTAR app currently uses less than half of the dataset by Rihel et al., 2010 for prediction of disrupted pathways. In the future, other sources could be used to enrich the annotations, for example using machine learning to predict target proteins[115].

Behavioural pharmacology from sorl1 F0 knockout’s fingerprint

We measured the cosine similarity (range −1.0–1.0) between the mean fingerprint of the two *sorl1* F0 knockout clutches and each of the 5,756 small molecule fingerprints from the Rihel et

al., 2010 database. We then ranked the 5,756 small molecule fingerprints from the most positive cosine (SU6656: cos = 0.83) to the most negative cosine (flumazenil: cos = −0.80).

At this stage, the general goal of the analysis is to detect whether compounds with a given annotation (indication, target, or KEGG pathway) are found more towards the top and/or bottom of the ranked list than expected by chance. For example, two cases suggest that inhibition of a pathway is what causes the knockout behavioural phenotype: all compounds *inhibiting* this pathway are found towards the top of the list (positive cosines); or all compounds *activating* this pathway are found towards the bottom of the list (negative cosines). The database may include both agonists and antagonists for a given pathway, so we also want to detect cases where compounds interacting with the pathway are found both towards the top *and* towards the bottom of the ranked list. Therefore, the null hypothesis for a given annotation is specifically that fingerprints with this annotation are found across the ranked list in a pattern that can be explained by chance, or that they are mostly found around the centre of the list (cos ~ 0 position).

In practice, we counted fingerprint positions starting at the centre (cos ~ 0 position) and counting in both directions. Namely, the fingerprint with the smallest positive cosine (6,7-dichloroquinoxaline-2,3-dione, cos = 0.0003) was position #1, then position #2 for the next smallest positive cosine, etc. We did not set negative positions, so the fingerprint with the smallest negative cosine (L-Histidine hydrochloride, cos = −0.0003) was also position #1, then position #2, etc. The fingerprint with the smallest positive cosine was not always at the centre of the list, as there could be more fingerprints with positive cosines than fingerprints with negative cosines, or vice-versa. In a case where there were more fingerprints with positive cosines, using these positions directly as ranks would have biased the analysis against detecting negative enrichment (i.e. more fingerprints towards the bottom of the list than expected by chance) as the random draws (see below) would have mostly picked fingerprints with large ranks on the positive-cosine side simply because there were more of them. We controlled for this by forcing ranks to be on the same range (same maximum rank) on either side of the list. Namely, we set the ranks of the fingerprints with positive cosines as:

$$rank = position \times \frac{1000}{n_{positive\ fingerprints}}$$

The same was done for the ranks of the fingerprints with negative cosines (i.e. no negative ranks). Using 1000 as the maximum rank was arbitrary; any number could have been used.

For example, there were 3,201 positive-cosine fingerprints for *sorl1*. Therefore, the rank of the fingerprint with the smallest positive cosine was 1 × 1000/3201 = #0.31; the next fingerprint was rank 2 × 1000/3201 = #0.62, etc., until the fingerprint with the largest positive cosine which had rank 3201 × 1000/3201 = #1000.00. On the opposite side, there were 2,555 negative-cosine fingerprints. Therefore, the rank of the fingerprint with the smallest negative cosine was 1 ×

1000/2555 = #0.39; the next fingerprint was rank 2 × 1000/2555 = #0.78, etc., until the fingerprint with the largest negative cosine which had rank 2555 × 1000/2555 = #1000.00.

At this stage, we had a list of fingerprints from largest positive cosine to largest negative cosine, each with a rank representing its distance from the cosine ~ 0 position. We swapped each compound for its annotations, for example its target(s). If a compound had no annotated target (or indication or KEGG pathway), it was simply deleted without editing any of the ranks. If a compound had multiple annotated targets (or indications or KEGG pathways), all targets received the same rank. For example, aspirin had rank #874.36 (cos = −0.50) and two annotated targets: HMG-CoA reductase and Prostaglandin G/H synthase. Therefore, swapping aspirin for its targets generated two rows with the same rank #874.36. The same compound could appear multiple times in the list, in which case its targets (or indications or KEGG pathways) were simply repeated.

To measure enrichment of a given annotation towards the top and/or bottom of the list, we summed the ranks of all its instances. For example, the serotonin transporter (SLC6A4) appeared 59 times in the list for *sorl1*. The sum of those 59 ranks was 34,958. Was this sum of ranks surprising or could it be explained by chance? To test this, we randomly drew 59 positions and measured the sum of ranks 100,000 times to generate a null distribution of sum of ranks (e.g. Fig. 5b). We counted how many random draws gave a larger sum of ranks than the observed sum of ranks (34,958) to calculate a simulated p-value. In the case of SLC6A4, 1,127 random draws gave a larger sum of ranks; therefore, the probability that a sum of ranks as high as 34,958 was obtained by chance was estimated at 1,127/100,000 = 0.01127, which we reported as the simulated p-value.

A simpler alternative for this analysis may be to sum absolute cosines directly, instead of ranks, as a measure of enrichment. In theory, this option would consider more directly how well the knockout fingerprint and the small molecule fingerprints match.

Behavioural pharmacology from psen2 F0 knockout's fingerprint

We measured the cosine similarity between the mean fingerprint of the two *psen2* F0 knockout clutches and each of the 5,756 small molecule fingerprints from the Rihel et al., 2010 database. We then ranked the 5,756 small molecule fingerprints from the most positive cosine (3-3-Acetoxypregn-16-en-12,20-dione: cos = 0.82) to the most negative cosine (isogedunin: cos = −0.87). We searched within the ~100 fingerprints with the most negative cosines (range of cosines: −0.72–0.87) for compounds which Rihel et al., 2010 labelled as shortlisted because it affected one behavioural parameter with a large effect size and/or affected the same parameter in the same direction across the two days/nights. From these compounds, we selected fenoprofen and betamethasone because they both had a replicate fingerprint with cosine <

−0.60. Tinidazole was selected based on a preliminary experiment in wild-type larvae (data not shown), although it was not shortlisted by Rihel et al., 2010.

To simplify this selection process in the ZOLTAR app (francoiskroll.shinyapps.io/zoltar/), the shortlisted compounds are labelled, and clicking on a candidate compound automatically plots all the fingerprints from this compound (same PubChem CID).

Protein alignment plots

This refers to Fig. 3a,b; Fig. 3–supplement 3a,b; Fig. 4a; Fig. 4–supplement 2a,b; Fig. 4–supplement 3a; and Fig. 4–supplement 4a. Amino acid sequences were obtained from UniProt. The ClustalOmega algorithm, implemented in R by the msa package, was used to align the sequences. Definitions of “highly similar” and “weakly similar” groups of amino acids were taken from the ClustalOmega online documentation. The following groups of amino acids were considered highly similar: STA, NEQK, NHQK, NDEQ, QHRK, MILV, MILF, HY, FYW. The following groups of amino acids were considered weakly similar: CSA, ATV, SAG, STNK, STPA, SGND, SNDEQK, NDEQHK, NEQHRK, FVLIM, HFY. Identity was the number of positions where the zebrafish amino acid matched the human amino acid divided by the total length of the alignment. Similarity was the number of positions where the zebrafish amino acid matched or was highly similar to the human amino acid divided by the total length of the alignment. UniProt IDs of the amino acid sequences used were (human vs. zebrafish): *appa*, P05067 vs. Q6NUZ1; *appb*, P05067 vs. B0V0E5; *psen1*, P49768 vs. Q9W6T7; *psen2*, P49810 vs. Q90ZE4; *apoea*, P02649 vs. Q503V2; *apoeb*, P02649 vs. O42364; *cd2ap*, Q9Y5K6 vs. F1R1N9; *clu*, P10909 vs. Q6PBL3; *sorl1*, Q92673 vs. Q90ZE4.

Gene schematics

This refers to Fig. 3c,d; Fig. 3–supplement 3c,d; Fig. 4b; Fig. 4–supplement 2c,d; Fig. 4–supplement 3b; and Fig. 4–supplement 4b. Coordinates of 5'-UTRs, 3'-UTRs, and exon boundaries were obtained from Ensembl accessed through R using the biomaRt package v2.54.1[116]. For each gene, we drew the transcript that was used as reference when selecting the crRNAs, usually the longest coding transcript annotated in Ensembl. Ensembl IDs of transcripts drawn were: *appa*, ENSDART00000166786; *appb*, ENSDART00000077908; *psen1*, ENSDART00000149864; *psen2*, ENSDART00000006381; *apoea*, ENSDART00000172219; *apoeb*, ENSDART00000058965; *cd2ap*, ENSDART00000102611; *clu*, ENSDART00000127173; *sorl1*, ENSDART00000156995.

Pictures

For the pictures of the *psen2* F0 knockout larvae and scrambled-injected siblings (Fig. 3f and Fig. 3–supplement 2a), larvae were anaesthetised and mounted in 1% low melting point agarose (Sigma-Aldrich) in fish water. Pictures were then taken with a Nikon SMZ1500 brightfield microscope with illumination from above the sample.

Pictures of the *psen1/psen2* double F0 knockout larvae were taken with an Olympus MVX10 microscope connected to a computer with the software cellSens (Olympus).

Statistics

For statistics on behavioural parameters, see *Statistics on behavioural parameters*. For the permutations procedure used in Fig. 5a,b and Fig. 5–supplement 1a,b, see *Behavioural pharmacology from sorl1 F0 knockout's fingerprint*.

Threshold for statistical significance was $\alpha = 0.05$. In figures, ns refers to $p > 0.05$, * to $p \leq 0.05$, ** to $p \leq 0.01$, and *** to $p \leq 0.001$. In text, data distributions are reported as mean ± standard deviation, unless stated otherwise.

In text, estimates of behavioural parameter effect sizes are often reported in % vs. scrambled-injected controls. To calculate those, we first calculated, for each clutch and day or night, the mean of all control data points for this parameter, typically returning four averages (e.g. clutch1 controls, night1 and night2; clutch2 controls, night1 and night2). To each average, the slope from the LME model (see *Statistics on behavioural parameters*) was added/subtracted to estimate the knockout averages. An effect size in % vs. controls ($ef\%$) was then calculated for each clutch and day or night as:

$$ef\% = 100 \times (-1 + \frac{ko}{con})$$

If the slope was positive; or

$$ef\% = -100 \times (1 - \frac{ko}{con})$$

If the slope was negative; where ko and con is the knockout or control average for one clutch and one day or night. The effect sizes were then averaged to return one effect size representing the estimated % increase or decrease vs. scrambled controls.

In Fig. 2–supplement 2d, the data were 47 observations, one per larva. Each observation was the time in hours when the larva had its first sleep bout (status 2). Every larva slept at least once during the experiment, so there were no censored (status 1) observations. We calculated the hazard ratio with a Cox proportional-hazards model and the p-value with a likelihood-ratio test. The functions we used were implemented in the R package survival v3.4.0. The FramebyFrame R package automatically performs this survival analysis when generating sleep latency survival plots with the function `ggSleepLatencyGrid(…)`.

In Fig. 5f and Fig. 5–supplement 1d, we compared values between groups (*sorl1* F0 knockouts vs. scrambled-injected) in each anatomical region using Welch's t-test. To test the null hypothesis that group assignment had no effect on values across regions, we used LME

modelling implemented in the `lmer` function of the R package lme4 v1.1.31[103]. Taking total signal intensity as an example, the command to create the LME model was:

$$lmer(total\ signal\ intensity \sim group + (1|larva) + (1|anatomical\ region)$$

The model provided the slope and its standard error reported in the figures. We then created a model without the fixed effect group, as:

$$lmer(total\ signal\ intensity \sim 1 + (1|larva) + (1|anatomical\ region)$$

We compared this null model with the full model created above with a likelihood-ratio test, which provided the p-value reported in the figures.

Software

Data analysis was performed in R v4.2.2 ran through RStudio 2023.06.0+421. Analysis of HCR on *sorl1* F0 knockouts used Jupyter notebooks written in Python 3. Figures were prepared with Adobe Illustrator 2019. Videos were prepared with Adobe Premiere Pro 2020.

Code availability

Source code of the FramebyFrame R package is available at github.com/francoiskroll/FramebyFrame. The package can be installed directly into R. The GitHub repository includes installation instructions, tutorial, and documentation.

The ZOLTAR online app (francoiskroll.shinyapps.io/zoltar/) was written in R using the Shiny package. Source code is available at github.com/francoiskroll/ZOLTAR.

The online app illustrating the simplified model of knockout by frameshift (francoiskroll.shinyapps.io/frameshiftmodel/) was written in R using the Shiny package. Source code is available github.com/francoiskroll/frameshiftShiny.

Other code used for analysis will be made available at github.com/francoiskroll/ZFAD.

Data availability

Data will be made available on Zenodo.

Acknowledgments

We thank the members of the Rihel lab and other zebrafish groups at University College London (UCL) for helpful discussions. We thank Daniel J. Stein and Douglas A. Lauffenburger (MIT) for inspiration. We thank Alexandra Lubin for the Illumina MiSeq runs; Chintan Trivedi for code used to design HCR probes and advice on analysis of the HCR images; Tom Ryan for help raising the *psen1*/*psen2* knockout larvae used for the Aβ measurements; Alizée Kastler for the *slc6a4b* HCR probes; Stephen Carter for his assessment of the *psen1*/*psen2* double knockout eye phenotype; Declan Lyons for the measurements of the 3D-printed plate's mesh. We thank all supporting staff at UCL including Fish Facility staff for fish care and husbandry. FK thanks Filippo Del Bene for the time spent in his lab working on the manuscript. Most of the behavioural small molecule dataset was generated by JR and David Prober in Alexander F Schier's lab at Harvard University. FK was supported and funded by the Leonard Wolfson PhD Programme in Neurodegeneration. The work was also funded by a Wellcome Trust Investigator Award awarded to JR (217150/Z/19/Z).

Bibliography

1. Schellenberg, G. D. *et al.* Genetic linkage evidence for a familial Alzheimer's disease locus on chromosome 14. *Science* **258**, 668–671 (1992).
2. Levy, E. *et al.* Mutation of the Alzheimer's Disease Amyloid Gene in Hereditary Cerebral Hemorrhage, Dutch Type. *Science* **248**, 1124–1126 (1990).
3. Van Broeckhoven, C. *et al.* Amyloid β Protein Precursor Gene and Hereditary Cerebral Hemorrhage with Amyloidosis (Dutch). *Science* **248**, 1120–1122 (1990).
4. Campion, D. *et al.* Mutations of the presenilin I gene in families with early-onset Alzheimer's disease. *Human Molecular Genetics* **4**, 2373–2377 (1995).
5. Rogaev, E. I. *et al.* Familial Alzheimer's disease in kindreds with missense mutations in a gene on chromosome 1 related to the Alzheimer's disease type 3 gene. *Nature* **376**, 775–778 (1995).
6. Glenner, G. G. & Wong, C. W. Alzheimer's disease and Down's syndrome: sharing of a unique cerebrovascular amyloid fibril protein. *Biochem Biophys Res Commun* **122**, 1131–1135 (1984).
7. Haass, C. & Selkoe, D. J. Cellular processing of β-amyloid precursor protein and the genesis of amyloid β-peptide. *Cell* **75**, 1039–1042 (1993).
8. Shoji, M. *et al.* Production of the Alzheimer amyloid beta protein by normal proteolytic processing. *Science* **258**, 126–129 (1992).
9. De Strooper, B. *et al.* Deficiency of presenilin-1 inhibits the normal cleavage of amyloid precursor protein. *Nature* **391**, 387–390 (1998).
10. Wolfe, M. S. *et al.* Two transmembrane aspartates in presenilin-1 required for presenilin endoproteolysis and gamma-secretase activity. *Nature* **398**, 513–517 (1999).
11. Hardy, J. & Selkoe, D. J. The amyloid hypothesis of Alzheimer's disease: progress and problems on the road to therapeutics. *Science* **297**, 353–356 (2002).
12. van Dyck, C. H. *et al.* Lecanemab in Early Alzheimer's Disease. *New England Journal of Medicine* **388**, 9–21 (2023).
13. Hardy, J. & Mummery, C. An anti-amyloid therapy works for Alzheimer's disease: why has it taken so long and what is next? *Brain* **146**, 1240–1242 (2023).
14. Lu, Q. *et al.* Systematic tissue-specific functional annotation of the human genome highlights immune-related DNA elements for late-onset Alzheimer's disease. *PLOS Genetics* **13**, e1006933 (2017).
15. Tansey, K. E., Cameron, D. & Hill, M. J. Genetic risk for Alzheimer's disease is concentrated in specific macrophage and microglial transcriptional networks. *Genome Medicine* **10**, 14 (2018).
16. Bellenguez, C. *et al.* New insights into the genetic etiology of Alzheimer's disease and related dementias. *Nat Genet* **54**, 412–436 (2022).
17. Kroll, F. From disease genes to behavioural screen in zebrafish: early onset Alzheimer's as case study. *Doctoral thesis, UCL (University College London).* (UCL (University College London), 2022).
18. Verschuur, C. V. M. *et al.* Randomized Delayed-Start Trial of Levodopa in Parkinson's Disease. *N Engl J Med* **380**, 315–324 (2019).
19. Kroll, F. *et al.* A simple and effective F0 knockout method for rapid screening of behaviour and other complex phenotypes. *eLife* **10**, e59683 (2021).
20. Ashlin, T. G., Blunsom, N. J., Ghosh, M., Cockcroft, S. & Rihel, J. Pitpnc1a Regulates Zebrafish Sleep and Wake Behavior through Modulation of Insulin-like Growth Factor Signaling. *Cell Reports* **24**, 1389–1396 (2018).
21. Hoffman, E. J. *et al.* Estrogens Suppress a Behavioral Phenotype in Zebrafish Mutants of the Autism Risk Gene, CNTNAP2. *Neuron* **89**, 725–733 (2016).
22. Schwartzentruber, J. *et al.* Genome-wide meta-analysis, fine-mapping and integrative prioritization implicate new Alzheimer's disease risk genes. *Nat Genet* **53**, 392–402 (2021).
23. Giambartolomei, C. *et al.* Bayesian Test for Colocalisation between Pairs of Genetic Association Studies Using Summary Statistics. *PLoS Genet* **10**, e1004383 (2014).
24. Raj, T. *et al.* Integrative transcriptome analyses of the aging brain implicate altered splicing in Alzheimer's disease susceptibility. *Nat Genet* **50**, 1584–1592 (2018).
25. Meyer, A. & Mélaga-Trillo, E. Vertebrate genomics: More fishy tales about Hox genes. *Current Biology* **9**, R210–R213 (1999).
26. Raj, B. *et al.* Emergence of Neuronal Diversity during Vertebrate Brain Development. *Neuron* **108**, 1058-1074.e6 (2020).
27. Yamazaki, Y., Zhao, N., Caulfield, T. R., Liu, C.-C. & Bu, G. Apolipoprotein E and Alzheimer disease: pathobiology and targeting strategies. *Nat Rev Neurol* **15**, 501–518 (2019).
28. Kunkle, B. W. *et al.* Genetic meta-analysis of diagnosed Alzheimer's disease identifies new risk loci and implicates Aβ, tau, immunity and lipid processing. *Nat Genet* **51**, 414–430 (2019).
29. Lambert, J.-C. *et al.* Meta-analysis of 74,046 individuals identifies 11 new susceptibility loci for Alzheimer's disease. *Nat Genet* **45**, 1452–1458 (2013).
30. Nicolas, G. *et al.* SORL1 rare variants: a major risk factor for familial early-onset Alzheimer's disease. *Mol Psychiatry* **21**, 831–836 (2016).
31. Pottier, C. *et al.* High frequency of potentially pathogenic SORL1 mutations in autosomal dominant early-onset Alzheimer disease. *Mol Psychiatry* **17**, 875–879 (2012).
32. Thonberg, H. *et al.* Identification and description of three families with familial Alzheimer disease that segregate variants in

the SORL1 gene. *Acta Neuropathologica Communications* **5**, 43 (2017).
33. Herbomel, P., Thisse, B. & Thisse, C. Zebrafish Early Macrophages Colonize Cephalic Mesenchyme and Developing Brain, Retina, and Epidermis through a M-CSF Receptor-Dependent Invasive Process. *Developmental Biology* **238**, 274–288 (2001).
34. Kudoh, T. *et al.* A Gene Expression Screen in Zebrafish Embryogenesis. *Genome Res.* **11**, 1979–1987 (2001).
35. Raymond, P. A., Barthel, L. K., Bernardos, R. L. & Perkowski, J. J. Molecular characterization of retinal stem cells and their niches in adult zebrafish. *BMC Dev Biol* **6**, 36 (2006).
36. Thiel, W. A., Esposito, E. J., Findley, A. P., Blume, Z. I. & Mitchell, D. M. Modulation of retinoid-X-receptors differentially regulates expression of apolipoprotein genes *apoc1* and *apoeb* by zebrafish microglia. *Biology Open* **11**, bio058990 (2022).
37. Wu, S. *et al.* Two phenotypically and functionally distinct microglial populations in adult zebrafish. *Sci. Adv.* **6**, eabd1160 (2020).
38. Lowery, L. A. & Sive, H. Initial formation of zebrafish brain ventricles occurs independently of circulation and requires the *nagie oko* and *snakehead/atp1a1a.1* gene products. *Development* **132**, 2057–2067 (2005).
39. Mu, Y. *et al.* Glia Accumulate Evidence that Actions Are Futile and Suppress Unsuccessful Behavior. *Cell* **178**, 27-43.e19 (2019).
40. Jiao, S. *et al.* The Conserved Clusterin Gene Is Expressed in the Developing Choroid Plexus Under the Regulation of Notch But Not IGF Signaling in Zebrafish. *Endocrinology* **152**, 1860–1871 (2011).
41. Lee, D., Oikonomou, G. & Prober, D. Large-scale Analysis of Sleep in Zebrafish. *Bio-protocol* **12**, (2022).
42. Rihel, J. *et al.* Zebrafish Behavioral Profiling Links Drugs to Biological Targets and Rest/Wake Regulation. *Science* **327**, 348–351 (2010).
43. Rihel, J., Prober, D. A. & Schier, A. F. Monitoring Sleep and Arousal in Zebrafish. in *Methods in Cell Biology* vol. 100 281–294 (Elsevier, 2010).
44. Ghosh, M. & Rihel, J. Hierarchical Compression Reveals Sub-Second to Day-Long Structure in Larval Zebrafish Behavior. *eNeuro* 7, (2020).
45. Prober, D. A., Rihel, J., Onah, A. A., Sung, R.-J. & Schier, A. F. Hypocretin/Orexin Overexpression Induces An Insomnia-Like Phenotype in Zebrafish. *J. Neurosci.* **26**, 13400–13410 (2006).
46. Haapasalo, A. & Kovacs, D. M. The Many Substrates of Presenilin/γ-Secretase. *JAD* **25**, 3–28 (2011).
47. Kang, J. *et al.* The precursor of Alzheimer's disease amyloid A4 protein resembles a cell-surface receptor. *Nature* **325**, 733–736 (1987).
48. Özcan, G. G., Lim, S. & Rihel, J. Genetic and chemical disruption of Amyloid Precursor Protein processing impairs zebrafish sleep maintenance. 2022.06.08.495312 Preprint at https://doi.org/10.1101/2022.06.08.495312 (2022).
49. Frånberg, J., Svensson, A. I., Winblad, B., Karlström, H. & Frykman, S. Minor contribution of presenilin 2 for γ-secretase activity in mouse embryonic fibroblasts and adult mouse brain. *Biochemical and Biophysical Research Communications* **404**, 564–568 (2011).
50. Herreman, A. *et al.* Presenilin 2 deficiency causes a mild pulmonary phenotype and no changes in amyloid precursor protein processing but enhances the embryonic lethal phenotype of presenilin 1 deficiency. *Proceedings of the National Academy of Sciences* **96**, 11872–11877 (1999).
51. Shen, J. *et al.* Skeletal and CNS Defects in Presenilin-1-Deficient Mice. *Cell* **89**, 629–639 (1997).
52. Sundvik, M., Chen, Y.-C. & Panula, P. Presenilin1 Regulates Histamine Neuron Development and Behavior in Zebrafish, *Danio rerio*. *J. Neurosci.* **33**, 1589–1597 (2013).
53. Jiang, H., Newman, M. & Lardelli, M. The zebrafish orthologue of familial Alzheimer's disease gene PRESENILIN 2 is required for normal adult melanotic skin pigmentation. *PLoS ONE* **13**, e0206155 (2018).
54. Yang, T., Arslanova, D., Gu, Y., Augelli-Szafran, C. & Xia, W. Quantification of gamma-secretase modulation differentiates inhibitor compound selectivity between two substrates Notch and amyloid precursor protein. *Molecular Brain* **1**, 15 (2008).
55. Musa, A., Lehrach, H. & Russo, V. E. Distinct expression patterns of two zebrafish homologues of the human APP gene during embryonic development. *Dev Genes Evol* **211**, 563–567 (2001).
56. Zhou, Y. *et al.* Therapeutic target database update 2022: facilitating drug discovery with enriched comparative data of targeted agents. *Nucleic Acids Res* **50**, D1398–D1407 (2022).
57. Andersen, J., S. Kristensen, A., Bang-Andersen, B. & Strømgaard, K. Recent advances in the understanding of the interaction of antidepressant drugs with serotonin and norepinephrine transporters. *Chemical Communications* **0**, 3677–3692 (2009).
58. Lillesaar, C. The serotonergic system in fish. *Journal of Chemical Neuroanatomy* **41**, 294–308 (2011).
59. Glerup, S. *et al.* SorLA Controls Neurotrophic Activity by Sorting of GDNF and Its Receptors GFRα1 and RET. *Cell Reports* **3**, 186–199 (2013).
60. Barthelson, K., Pederson, S. M., Newman, M. & Lardelli, M. Brain transcriptome analysis reveals subtle effects on mitochondrial function and iron homeostasis of mutations in the SORL1 gene implicated in early onset familial Alzheimer's disease. *Molecular Brain* **13**, 142 (2020).
61. D'Atri, A. *et al.* EEG alterations during wake and sleep in mild cognitive impairment and Alzheimer's disease. *iScience* **24**, 102386 (2021).

62. Prinz, P. N. *et al.* Sleep, EEG and mental function changes in senile dementia of the Alzheimer's type. *Neurobiol Aging* **3**, 361–370 (1982).
63. Lim, A. S. P., Kowgier, M., Yu, L., Buchman, A. S. & Bennett, D. A. Sleep Fragmentation and the Risk of Incident Alzheimer's Disease and Cognitive Decline in Older Persons. *Sleep* **36**, 1027–1032 (2013).
64. Shokri-Kojori, E. *et al.* β-Amyloid accumulation in the human brain after one night of sleep deprivation. *Proc Natl Acad Sci U S A* **115**, 4483–4488 (2018).
65. Lucey, B. P. *et al.* Effect of sleep on overnight cerebrospinal fluid amyloid β kinetics. *Ann Neurol* **83**, 197–204 (2018).
66. Holth, J. K. *et al.* The sleep-wake cycle regulates brain interstitial fluid tau in mice and CSF tau in humans. *Science* **363**, 880–884 (2019).
67. Kang, J.-E. *et al.* Amyloid-beta dynamics are regulated by orexin and the sleep-wake cycle. *Science* **326**, 1005–1007 (2009).
68. Zhao, B. *et al.* Chronic Sleep Restriction Induces Aβ Accumulation by Disrupting the Balance of Aβ Production and Clearance in Rats. *Neurochem Res* **44**, 859–873 (2019).
69. Jagirdar, R. *et al.* Restoring activity in the thalamic reticular nucleus improves sleep architecture and reduces Aβ accumulation in mice. *Sci Transl Med* **13**, eabh4284 (2021).
70. Herring, W. J. *et al.* Polysomnographic assessment of suvorexant in patients with probable Alzheimer's disease dementia and insomnia: a randomized trial. *Alzheimers Dement* **16**, 541–551 (2020).
71. Ednick, M. *et al.* A review of the effects of sleep during the first year of life on cognitive, psychomotor, and temperament development. *Sleep* **32**, 1449–1458 (2009).
72. Dean, D. C. *et al.* Brain Differences in Infants at Differential Genetic Risk for Late-Onset Alzheimer Disease A Cross-sectional Imaging Study. *JAMA Neurol* **71**, 11–22 (2014).
73. Quiroz, Y. T. *et al.* Brain Imaging and Blood Biomarker Abnormalities in Children With Autosomal Dominant Alzheimer Disease: A Cross-Sectional Study. *JAMA Neurol* **72**, 912–919 (2015).
74. Jensen, A. M. G. *et al.* Dimerization of the Alzheimer's disease pathogenic receptor SORLA regulates its association with retromer. *Proceedings of the National Academy of Sciences* **120**, e2212180120 (2023).
75. Mishra, S. *et al.* The Alzheimer's gene SORL1 is a regulator of endosomal traffic and recycling in human neurons. *Cell. Mol. Life Sci.* **79**, 162 (2022).
76. Burd, C. & Cullen, P. J. Retromer: a master conductor of endosome sorting. *Cold Spring Harb Perspect Biol* **6**, a016774 (2014).
77. Mishra, S. *et al.* Pharmacologic Stabilization of Retromer Rescues Endosomal Pathology Induced by Defects in the Alzheimer's gene SORL1. 2022.07.31.502217 Preprint at https://doi.org/10.1101/2022.07.31.502217 (2023).
78. Small, S. A. & Petsko, G. A. Retromer in Alzheimer disease, Parkinson disease and other neurological disorders. *Nat Rev Neurosci* **16**, 126–132 (2015).
79. Joubert, L. *et al.* New sorting nexin (SNX27) and NHERF specifically interact with the 5-HT4a receptor splice variant: roles in receptor targeting. *J Cell Sci* **117**, 5367–5379 (2004).
80. Huang, T. Y. *et al.* SNX27 and SORLA Interact to Reduce Amyloidogenic Subcellular Distribution and Processing of Amyloid Precursor Protein. *J Neurosci* **36**, 7996–8011 (2016).
81. Cirrito, J. R. *et al.* Serotonin signaling is associated with lower amyloid-β levels and plaques in transgenic mice and humans. *Proc Natl Acad Sci U S A* **108**, 14968–14973 (2011).
82. Terzioglu, N., van Rijn, R. M., Bakker, R. A., De Esch, I. J. P. & Leurs, R. Synthesis and structure–activity relationships of indole and benzimidazole piperazines as histamine H4 receptor antagonists. *Bioorganic & Medicinal Chemistry Letters* **14**, 5251–5256 (2004).
83. Pereira, T. D. *et al.* SLEAP: A deep learning system for multi-animal pose tracking. *Nat Methods* **19**, 486–495 (2022).
84. Mathis, A. *et al.* DeepLabCut: markerless pose estimation of user-defined body parts with deep learning. *Nat Neurosci* **21**, 1281–1289 (2018).
85. Myers-Turnbull, D. *et al.* Simultaneous analysis of neuroactive compounds in zebrafish. 2020.01.01.891432 Preprint at https://doi.org/10.1101/2020.01.01.891432 (2022).
86. Marques, J. C., Lackner, S., Félix, R. & Orger, M. B. Structure of the Zebrafish Locomotor Repertoire Revealed with Unsupervised Behavioral Clustering. *Current Biology* **28**, 181-195.e5 (2018).
87. Wiltschko, A. B. *et al.* Revealing the structure of pharmacobehavioral space through motion sequencing. *Nat Neurosci* **23**, 1433–1443 (2020).
88. Aleström, P. *et al.* Zebrafish: Housing and husbandry recommendations. *Lab Anim* **54**, 213–224 (2020).
89. Uribe-Salazar, J. M. *et al.* Evaluation of CRISPR gene-editing tools in zebrafish. *BMC Genomics* **23**, 12 (2022).
90. Labun, K. *et al.* CHOPCHOP v3: expanding the CRISPR web toolbox beyond genome editing. *Nucleic Acids Research* **47**, W171–W174 (2019).
91. Moreno-Mateos, M. A. *et al.* CRISPRscan: designing highly efficient sgRNAs for CRISPR-Cas9 targeting in vivo. *Nat Methods* **12**, 982–988 (2015).
92. Shen, M. W. *et al.* Predictable and precise template-free CRISPR editing of pathogenic variants. *Nature* **563**, 646–651 (2018).
93. Naert, T. *et al.* Maximizing CRISPR/Cas9 phenotype penetrance applying predictive modeling of editing outcomes in Xenopus and zebrafish embryos. *Sci Rep* **10**, 14662 (2020).

94. Höijer, I. *et al.* CRISPR-Cas9 induces large structural variants at on-target and off-target sites in vivo that segregate across generations. *Nat Commun* **13**, 627 (2022).
95. Butler, M. G. *et al.* SNPfisher: tools for probing genetic variation in laboratory-reared zebrafish. *Development* **142**, 1542–1552 (2015).
96. Terzioglu, M., Saralahti, A., Piippo, H., Rämet, M. & Andressoo, J.-O. Improving CRISPR/Cas9 mutagenesis efficiency by delaying the early development of zebrafish embryos. *Sci Rep* **10**, 21023 (2020).
97. Meeker, N. D., Hutchinson, S. A., Ho, L. & Trede, N. S. Method for isolation of PCR-ready genomic DNA from zebrafish tissues. *Biotechniques* **43**, 610, 612, 614 (2007).
98. Li, H. *et al.* The Sequence Alignment/Map format and SAMtools. *Bioinformatics* **25**, 2078–2079 (2009).
99. Quinlan, A. R. & Hall, I. M. BEDTools: a flexible suite of utilities for comparing genomic features. *Bioinformatics* **26**, 841–842 (2010).
100. Labun, K. *et al.* Accurate analysis of genuine CRISPR editing events with ampliCan. *Genome Res* **29**, 843–847 (2019).
101. Joo, W., Vivian, M. D., Graham, B. J., Soucy, E. R. & Thyme, S. B. A Customizable Low-Cost System for Massively Parallel Zebrafish Behavioral Phenotyping. *Frontiers in Behavioral Neuroscience* **14**, (2021).
102. Bachour, R.-L., Golovko, O., Kellner, M. & Pohl, J. Behavioral effects of citalopram, tramadol, and binary mixture in zebrafish (Danio rerio) larvae. *Chemosphere* **238**, 124587 (2020).
103. Bates, D., Mächler, M., Bolker, B. & Walker, S. Fitting Linear Mixed-Effects Models Using lme4. *Journal of Statistical Software* **67**, 1–48 (2015).
104. Winter, B. Linear models and linear mixed effects models in R with linguistic applications. Preprint at https://doi.org/10.48550/arXiv.1308.5499 (2013).
105. Choi, H. M. T. *et al.* Third-generation in situ hybridization chain reaction: multiplexed, quantitative, sensitive, versatile, robust. *Development* **145**, dev165753 (2018).
106. Lister, J. A., Robertson, C. P., Lepage, T., Johnson, S. L. & Raible, D. W. nacre encodes a zebrafish microphthalmia-related protein that regulates neural-crest-derived pigment cell fate. *Development* **126**, 3757–3767 (1999).
107. Vladimirov, N. *et al.* Light-sheet functional imaging in fictively behaving zebrafish. *Nat Methods* **11**, 883–884 (2014).
108. Marquart, G. D. *et al.* A 3D Searchable Database of Transgenic Zebrafish Gal4 and Cre Lines for Functional Neuroanatomy Studies. *Frontiers in Neural Circuits* **9**, (2015).
109. Marquart, G. D. *et al.* High-precision registration between zebrafish brain atlases using symmetric diffeomorphic normalization. *GigaScience* **6**, gix056 (2017).
110. Avants, B. B. *et al.* A reproducible evaluation of ANTs similarity metric performance in brain image registration. *NeuroImage* **54**, 2033–2044 (2011).
111. Antinucci, P., Folgueira, M. & Bianco, I. H. Pretectal neurons control hunting behaviour. *eLife* **8**, e48114 (2019).
112. Schindelin, J. *et al.* Fiji: an open-source platform for biological-image analysis. *Nat Methods* **9**, 676–682 (2012).
113. Walt, S. van der *et al.* scikit-image: image processing in Python. *PeerJ* **2**, e453 (2014).
114. Szöcs, E., Stirling, T., Scott, E. R., Scharmüller, A. & Schäfer, R. B. webchem: An R Package to Retrieve Chemical Information from the Web. *Journal of Statistical Software* **93**, 1–17 (2020).
115. Chatterjee, A. *et al.* Improving the generalizability of protein-ligand binding predictions with AI-Bind. *Nat Commun* **14**, 1989 (2023).
116. Durinck, S., Spellman, P. T., Birney, E. & Huber, W. Mapping identifiers for the integration of genomic datasets with the R/Bioconductor package biomaRt. *Nat Protoc* **4**, 1184–1191 (2009).